Masters's Thesis

Understanding the Parasitic Effects on the Microwave Interferences at Hearing Instrument Level up to 6GHz

Thomas Sofya



Department of Electrical and Information Technology,
Faculty of Engineering, LTH, Lund University, 2016.

Understanding the Parasitic Effects on the Microwave Interferences at Hearing Instrument Level up to 6GHz

Thomas Sofya

Department of Electrical and Information Technology
Lund University

Advisor: Andreas Jakob
Johan Wernehag

Acknowledgements

This thesis was made available and financially supported by Sonova AG in Switzerland (Staefa). I am grateful to Andreas Jakob, for his support and enthusiasm in providing this opportunity and his valuable technical input, altogether making my work and stay at Sonova more interesting and pleasant.

The writing of this thesis was one of the most significant challenges in my academic life. I wish to also thanks the following colleagues for their support, guidance and patience in helping me improve the quality and value of this work. Our deepest gratitude to all the people who helped us throughout this thesis.

*Andreas Jakob, my first supervisor at Sonova AG.

*Johan Wernehag, my second supervisor in Lund University.

*Professor Daniel Sjöberg, my examiner in Lund University.

The following persons contributed to the master thesis:

Gerard van Oerle, Manager HIMS R&D, Sonova AG

Fethi Cherigui, Manager Electronic Systems R&D, Sonova AG

Laich Rolf, Manager Microsystem Software Engineer Services, Sonova AG

Sahba Aazami, Electronics System Architect, Sonova AG

Claudio Zuin, RF expert, Sonova AG

Javier Abadiadel Castillo, 3D-EM simulation expert, Phonak Communications, Murten

Anton Tombeur, EMC expert, NXP Eindhoven

Harry Neuteboom, Analog CMOS architect, NXP Semiconductors Eindhoven

Michiel van Nieuwkerk, ASIC Development Engineer, Sonion Netherlands

Yang Gao, ASIC Development Engineer, Sonion Netherlands

Jan P. Koopman, Application Engineer, Sonion Netherlands

Sven Kuehn, RF expert, IT'IS Foundation, Zurich

Abstract

In recent decades, an increase in the number of electromagnetic sources, such as mobile phones, has occurred in parallel with developing smaller hearing instrument (HI) devices with low power consumption. All these factors have made the HI devices more susceptible to electromagnetic interference (EMI). Because previous standardized electromagnetic immunity measurement methods (like IRIL measurements according to the HI EMC standards IEC 60118-13 or ANSI C63.19) do not deliver enough insight into the EMI processes and EM coupling paths inside an HI, it has become important to look for new and other EMI measurement methods which could accommodate the design of HI devices with better immunity to EMI.

In order to increase the RF immunity of the HI during its design process, a better understanding of the effects of the hearing instrument (HI) parasitic microwave antennas (PMWAs) and other non-linear HI components causing electromagnetic interference (EMI) in a HI up to frequencies of 6 GHz should be accomplished. The PMWAs pick up RF signals from external and even internal (HI) sources. These RF signals are demodulated by non-linear HI components in the signal path. Amplifying components of the HI electronics always exhibit some non-linear behavior and therefore act as demodulator circuits. They cannot be avoided and cause unwanted distortion and noise in the output of the HI.

We have studied two important parts of the HI:

A) The Hybrid, which amplifies and processes the audio signal and

B) The HI Microphone, which converts the acoustical sound into an electrical signal.

Both parts, Hybrid and HI Microphone, were implemented on two separated test boards. During the study we applied Direct Power Injection (DPI) method to these test boards (which is able to work with active components) and then studied the RF power distribution and the RF voltage transfer inside the components/sections of interest, mentioned above, by creating electrical models of these components/sections while taking into account the circuit connection to the test boards.

One major issue is the lack of physical access to the Hybrid and HI Microphone internal electronic circuit nodes which would allow us to perform RF voltage transfer measurements. The Hybrid and HI Microphone are therefore “black boxes” which could only be characterized by impedance and “transfer”

measurements at the acoustical HI output, hence allowing us to make an informed behavioral estimation of the internal electronic circuit.

Furthermore we tried to investigate the PMWAs behavior and efficiency and carried out measurements with 2 special demodulator circuits (instead of the Hybrid) mounted in a dummy HI. The measurements with these dummy HI were done in a GTEM cell.
Instead of using the complex PMWAs of a HI we also measured some artificial antennas (monopole and L-shape antennas) in a GTEM cell.

We were not able to accurately model the impedance and the RF voltage transfer in the Hybrid and the HI microphone for radio frequencies (RF) > 1 GHz because of unknown RLC parasitics of the test boards. These unknown RLC parasitics impacted the DPI measurements as well.
A better RF model accuracy (or better lumped element models) can be achieved by A) applying extended 3D-EM simulations for the test boards, the Hybrid and the HI Microphone,
B) getting more RF data about the integrated circuits (IC) inside the Hybrid and HI Microphone from the corresponding manufacturers/designers, i.e. more accurate lumped element models and demodulator circuit behavior of ESD protection diodes and audio low-noise amplifiers (LNA).

Nevertheless, the models for RF < 1 GHz are helpful to show if on-/off-chip components of MW filters are useful. Therefore, these components were studied more closely during the thesis. The on-/off-chip components of MW filters can make HIs more immune against EMI in the frequency range of 50 MHz- 4 GHz.

Contents

Acknowledgements 2
Abstract 4
Glossary 13
Introduction 15
1. Summary of work 17
2. Background 22
2.1 Equipment 22
RF signal generator (Agilent N5182B, 9 kHz – 6 GHz): 22
Power meter with power sensors 22
Network Analyzer (R&S ZVL, 9 kHz – 6 GHz): 22
Audio Analyzer (UPD and UPL R&S, 2 Hz – 300 kHz): 22
Measurement Microphone (B&K) with Ear Simulator: 22
Microphone Power supply (Norsonic 324): 22
Oscilloscope: 22
GTEM cell teseq 250V: 23
Directional Coupler: 23
2.2 GTEM cell measurements 24
IT'IS Foundation demodulator circuit for GTEM cell measurements 24
Golden Unit HI measurements 25
Antenna measurement 26
2.3 Julstrom Method 29
2.4 Integrated Circuit Specialties and Limitations 30
3. Direct Power injection (DPI) 33
3.1 Computed power loss using S11 parameter (program 2) 35
3.2 Computed reflected power method (Program 3): 38
3.3 Measurements for computed power loss using S11 parameter: 39
4. Modeling of the Circuits 47
4.1 Matching parameters 49

Strange matching 52
Power Distribution inside circuits 57
4.2 Microphone test board circuit: 61
4.3 Hybrid MIC1 circuit: 67
4.4 Hybrid TCOILN&P circuit: 72
5. Measurements of parasitic microwave antennas (PWMA) 78
5.1) The IT'IS foundation demodulator circuit 78
5.2) Real HI measurements 83
5.3) L-shape and monopole antenna 87
6. General Findings and Conclusions, Future Improvements 93
Reference: 96
Appendix 98
A. Cubicle and manipulator setup 98
B. Input circuit of microphone 99
C. Voltage AC source of the artificial antenna circuit 102
D. ESD protection diodes 103
E. Simple ESD diode demodulation model for MIC1 103
F. Network Analyzer Calibration 106
G. Tcoil (or Telecoil) 107
H. 3D-EM models and interconnections 109
I. Converting from S11 parameter to impedance 110
J. Creating the DPI voltage AC source 111
K. Directional coupler measurements 113
Setup for $\boldsymbol{S11, S12, S21, S22}$ measurements 114
Setup for $\boldsymbol{S13, S33}$ measurement: 114
The setup for $\boldsymbol{S24, S44}$measurement: 115
L. Ferrite bead model BLM18AG471SN1D: 116
Part 1: Accurate impedance measurements 116
Part 2: Electrical circuit topology 122

Part 3: Matching between measured and simulated ferrite bead 122
M. SMA-connector short circuit measurements 126
O. Side effect of measuring reflected power, program 3 130
P. Full frequency range 132
Q. Julstrom correction 133
MIC1 and TCOILN/TCOILP: 133
IT'IS Foundation demodulator circuit calibration data and Julstrom method 133
R. GTEM Cell Input Power Corrections: 134
S. Matlab code 136
Demodulator circuit code 136
Julstrom calculation for Golden HI 138

List of Figures

Fig.1. General structure of a Directional coupler component. 23
Fig.2.Measurement setup for IT'IS Foundation demodulator circuit with dummy HI..... 24
Fig.3. Setup for Golden Unit HI IRIL measurements 26
Fig.4. SMA chassis connector in metal plate 27
Fig.5. Monopole and L-shape antenna measurement. 28
Fig.6. The 6 different orientations of the Julstrom method. 29
Fig.7. Magnetic-acoustical T-coil gain measurement for test board 7 31
Fig.8. The setup of Magnetic-Acoustical gain measurement with Tcoil..... 32
Fig.9. Original setup of DPI measurement. 34
Fig.10. DPI measurement setup for active electronic HI component. 35
Fig.11.Example of relation between S11 parameter, incident, reflected and transmitted power. 37
Fig.12. Comparing the S11-parameter measurement for all test boards with Hybrid MIC1 connection. 40
Fig.13. Firstharmonic output for changing RF power at Hybrid MIC1 input. 41
Fig.14. First harmonic output for changing RF power at Microphone input..... 42
Fig.15. First harmonic output for changing RF power at Hybrid TCOILN&P input. 43
Fig.16.The first four harmonics for Hybrid 5 MIC1 45
Fig.17.The first four harmonics for microphone 4 test board..... 45
Fig.18. The first four harmonics for TCOILN&P Hybrid 1 test board. 46
Fig.19. The RF signal of the microphone IC output. 51
Fig.20. Comparing the RF signal at the ASPIC branch with the IRIL output (DPI measurement). 54
Fig.21. Comparing the MW filter output with the DPI measurement. 54
Fig.22. Comparing ASPICn Output of TCOILN&P connection with DPI measurement. 55
Fig.23. Comparing ASPICp Output of TCOILN&P connection with DPI measurement. 55
Fig.24. Comparing the RF signal from the middle branch in the microphone integrated circuit with the DPI measurement. 56
Fig.25. Shows the output voltage of the Microphone integrated circuit..... 56
Fig.26. Microphone test board circuit 58
Fig.27. Real Power Distribution. 59

Fig.28. Microphone output with both DPI voltage source and regular AC voltage source curves. 61
Fig.29.Electrical circuit model of the microphone test board 62
Fig.30. A picture for the microphone test board..... 63
Fig.31. PCB layout showing the microphone test board connections on a PCB. .. 63
Fig.32. First frequency range results for microphone test board. 65
Fig.33. Second frequency range results for microphone test board..... 66
Fig.34. The third frequency range results for microphone test board..... 66
Fig.35. The PCB layout of Hybrid test boards with MIC1 connection on PCB layout. 67
Fig.36. Hybrid test board fully assembled..... 68
Fig.37. Hybrid test board electrical model with MIC1 connection. 69
Fig.38. The first frequency range results for Hybrid MIC1 input test board..... 70
Fig.39. The second frequency range results for MIC1 test board..... 71
Fig.40. The third frequency range results for MIC1 test board. 71
Fig.41. TCoil component..... 72
Fig. 42. TCoil Hybrid Testboard. 73
Fig.43. Hybrid test board with TCOILN&P connection on PCB layout. 73
Fig.44. The first frequency range results for Hybrid test board with TCOILN&P connection..... 74
Fig.45. The second frequency range results for Hybrid test board with TCOILN&P connection..... 74
Fig.46. The third frequency range results for Hybrid test board with TCOILN&P connection..... 75
Fig.47.Hybrid test board with TCOILN&P connection 77
Fig.48. Impedance magnitude and phase matching for the first frequency range for the Hybrid test board TCOILNP. 77
Fig.49. Schematic of IT'IS Foundation demodulator circuit..... 79
Fig.50. IT'IS Foundation demodulator circuit mounted on a dummy HI..... 80
Fig.51. TCOILN&P demodulator circuit results of orientation A..... 81
Fig.52. Julstrom calculation for TCOILN&P demodulator circuit..... 82
Fig.53. MIC1 demodulator circuit results of orientation A 82
Fig.54. Julstrom calculation for MIC1 demodulator circuit. 83
Fig.55. Golden Unit HI1 with Tcoil, GTEM cell measurement. 85
Fig.56. Golden Unit HI1-HI3 with Tcoil, GTEM cell measurement. 85
Fig.57. Golden Unit HI1 with Omni Mic, GTEM cell measurement..... 86
Fig.58. Golden Unit HI1-HI3 with Omni Mic..... 86
Fig.59. Measured monopole antenna..... 87

Fig.60. Measured L-shape antenna with 2 cm bending. 87
Fig.61. Measured L-shape antenna with 4 cm bending. 88
Fig.62. Schematic of loaded, artificial antenna. 89
Fig.63. HI with L-shape antenna RF voltage transfer inside HI for frequency Range1. 90
Fig.64. HI with L-shape antenna RF voltage transfer inside HI for frequency Range 2 91
Fig.65. The HI with L-shape antenna RF voltage transfer inside HI for frequency Range 3. 92
Fig.66. Golden Unit HI mounted inside a cubicle 98
Fig.67. Cubicle orientations 99
Fig.68. Cubicle mounted on a plexiglass plate with manipulator rod 99
Fig.69. Opened microphone 100
Fig.70. Microphone PCB layer 1 101
Fig.71. Microphone PCB layer 2 102
Fig.72. Demodulation caused by the ESD diodes together with a squarer..... 103
Fig.73.Vout, biasing with 8uA 104
Fig.74. 1KHz-harmonic output..... 105
Fig.75. Checking the Smith Chart directly after the calibration. 106
Fig.76. Port extensions 107
Fig.77. Simple Tcoil topology for frequency range between 50 MHz - 1 GHz. . 108
Fig.78. A more complex Tcoil topology for frequency range between 1-6 GHz.108
Fig.79. Matching of the Tcoil impedance for f-Range1. 109
Fig.80. 3-D model of part in the Hybrid test board 110
Fig.81. S21 parameter of the directional coupler 115
Fig.82. S24 parameter of the directional coupler 116
Fig.83. Circuit for a SMA connector with a simple ferrite bead. 117
Fig.84. Impedance of a short circuit 118
Fig.85. Impedance of an open circuit. 118
Fig.86. Open SMA-connector 119
Fig.87. Shorted SMA-connctor 119
Fig.88. A ferrite connected to a SMA-connector 119
Fig.89. One port de-embedding idea 120
Fig.90. Comparison of ideal and extracted impedance of the ferrite bead 121
Fig.91. Impedance match of measured and simulated ferrite bead data, frequency range 50 MHz - 1 GHz. 123
Fig.92. Impedance magnitude 124
Fig.93. Impedance phase 124

Fig.94. Adjusting the impedance magnitude and phase 125
Fig.95. Ferrite bead circuit 125
Fig.96. Different short circuit measurements 126
Fig.97. One conductive short circuit pin 127
Fig.98. Impedance for a short circuit with one conductive pin 127
Fig.99. Two conductive pin short circuit..... 128
Fig.100. Impedance of a short circuit with two conductive pins..... 128
Fig.101. A very good short circuit for SMA-connector. 129
Fig.102. Impedanceof a short circuit with fully conductive pins 129
Fig.103. The s11-parameter measurement for Hybrid 2..... 130
Fig.104. The result of using program 3 131
Fig.105. The results of program 2 131
Fig.106. The full frequency range for Hybrid test board with TCOILN&P connection..... 132
Fig.107. The full frequency range for microphone test board..... 132
Fig.108. The full frequency range for Hybrid test board with MIC1 connection 133

Glossary

HI	Hearing instrument
MW	Microwaves; frequency range 600 MHz – 6 GHz
GTEM cell	Gigahertz-TEM cell (waveguide which produces quite a homogenous electromagnetic (EM) field over a large frequency range.
Parasitic MW Antenna (PMWA)	A combination of metallic HI objects (like PCB traces, connecting wires, housing of microphone and earphone, etc.) with the following RF properties: A) A monopole antenna with an electrical length of one quarter of the wavelength or a multiple of that. B) A dipole antenna with electrical length of one half of the wave length or a multiple of that. C) An electrically short, high-Q antenna (with electrical length << wavelength) well matched to the loading circuit.
3D EM simulation	3 dimensional electromagnetic simulation, e.g. with "CST Microwave Studio" or similar
ASIC	Application Specific Integration Circuit. Both hybrids and microphones use ASICs for signal processing
Chip	Rectangular piece of silicon on top of which the ASIC is implemented.
PCB	Printed Circuit Board
HI electronics	Consists of a hybrid and parts like 1 or 2 microphones, an earphone (named in the acoustic domain as "receiver"), switches (to control program and volumes), a passive telecoil, a HIBAN antenna coil (for the transceiver running at 10.6 MHz), a programming interface (mechanical connector), a 4- layer flex-PCB, a battery (Zn-Air). All these parts are relatively small (or even tiny).
Hybrid	Part of the HI electronics with 3 ASICs and a few passive components (mainly for power supply decoupling) encapsulated in a small brick of size: 5.5 x 3.5 x 1.6 mm
EHIMA	European Hearing Instrument Manufacturer Association
EMI	Electromagnetic Interference, functional disturbances caused by RF signals radiated onto or conducted into an electronic device

EM immunity	Electromagnetic immunity, the electronic device's immunity against RF signals originating from outside of the device
EMC	Electromagnetic Compatibility. EMC is the branch of electrical engineering concerned with the unintentional generation, propagation and reception of electromagnetic energy which may cause unwanted effects such as electromagnetic interference (EMI) or even physical damage in operational equipment (or electronic devices). The goal of EMC is the correct operation of different equipment (or electronic devices) in a common electromagnetic environment.
Julstrom approach	Proposal for new HI positions to achieve better immunity (and emission) results. See reference [2].
IRIL	Input related interference level in [dB-SPL]
ORIL	Output related interference level [dB-SPL]
DPI	Direct RF power injection

Introduction

In the period from 1980 – 2010, many wireless communication standards (like GSM, DECT, PCS, (WCDMA, IDEN, 2.4GHz-WLAN, Bluetooth) have been introduced. The mobile phone standard GSM became widespread in 1990 and subsequently has presented the Hearing Instrument industry with the challenge of dealing with potentially interfering Microwave emissions. Among these mobile phone standards, GSM has caused the largest interference in Hearing Instrument (HI) electronics because of the high RF peak power radiated by the mobile phone and the time-division-multiplexing transmission scheme used by GSM.
The hearing aid industry in cooperation with EHIMA (European Hearing Instrument Manufacturer Association), HIA (Hearing Instrument Association (US)) and other organizations tackled the issue with a threefold approach:

- Investigation and survey of Microwave power levels, frequencies and modulation schemes emitted by mobile phones, [4]
- Introducing new EMC standards, such as, ANSI C63.19 and IEC 60118-13 for mobile phones and HI, [3]
- Making the HI electronics reasonably immune against the widespread radiation from mobile and smart phones.

Because telecommunication standards for mobile and smart phones have rapidly evolved to other (higher) frequency bands and transmission schemes (e.g. GSM, 2G, 3G, 4G and LTE) [4], there has been an ongoing demand for amendments of the HI EMC standards and making the HI electronics immune against Microwave emissions. It is a design secret of each HI manufacturer to achieve the HI EM immunity required by the HI EMC standards at low cost.

The main goal of the master thesis work was to understand the effect of the HI parasitic microwave antennas (PMWAs) and other non-linear HI components on the electromagnetic interference (EMI) or input related interference level (IRIL) performance for frequencies up to 6 GHz.

Considered from the radio frequency (RF) or MW viewpoint the HI is a highly complex system. Therefore, it was important to break down this complex system into smaller parts in order to have a simpler system to study. The parts we focused on were mainly the HI microphone and hybrid (audio amplification system).
In the main study we applied the direct RF power injection (DPI) method for these smaller parts. The DPI method was analyzed by RF and EMI measurements and RF models for simulation were created. Afterwards measurement and simulation

results of the models were compared. Even though we had some modeling issues it turned out that DPI and constant EMF voltage could be a competitive method compared to those presented in both EMC standards ANSI C63.19 [3] and IEC 60118-13 [3], when analyzing the EMI behavior of HI microphones and hybrids. As a side effect of this main study, we found that ESD protection circuits in integrated circuits can largely contribute to EMI or even be the main cause.

In a further part of the study, we looked at the HI electronics as multiples of PMWAs. For a few of these PMWAs, the EMI output and their foot point voltage was measured with the aid of a tiny demodulator circuit. One PMWA was further simplified to an L-shape antenna and their scattering parameters were measured in a GTEM cell environment.

In a last step we tried to combine the RF simulation models obtained by the DPI measurements with the PMWA measurement results to get an overall RF or MW model. This worked quite well for the case of the L-shape antenna. For the other distinct PMWAs, their scattering parameters were lacking, but we were able to sketch a way to overcome this issue in a future work.

Essential and simple solutions to lower EMI in HI will help thousands of people who use HI and mobile communication devices together (e.g. 3% of population in USA and EU).

Furthermore, EMC and design knowledge to lower EMI will also help other industries to manufacture better products and bring them to the market. The industry providing any sort of audio electronic goods might therefore be interested in our findings.

1. Summary of work

Having a good idea about the parasitic RLC-circuits inside your model is the main point in studying the behavior of the transferred RF voltage. The deficiency in understanding the behavior of the parasitic microwave antennas (PMWA) in a HI is mainly because the standardized electromagnetic (EM) immunity measurement method (like IRIL measurements according to the HI EMC standards IEC 60118-13 or ANSI C63.19 [3] do not deliver enough insight into the EMI processes and EM coupling paths inside a HI. Therefore, it is important to find new methods.

The PMWAs inside a HI consist of PCB traces, connecting wires and relatively large metallic objects (like the HI battery and the microphones). The connecting wires from the HI to the external earphone can form parts of PMWAs. In general the PMWAs of a HI can be thought of as many MW antennas which are mutually coupled and differently loaded by electrical components. Therefore, it was very important to include all the possible parasitic RLC-circuits in our electrical circuit model. Our test boards consist mainly of analogpassive parts consisting of traces, wires, ferrite beads and integrated circuits represented by the microphone and Hybrid chips.

The strategy we used to get some accuracy and match between the test boards, which were used in our measurements, and the created electrical circuits for them, was first to define an accurate electrical circuit model of our test boards, and second to match the impedance and/or S11 parameter between the measured and simulated test boards. The network analyzer was used for the impedance and S11 parameter measurements.

As mentioned before the lack of physical access to the HI internal electronic circuit nodes to allow RF voltage transfer measurements, presents a major problem. You have to characterize your “black box” by impedance measurements and “transfer” measurements at the acoustical HI output in order to estimate the RF behavior of the internal electronic circuit. During this approach we guessed the RLC parasitic components derived from MCAD and ECAD design data. 3D-EM modeling and circuit simulation tools were applied on the Hybrid PCB (assembled with components) to get a 2-port RF model for further simulation and analysis. Both results, which we obtained by impedance and acoustical output measurement, were used to refine the RF circuit simulation model of the black box. However, because of complexity we could not perform 3D-EM modeling and simulations of the whole test board and/or the HI. Later on, it was discovered that

these missing models were the main limitation for a better model accuracy at RF > 1 GHz.

In the beginning of our work the frequency range of interest was between (50 MHz – 6 GHz), but we realized that it is too difficult to get accurate results with this large frequency range. Therefore, we split this large range into three parts in order to get more accurate models for each frequency span.

In chapter 3 and 4, we describe how we measured the input and output of test boards applying the Direct Power Injection (DPI) method. DPI accurracy to the standard IEC 62132-4 [5] is a common measurement method in the automotive industry when the RF immunity of an integrated circuit must be analyzed. We have tried to apply DPI also for active electronic HI components, see Fig.10. In the automotive industry DPI is mainly used to test the RF power immunity of a distinct integrated circuit (IC) and looks for permanent failures or malfunctions of the IC, see Fig.9. Here, we used DPI for active electronic HI components by investigating their acoustical audio frequency output in a large dynamic range. This acoustical output is the unwanted EMI signal caused by the demodulation (or audio rectification process) in the analogue front-end circuitry of the HI IC and the HI microphone IC.
The output signal was evaluated according to the HI EMC standards, mentioned before. We based our DPI measurement on a s11-parameter measurement at the HI circuit input which we used to calculate the "incident" power delivered by the RF generator and to get a constant "transferred" RF power delivered to the input of the active electronic HI component. (See section "3.1 Computed power loss using S11 parameter (program 2)"). The same s11-parameter measurement was used to calculate the circuit input impedance. The measured RF input impedance was first mapped onto a hypothetical electrical circuit (with reasonable circuit topology and component values) which gave approximately the same simulated impedance as measured. For this mapping process different approaches and tools were used. The final hypothetical circuit was then analyzed with the circuit simulator SPICE which allowed the simulation of the RF voltage transfer from the HI or microphone input to the demodulating part(s) deep inside the electronic circuit, see Fig.29, Fig.37 and

Fig.47).

We studied 3 different cases by using Hybrid and microphone test boards. The names that we gave for the Hybrid test boards are the following: 1) MIC1 connection, seeFig.37; 2) TCOILN&P connection, see

Fig.47.
For the microphone test board we used a distinct microphone from Sonion see Fig.29.

In chapter 5.1, the modeling of the demodulating parts is considered. These are all active electronic HI components with non-linear behavior, especially pn-junctions on the IC, which are met by the RF signal when travelling from the HI input through the analogue front end circuit. It turned out that the input ESD protection diodes at the IC, which were designed for a completely different function, turn on when the RF input signal is large enough and can contribute largely to the EMI signal. In order to investigate the demodulating parts more closely we obtained a rough model for the ESD protection diodes from NXP, see chapter 5.1. For other parts, like the audio low-noise amplifier (LNA) on the HI IC (after the MW filter) we did not get a model, see Fig.29. The same was true for the PMOS transistor on the IC of the Sonion microphone. Obviously, it's very difficult for the IC designer and manufacturer to model the RF demodulator behavior of an IC for which the main function is audio signal processing and the IC design and manufacturing process is unsuitable for RF applications.
Because of the missing models for the demodulating parts we cannot compare the measured demodulated voltage with a simulated one. However, the changes and maximum values of the RF voltage at the demodulator input over a distinct frequency range should also show up at the demodulated output (or DPI measurement output). This at least allows a rough comparison between DPI measurement and simulation results based on an estimated circuit.

In chapter 5.2, we performed GTEM cell measurements to 3 golden unit HIs and to dedicated demodulator circuits (MIC1, TCOILP &TCOILN&P) mounted in dummy HIs of the same design as the golden units.
Finally we also used the GTEM cell to apply some measurements for simple antennas, like monopole antenna and L-shape antenna with different length and bending, see Fig.60.

In chapter 5.3, we investigated the parasitic microwave antennas (PMWA) of a HI. The PMWAs inside a HI consist of metallic interconnections (PCB traces, connecting wires) and relatively large metallic objects (like the battery and microphone case). The connecting wires from the HI to the external earphone can also form the PMWAs. In general the PMWAs of a HI can be thought of as

multiple MW antennas which are mutually coupled and differently loaded by passive and active electrical components.

We tried to tackle the PMWA topic threefold by measuring:
A) The antenna foot point voltages in a dummy HI without Hybrid (i.e. without HI amplifier and signal processor IC), but with a tiny demodulator circuit built up by IT'IS foundation. The output leads of this tiny demodulator circuit are high-ohmic carbon fibers and therefore do not disturb the EM-fields inside the GTEM cell.
B) IRIL (or acoustical demodulator output) of 3 functional HIs which had exactly the same mechanical and electrical construction as the dummy HI used under A)
C) Measuring the S-parameters (s11, s21, s22) of a small L-shaped antenna placed in the GTEM cell

None of these measurement setups gave all the required information about a loaded PMWA of a HI. For more information and special findings please refer to chapter 5.
For case A) we got only an impression about the max. magnitude of the unloaded PMWA foot point voltages.
Case B) clearly showed that it is not sufficient to measure the HI RF immunity with only 4 positions of the HI with respect to the transmitted E-field. (Which is exactly what is required by the HI EMC standard IEC 60118-13 [3] with 4 rotations (angles of 0, 90, 180, 270 degrees) done in a plane in parallel to the GTEM cell GND-plane.) For this reason we applied for both cases B) and A) the Julstrom approach [1] (which measures the HI immunity in 6 different HI orientations and sums up their maximums).
For case C) we obtained the base data (foot point voltage and antenna impedance) of an "artificial" PMWA connected to the HI Hybrid pads and therefore reasonably loaded. This model can be used for further RF circuit simulation.

Finally we have seen that it should be possible to measure the impedance of the PMWAs directly from the HI but without the Hybrid. Measuring directly on HI will give more accurate data because it will include all the possible parasitics in the HI. To perform this step, an HI, without the Hybrid, connected to a network analyzer via a coaxial cable, is required. To get the impedance of the PMWAs, you will have to de-embed the effect of the coaxial cable, a method which we used many times during the thesis work.

2. Background

2.1 Equipment

RF signal generator (Agilent N5182B, 9 kHz – 6 GHz):
Radio frequency signal generator is widely used in RF microwave design and test applications. The available frequency range is between 10 Hz to 6 GHz. The maximum power is around 30dBm. The output impedance is 50 Ω.

It is recommended to use an additional RF power amplifier to reach the maximum required forwarded power in case the mismatch load is higher than the abilities of the RF power source. The maximum power level depends on the DUT application. In our case, we did not need to produce power above 20 dBm, therefore, it was not important to use an additional amplifier.

Power meter with power sensors: An instrument for measuring the RF or MW power. The power meter (Giga-tronics 8542C) has two input ports to connect the power sensors 80301A and 80320A. They are used to measure the forward and reflected power.

Network Analyzer (R&S ZVL, 9 kHz – 6 GHz): Are particularly useful in measuring linear characteristics of radio frequency (RF) components and devices. You can also use modern network analyzer in more specific applications, such as signal integrity and materials measurements. In our case, the main use for the Network Analyzer was to take impedance and S-parameter measurements.

Audio Analyzer (UPD and UPL R&S, 2 Hz – 300 kHz): is a test and measurement instrument used to objectively quantify the audio performance of electronic and electro-acoustical devices. The device has been mainly used to measure the acoustical output from the test boards under test.

Measurement Microphone (B&K) with Ear Simulator: any calibrated measurement microphone can be taken. The ear simulator is a standardized acoustical cavity which is put on top of the measurement microphone.
Microphone Power supply (Norsonic 324): used to supply the measurement microphone.

Oscilloscope: This has been used to check the acoustical output for heavy distortion before it was measured by the Audio Analyzer.

GTEM cell teseq 250V:

Is a type of electromagnetic compatibility (EMC) test chamber which has the capability to operate up to many gigahertz and is intended for radiated immunity and emissions testing. It works like a shielded TEM cell and provides - depending on the brand - quite homogenous E- and H-fields in a measurement plane perpendicular to the pointing vector.

Directional Coupler:

A directional coupler consists basically, of a 4-port network, which is also called ”bi-directional coupler”, (bi-directional means that both incident and reflected coupled power are available). The directional coupler is widely used as power monitor in microwave systems and test equipment.

The basic function of the directional coupler is to operate on an input, so that the two output signals are made available. However, when the input is applied to the opposite port of an internally terminated coupler, only one output signal is produced.

In Fig.1 below, we can see an example depiction of a simple directional coupler and how the ports connect with each other.

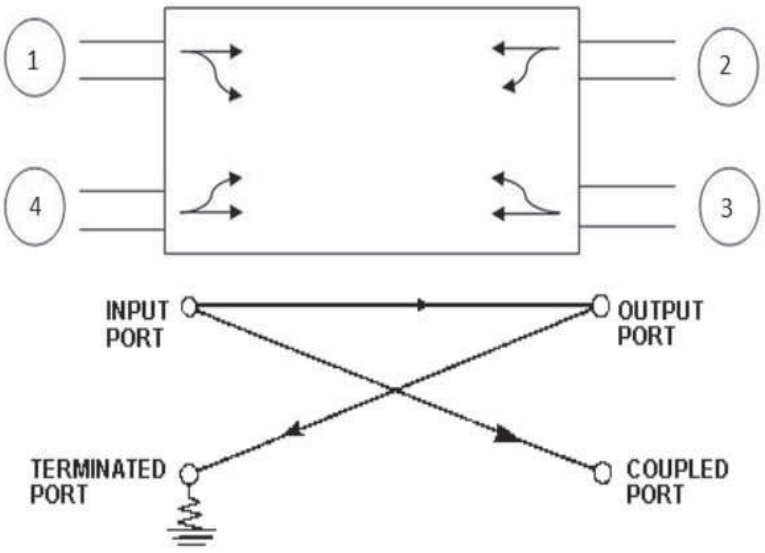


Fig.1. General structure of a Directional Coupler component.

We are using two kinds of directional coupler; one with three ports (Fairview MW MC51008-20) for low frequency (50 MHz – 1 GHz) measurements; the second with 4 ports (Fairview Microwave MC 0512-20) for high frequency (500 MHz – 6 GHz) measurements.

2.2 GTEM cell measurements

We used the GTEM cell to measure HI dummies with built-in demodulator circuit, golden unit hearing instruments and simple antennas.

IT'IS Foundation demodulator circuit for GTEM cell measurements

The demodulator circuit has been designed by IT'IS foundation and is used for special measurements with the GTEM cell. The calibration data came along with the designed model to correct the special GTEM cell measurement for the demodulator circuit. The frequency range for the calibration data was between 50 MHz – 4GHz. We aimed for 6 GHz but achieved only 4 GHz because of some design limitations of the demodulator circuit. During the GTEM cell measurement, we decreased the electrical field in the GTEM cell from 50V/m to 20V/m to be able to use the calibration data and to be in the correct RF input range of the demodulator circuit, see chapter 5.1 for more detailed information. The results of these data have been also corrected by Julstrom method, see Julstrom method section below.

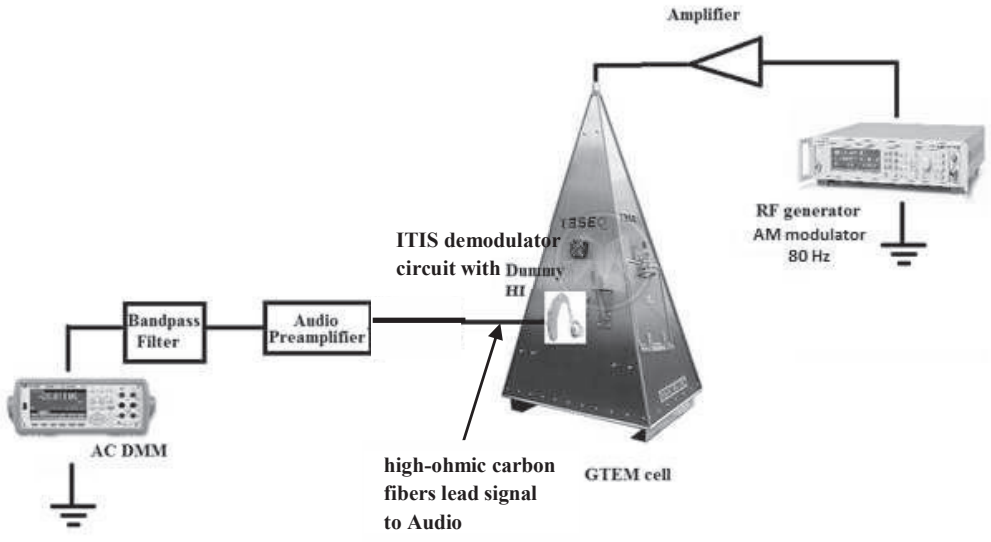


Fig.2.Measurement setup for IT'IS Foundation demodulator circuit with dummy HI

The IT'IS demodulator circuit is placed inside the dummy HI. See appendix "A. Cubicle and manipulator setup"

To measure the IT'IS Foundation demodulator circuit, AM modulated power was produced by the RF generator. The generated power is amplified before it is injected at the input of the GTEM cell. The modulation frequency of the injected power has a low value (80 Hz) so the demodulator output is not affected by the high-ohmic leads of the tested circuit. The audio preamplifier, the 80Hz-bandpass filter and the AC DMM are used to measure the demodulated signal, see Fig.2. IT'IS foundation delivered calibration tables for RF input voltage versus demodulator output voltage and for carrier frequencies from 50MHz up to 4GHz. Some post-processing in Matlab was necessary because the measurement points did not match the calibration points. For the Matlab code please refer to section "Demodulator circuit code" in the appendix.

Golden Unit HI measurements

Three Golden Unit HI were measured with the GTEM cell to test the efficiency of the Julstrom method, see Julstrom method section below.
The setup of this measurement is shown in Fig.3 and it seems to be similar to the demodulator circuit measurement, but there are important differences compared with Fig.2. The Golden Unit HI provides acoustical output while the IT'IS demodulator circuit has electrical output. This means that different equipment must be used to handle the outputs. The IT'IS demodulator circuit and audio pre-amplifier must be replaced by the measuring MIC which converts the acoustical output of the Golden Unit HI into an electrical output.

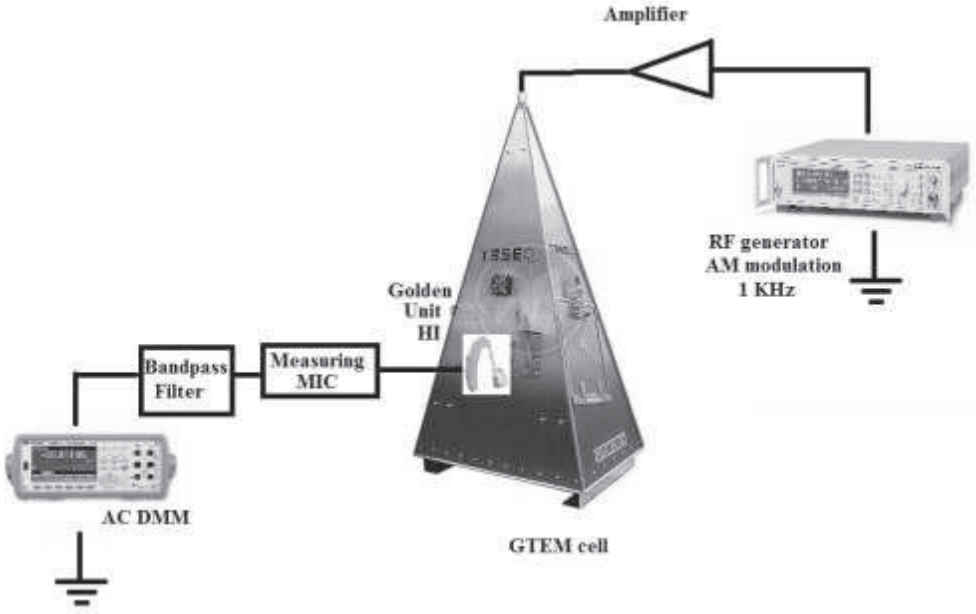


Fig.3. Setup for Golden Unit HI IRIL measurements

For more details see "A. Cubicle and manipulator setup" in appendix.

Antenna measurement

The HI PMWAs work as multiple antennas and it has not yet been possible to get accurate information about these antennas.
The purpose of these measurements is to give a rough idea about very simplified PMWAs, especially the output (or footpoint) voltage and the impedance of this artificial MWAs in form of a monopole or a L-shaped antenna. This simplification allows us to study both the output (or footpoint) voltage and the impedance of the antenna, which can then be used to model the behavior of the transferred RF signal in the electrical circuit of the test boards.

Different types monopole or L-shaped of antenna have been measured with the GTEM cell and a network analyzer. The antennas were placed perpendicular to the GTEM cell ground plane and rotated around its longer axis, see Fig.4 and Fig.5. Because of the L-shape antenna form, the measured voltage was impacted by the rotation angle. This has increased the importance of taking more than one measurement for this type of antenna to get the maximum possible power. Four measurements have been taken for L-shape antenna with four different rotation angles (0°, 90°, 180°, 270°). The S-parameter (S11, S21, S12, S22) measurement have been taken for each angle. Among the measured S-parameters, S21 (or S12)

was impacted by different orientations, therefore, the maximum power between these four measurements was considered. The monopole antenna was simply a straight rod-shaped conductor, with length of 65 mm and dimension of 1.5mm, see Fig.59, which means that there is no need to consider the maximum power of different angles.

A special setup has been used to perform the antenna measurements. The setup consisted of a metal plate with SMA-connector, where the SMA-connector was placed in the drilled hole of the metal plate. The metal plate was used as door for the GTEM cell and the SMA-connector used to connect between the measured antenna and network analyzer, see Fig.4 and Fig.5.

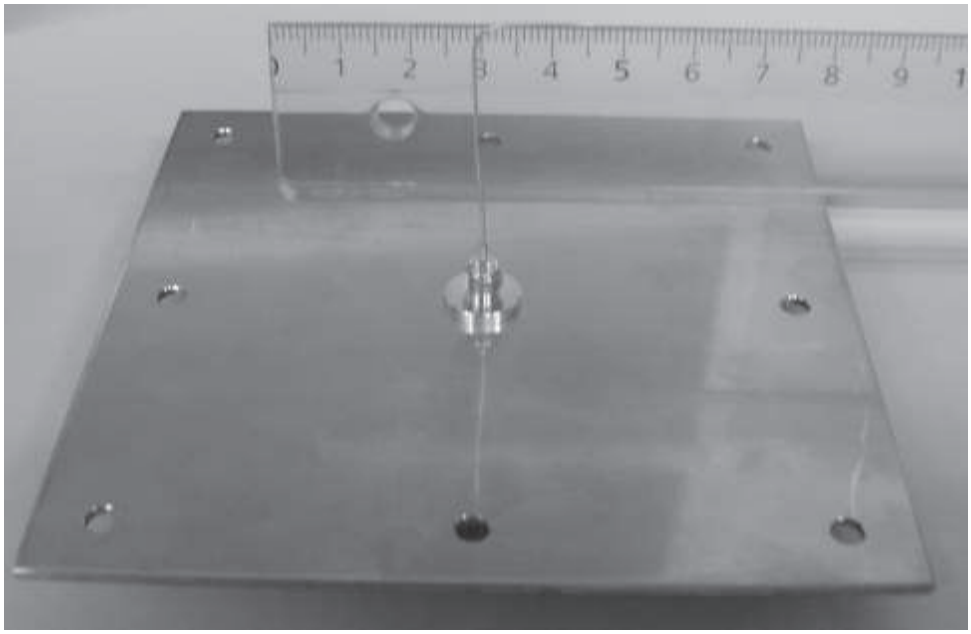


Fig.4. SMA chassis connector in metal plate

The retrieved S-parameter measurements showed the behavior of these antennas.

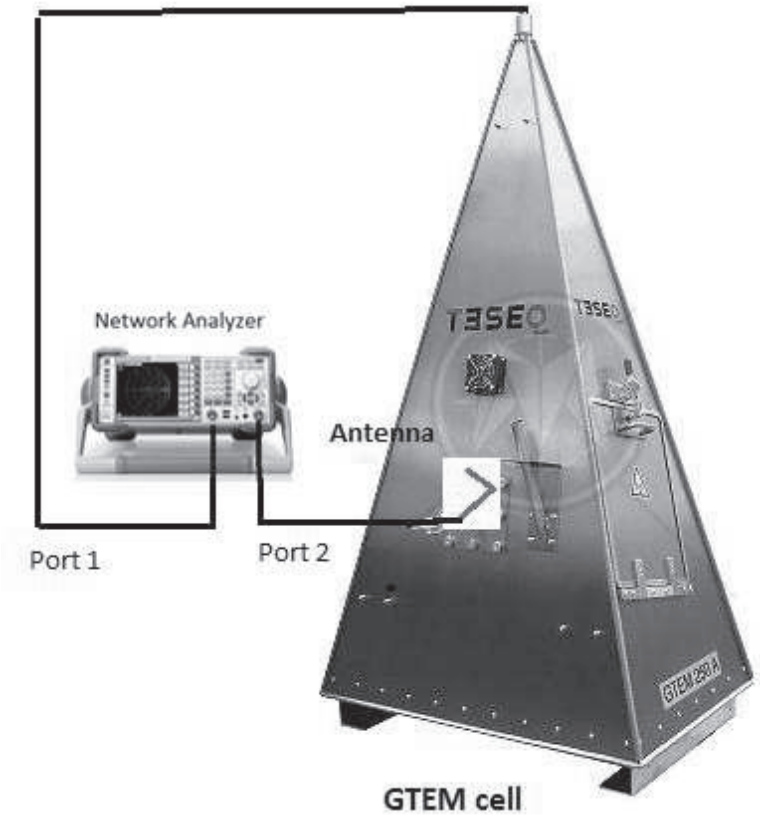


Fig.5. Monopole and L-shape antenna measurement.

Fig.5above shows the connection for measuring different types of antenna. Each antenna was placed inside the GTEM cell and connected to port 2 of the network analyzer.

The S22 parameter was useful to calculate the impedance of the measured antenna (the antenna was placed inside the GTEM cell and connected to port 2 of the network analyzer). The impedance data was used later to study its effects on a Hybrid test board electrical circuit. For more details refer to chapter 5.3.

S21 parameter was used to get the power transfer from port 1 to port 2. Furthermore calibration data for the GTEM cell (Pin vs. E-field) had to be applied. S21 was also used to calculate the data for the voltage AC source which was used in the artificial antenna circuit. For more details see chapter 5.3.

2.3 Julstrom Method

Julstrom method [2] represents a more accurate way to measure hearing aid immunity and emission [3]. The method uses a cubical container, into which the HI is placed during the measurement process. This method is particularly useful to calculate the maximum sum of the RF immunity for six different orientation measurements for each device, see Fig.6.

Compared with the common immunity measurement method used by the HI industry, where only 4 different orientations are measured to calculate the max. IRIL of the HI, this method shows superior results for most HIs.

The maximum sum formula is as follows:

$$MAX_{odd} = MAX(+X1, -X1) + MAX(+Y1, -Y1) + MAX(+Z1, -Z1) \text{ eq.1}$$

Where three mutual orthogonal orientation +X1, +Y1 and +Z1 are defined with their opposing orientation -X1, -Y1 and -Z1. The maximum between each orthogonal orientation and its opposing orientation is taken separately before they all are summed up to give the maximum sum.

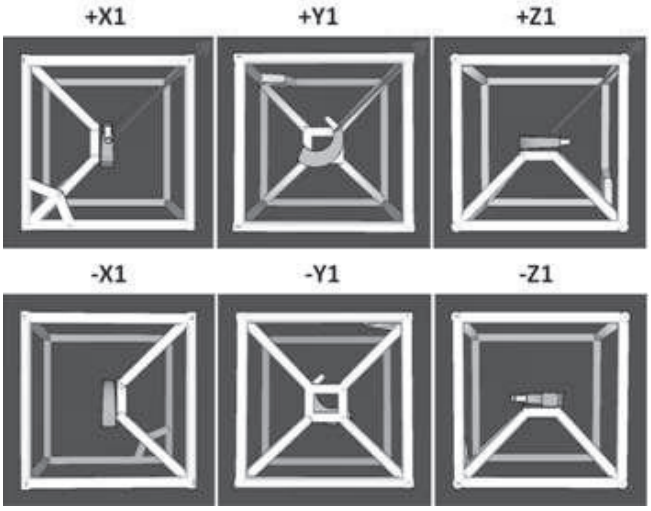


Fig.6. The 6 different orientations of the Julstrom method.

The Julstrom method was also applied for the measurements we did with IT'IS demodulator circuit together with the dummy HI but there in a different way. For more information and calculation please refer to the section "Q. Julstrom correction" in the appendix.

2.4 Integrated Circuit Specialties and Limitations

Analogue and digital audio signal processing is the main function which has to be provided by the HI integrated circuits (IC), but special features like HI immunity against microwaves and ESD protection are also required.

Special requirements like ESD protection (for HBM > 2kV) and MW low-pass filtering of MW frequencies are difficult to achieve with modern IC technologies (like CMOS 32nm). These IC technologies are preferably used for digital signal processing, but not for analog signals with frequencies beyond hundreds of MHz. In order to fulfill RF requirements special and highly expensive IC design solutions with an “unsuitable” IC technology are requested. In most cases such IC design solutions consume a lot of expensive chip area and occasionally, they are not feasible because of severe limitations. In many cases it is difficult to get a good “low-ohmic” connection between the “RF reference ground plane” of the PCB and the IC GND rails even if you apply special IC mounting and packaging technologies.

The IO-pads of modern IC technologies have the drawback of contributing to EMI if RF power is injected. The ESD protection diodes of the IO-pads get into the conductive mode and start to demodulate the RF signal. Please see section "ESD diodes" in the appendix to get a better idea about such parasitic demodulator circuits.

Large pn- or np-diffusion capacitors are another specialty of any CMOS IC technology. Their capacitance is largely dependent on the DC-voltage. We have such a capacitor at the output of the MW filter of the audio signal processing IC (ASPIC), see Fig.29. In spite of capacitance changes due to different DC voltages (caused by the parasitic demodulation of ESD protection diodes), we do not expect a large impact on the RF voltage transfer from the IO-pad up to the input of the MW filter. The capacitance value change is almost “isolated” by the MW filter resistor (180 Ohm in series) from the input pad circuit and the remaining RLC-parasitic circuit on the ASPIC and the Hybrid PCB.

The acoustical interference output from the measured test boards is called ORIL (output related interference level). When we relate the interference to the HI input we call it IRIL (input related interference level). The input and output can be related with the acoustical gain of the test board.

The formula can be described as follows.

$$ORIL\ [dB_SPL] = IRIL\ [dB_SPL] + gain\ [dB]$$

IRIL is the principle information of interest. The ORIL is acoustically measured at the output of the test boards, see chapter 3, DPI measurements.

The gain measurement were done by the Electroacoustics department at Sonova, see Fig.8. They did different types of input and output measurements (acoustical/acoustical) and (electrical/acoustical) with purely sinusoidal signals in the audio frequency band. An example measurement is given in the figure below.

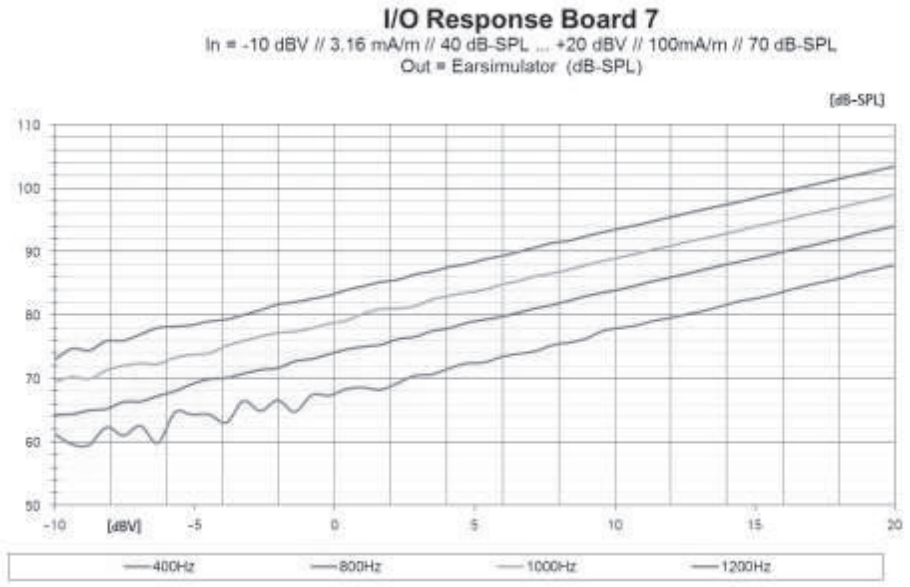


Fig.7. Magnetic-acoustical T-coil gain measurement for test board 7

Note: The Tcoil was connected between TCOILN and TCOILP. An input of +20dBV corresponds to H = 100 mA/m (or equivalent to 70 dB-SPL input).

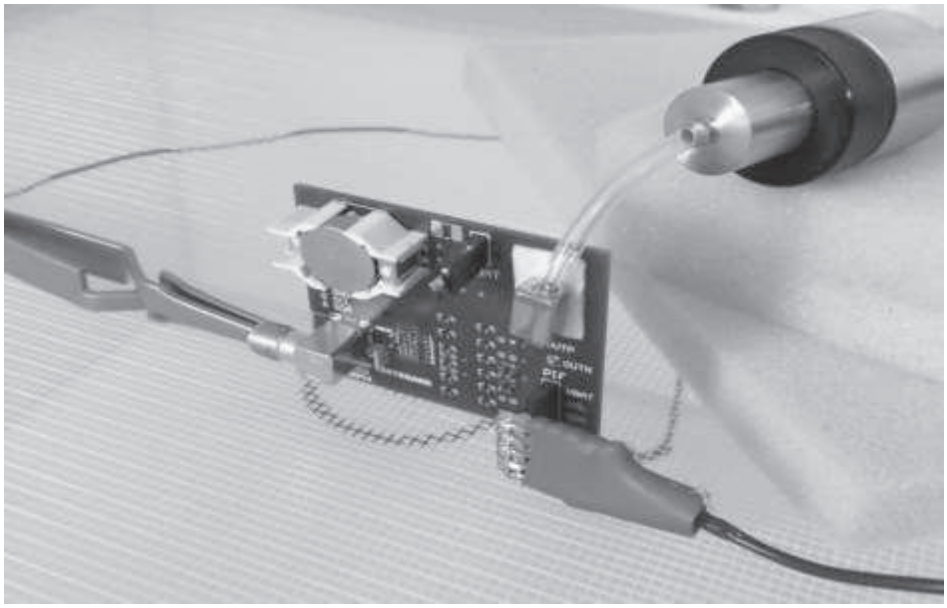


Fig.8. The setup of Magnetic-Acoustical gain measurement with Tcoil

3. Direct Power injection (DPI)

DPI is a widespread technique to measure the immunity of an integrated circuit. The method is explained in the standard IEC 62132-4 [9]. [1]
The amplitude modulated (AM) signal recommended by the standard is 1 kHz with modulation index of 80%. We used the same modulation index in our setup, but a different modulation frequency (400 Hz).

DPI is mainly used by the automotive industry to analyze the RF or microwave (MW) immunity of integrated circuits, the integrated circuit is shown as Device Under Test (DUT) in the Fig.9 below. In our case, we tried to use this method with active electronic HI components, which are made up from both the surrounding electronic circuit (mainly passive RLC components used for supply and biasing of the IC) and the IC itself (represented as DUT in Fig.9).

Looking at the test PCB of Fig. 7 it is clear it cannot be avoided that a certain amount of RF power is dissipated elsewhere in the surrounding electronic circuit but not in the IC itself. Furthermore, even if the IC is a miniaturized circuit it cannot be guaranteed that the main part of the RF power is dissipated (or used for electronics malfunctions) exactly at the IC location where we would like to have it (e.g. at the input of a low-noise amplifier).

DPI can successfully be used to stress the IC with RF or MW power in a "global" manner, but not to disturb a distinct node deep inside the IC in a well-defined way.

Ideally, when you know the internal RLC parasitic elements inside the IC, you can estimate or simulate the RF voltage at a distinct location inside the IC. (The magnitude of RF or MW power you inject there is then of less importance.)

Despite this fact we decided to continue with DPI because we simply did not have a better solution when we started the investigation.
As a future idea, we found that it might be sufficient to apply the RF voltage directly to the IC pad without considering which part of the RF or MW power is reflected at the IC pin and which part of the power is finally transferred to the IC location we want to disturb. For us, it is sufficient to know the RF voltage transfer from the entry port (e.g. the Microphone of Hybrid pads) to the location on the IC where the demodulation is expected. Going this way means, however, that you have to know all RLC parasitic elements of the test board, the Hybrid (or

[1] IEC (International Electrotechnical Commission) is an organization that prepares and publishes international standards for electrical, electronics and related technologies.

Microphone) PCB and inside the IC as well. Read more about that in chapter 6 (Future Work).

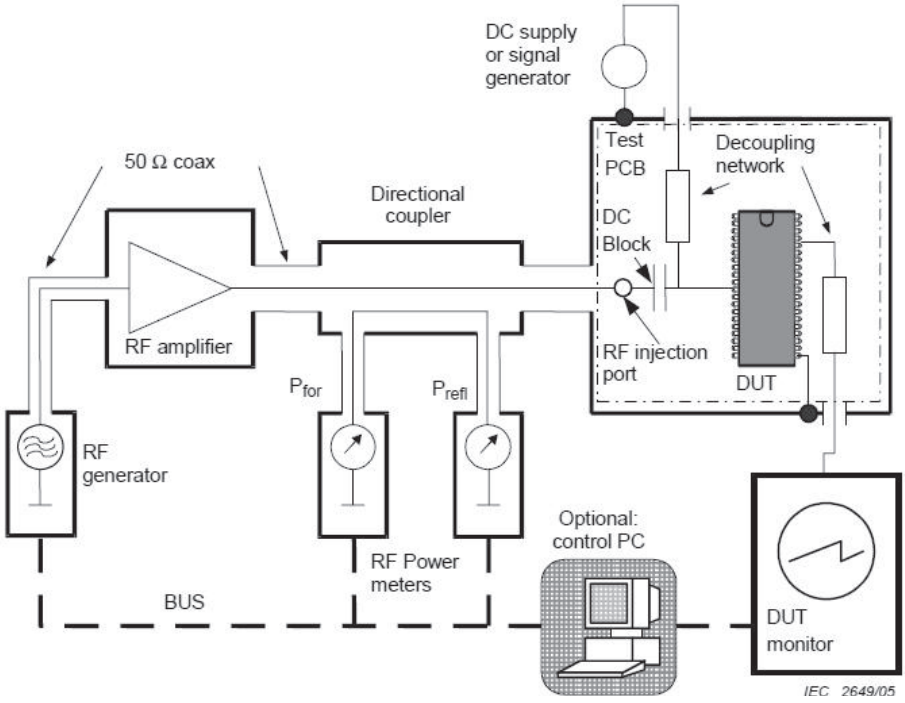


Fig.9. Original setup of DPI measurement.

The setup in Fig.9 above is used in the automotive industry to test the RF power immunity of Integrated Circuits. The figure is retrieved from the IEC standard [9].

The essential parts in the setup of the DPI measurements are the RF power generator, amplifier, power meter, Device Under Test (DUT), DUT monitor (or Audio analyzer in our case) and a computer to control all this equipment, see Fig.8 andFig.9.

Describing the measurement flow of the standard DPI measurement, seeFig.9 above. The measurement starts by producing power from the RF generator. The power is amplified before it continues to the directional coupler. The directional coupler, see directional coupler section in Background provides the possibility of measuring the forwarded and reflected power. This information is used to control the next generated power. Whenever the program finds the suitable injected power, the iteration stops and the power is injected directly to the DUT. The DUT

is a device which works with DC power and to stop any DC disturbance that can be caused by the injected power, a DC coupler capacitor has been added in the input port of the DUT. In the end, the output is to read at the DUT monitor.

In our DPI setup, we did not need to use the amplifier and an audio analyzer has been used as a DUT monitor.

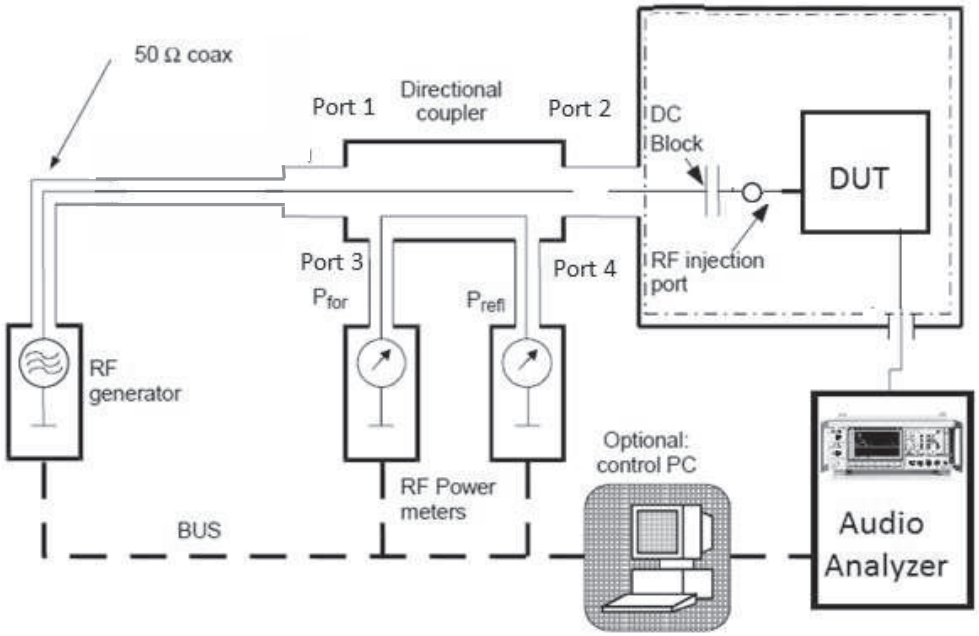


Fig.10. DPI measurement setup for active electronic HI component.

We tried two ways to implement the DPI measurements.

Briefly, the main difference between the 2 methods is how we consider the reflected power. The first method (computed power loss by using S11 parameter (program 2)) measures the reflection using insertion loss parameter (S11); while the second method (measuring reflected power method, program 3) measures the reflected power by using an extra power meter sensor on port 4, see Fig. 5.

3.1 Computed power loss using S11 parameter (program 2)

We relied on the measured S11-parameter by first using a network analyzer to calculate the transmitted power. Depending on the used formulas, the program corrected the injected power to get the proper transferred power.

The formulas to perform the calculation were found in [7].

Besides the formulas we needed to correct some other losses; RF cables, connectors, the directional coupler transmission loss $|S_{21}|$ and the DC blocking capacitor (Agilent 11742A).

Correction of the Injected RF Power:

According to (eq. 1) in [7] we get:

$$P_{tran} = (1 - |S_{11}|^2) * P_{inc} \qquad \text{Equation 2}$$

with

P_{tran}: transferred power to the Hybrid/microphone pad;
P_{inc}: incident power at the SMA input connector of the directional coupler;
S_{11}-parameter: measured at SMA connector (J1; female) of the directional coupler. The directional coupler is connected (J2) in series with the DC blocking capacitor (Agilent 11742A) and with an SMA connector on the test board.
$|S_{11}|$ is identical with the magnitude of the reflection coefficient

$$\rho = \frac{|Z_L - Z_0|}{|Z_L + Z_0|} = \left|\frac{V_{reflected}}{V_{forward}}\right|$$

Equation (2) can be rewritten as $P_{tran} = C_1$ (constant) . So, we get

$$P_{inc} = \frac{P_{tran}}{(1 - |S_{11}|^2)} \qquad \text{Equation 2A}$$

or with log units:

$$p_{inc}\ [\text{dBm}] = p_{tran}\ [\text{dBm}] - 10 * \text{LOG}_{10}(1 - |S_{11}|^2)$$

$$p_{inc}\ [\text{dBm}] = p_{tran}\ [\text{dBm}] - 10 * \text{LOG}_{10}(1 - 10^{(s11\ [\text{dB}]\ /\ 10)}) \qquad \text{Equation 3B}$$

Example: Based on a s11-measurement we plotted (p_{inc} [dBm] - p_{tran} [dBm]) and (p_{refl} [dBm] - p_{tran} [dBm])

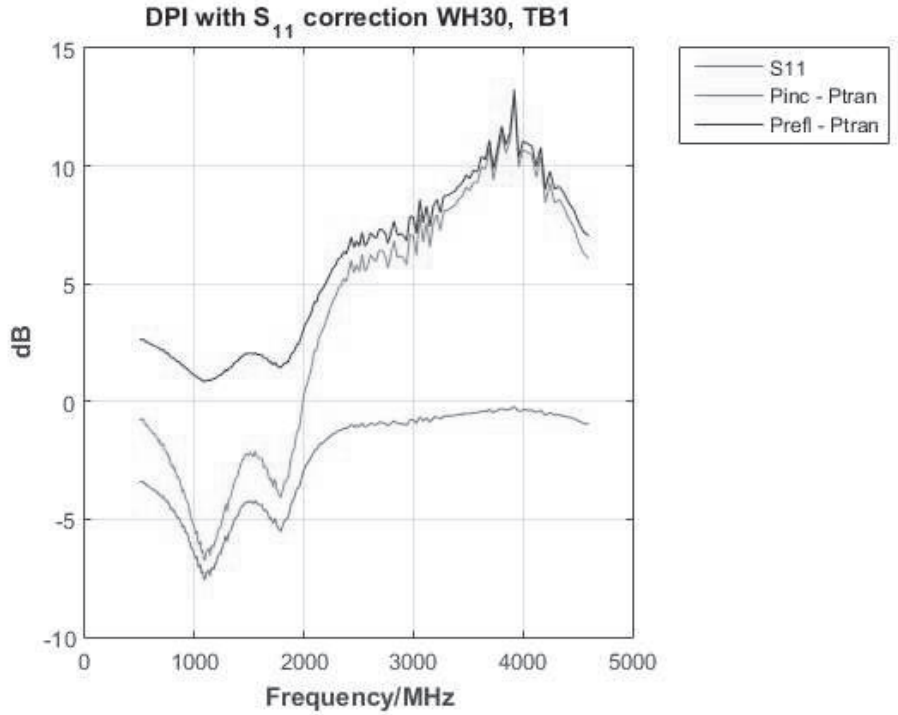


Fig.11.Example of relation between S11 parameter, incident, reflected and transmitted power.

As mentioned before, in this implementation method, the DPI measurement depends mainly on using the measured S11-parameter to calculate the transmitted power to the DUT. Therefore, it is reasonable that the incident and reflected power will follow a similar curve structure as the S11-parameter. From Fig.11 above, it is clear that when S11 values come close to 0 dB the incident and reflected power get very high.

Program 2: This program depends mainly on calculating the coupler power of the incident signal (P_3), which is compared later on with the measured (P_3) using the power meter, there are four parameters needed to do this calculation, see the formula below:

$$P_3[\mathrm{dBm}] = \mathrm{P_{transmitted}} - 10 * \mathrm{LOG}\left(1 - 10^{\frac{S_{11}[\mathrm{dB}]}{10}}\right) + C_{31} - C_{21} \qquad \text{Eq.4}$$

Where (P_3) is the coupler power of the incident signal, ($P_{transmitted}$) the transmitted power, (s_{11}) is s-parameter magnitude (dB) and (C_{31}) is the coupling factor between port 1 and 3, (C_{21}) is coupler loss between port 1 and 2. (All variables in the upper equation are given in dB and/or dBm).

The reflection of the power toward the source occurs mainly because of the impedance mismatch, therefore a good knowledge of the impedances inside the test board, could help to estimate the amount of the power reflection that happens at a certain frequency. In this program, the S11-parameter is measured using a network analyzer and smoothed later on by using Matlab. The S11-parameter represents the impedance of the test board, which is used to estimate the transmitted power, using the previous formula Eq.2:

$$P_{transmitted} = (1 - |S_{11}|^2) * P_{inc}$$

(All variables in the upper equation are in linear scale).

The calculated (P_3) is treated as an ideal value. The program will stay in a loop till the measured (P_3) become close enough the calculated (P_3) value.

3.2 Computed reflected power method (Program 3):

With this measurement we used the same setup as in the IEC 62132-4, ed1.0 [3] standard. Program 3, is a very general method, which depends on calculating the transmitted power, which is the main parameter in this program. The program uses this parameter as reference for its calculation. The transmitted power (P_{trans}) is simply the difference between the incident ((P_{inc}) and reflected power (P_{ref}). P_{trans} is the power which is absorbed by the test board.

The transmitted power was calculated by this formula:

$$P_{trans} = P_{inc} - P_{ref} \qquad \text{Equation 5}$$

(All variables in the upper equation are given in linear scale).

Incident power (P_{inc}): Three parameters are needed to calculate this. The first one is the coupled power of the incident signal (port3), see Fig.10, which is measured by the power sensor B (of the power meter). The second is the coupling factor between ports 1 and 3 of the directional coupler and the third parameter is the coupler loss between port 1 and 2.

$$P_{inc} = P_3 - C_{31} + C_{21} \qquad \text{Equation 6}$$

Where (P_{inc}) is the incident power, (P_3) is coupled power of the incident signal,(C_{31}) is coupling factor between ports 1 and 3, (C_{21}) is coupler loss between ports 1 and 2. All variables in the upper equation are given in dB and/or dBm.

Reflected power (P_{ref}): It is the power that is reflected back from the test board. Two parameters are needed to calculate it, the first one is coupled power of the reflected signal (port4), which is measured by the sensor A of the power meter, and the second one is the coupling factor between 2 and 4.

$$P_{ref} = P_4 - C_{42} \qquad \text{Equation 7}$$

Where (P_{ref}) is the reflected power, (P_4)is the coupled power of the reflected signal and (C_{42}) is the coupling factor between port 2 and 4. (All variables in the upper equation are given in dB and/or dBm).

The transmitted power is used to regulate the coupler input power, which will be declared in the signal generator part. The program stays in the loop till the wanted transmitted power is reached. After that, the program retrieves the magnitudes of the audio harmonics from the audio analyzer and saves them in a file. The file location should be defined before starting the program.

We did not use Program 3 because of some artifact. See appendix (Side effect of measuring reflected power, Program 3) to get more information about the problem we had with this DPI method.

3.3 Measurements for computed power loss using S11 parameter:

In our study we used 10 test boards, 5 of them were used with Hybrids and the rest were HI microphones. DPI measurements have been applied for each test board with six different power levels. The RF powers we used in our measurements were [-18, -12, -6, -4, -2, 0] dBm.
From these levels, we chose the DPI measurement of -6 dBm RF amplitude to be the input in our simulated model with LTSPICE. In this case the RF output of our simulated circuit will be compared with the acoustical output of our -6 dBm DPI measurements.

As the previously mentioned program 2 depends mainly on the measured S11 parameter to regulate the transmitted power to the DUT. The Fig.12 below gives

an idea about the reflection coefficient S11 parameter that has been measured for five Hybrid MIC1 connection test boards.

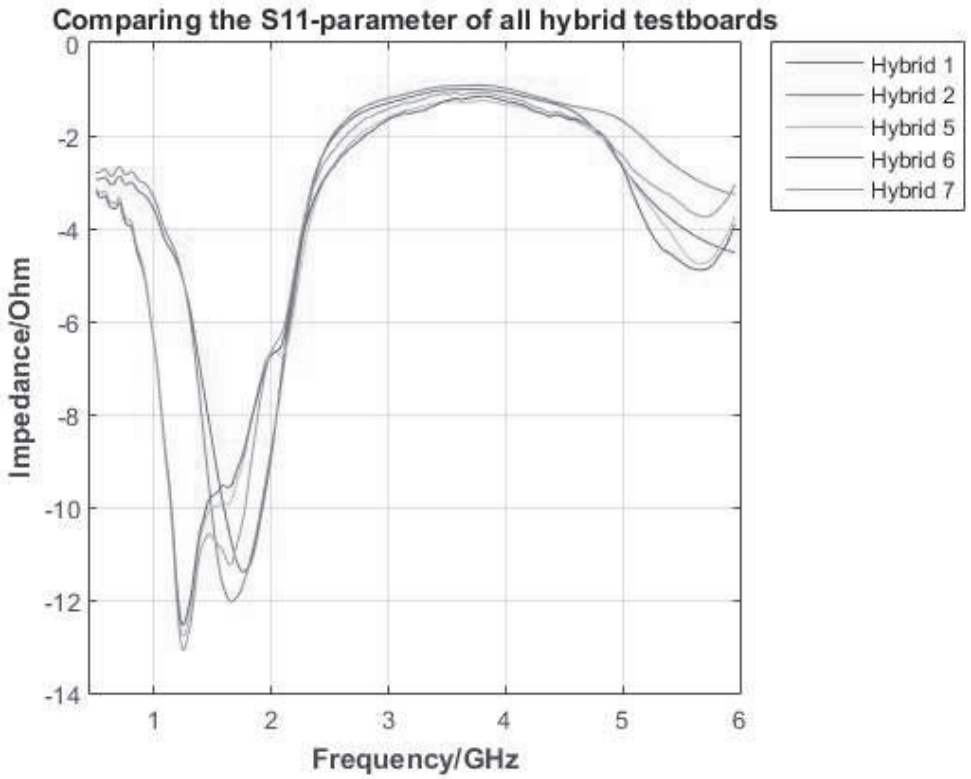


Fig.12. Comparing the S11-parameter measurement for all test boards with Hybrid MIC1 connection.

This and other measured data for S11 will be used to adjust the transmitted power in the figures that follows:

All the measurements that follow here were taken by using program 2.
The limitations we had with our directional couplers made us divide the DPI measurement for each power level into two frequency ranges which we named as low and high frequency DPI measurement.
The first frequency range is 50 MHz - 1GHz; the second frequency range is between 500 MHz - 6 GHz.
These two measurements overlap in the frequency range between 500 MHz - 1 GHz, as we can see from the double curves within the mentioned frequency range in all the DPI measurements below.

The benefit of the overlapping frequency range 500 MHz - 1 GHz is to show if the measurement that were taken by the two types of directional couplers are close to each other or not. As you can see in all the figures below, there is a good match in this frequency range but we have also some artifact measurements, for example in Fig.13, the first harmonic of the low frequency curve for 0dBm transmitted power show high decrease in its power at some points. These huge decreases at some points can be related to the ESD protection diodes in the integrated circuit of the Hybrid which start to conduct at high injected power (0dBm), see ESD protection diode in the appendix.

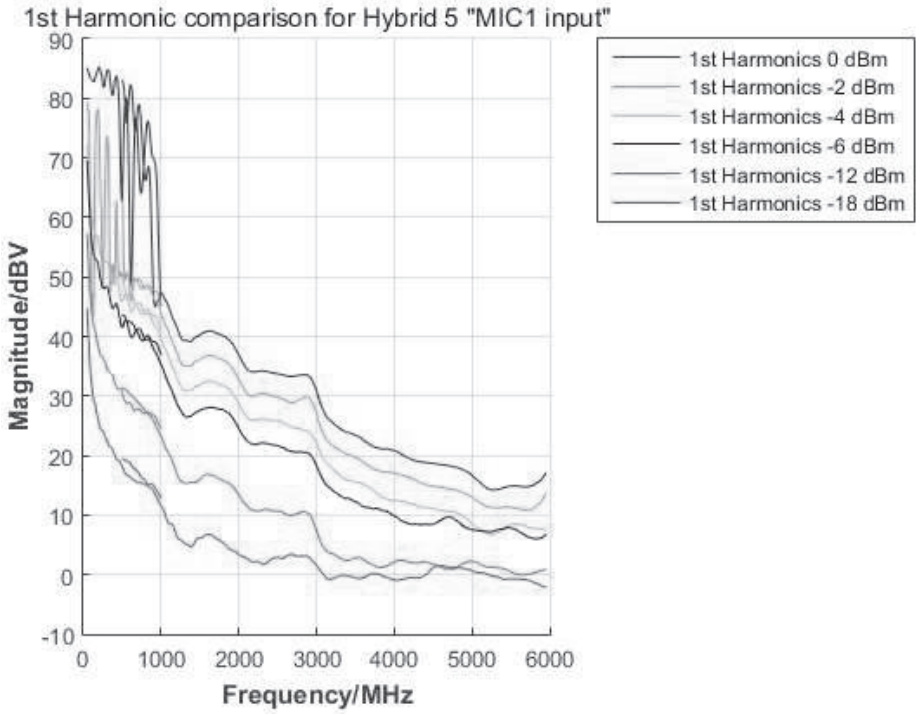


Fig.13. First harmonic output for changing RF power at Hybrid MIC1 input.

The output acoustical behavior of the microphone test board is shown inFig.14. As you can see we can be below the noise floor at the frequency range between 2-6 GHz, Depending on the injected power, it is possible that we get another behavior at this frequency range e.g. if we inject a much higher power, e.g. +12 dBm, but then the ESD protection diodes on the ASPIC start to conduct.

It is important to consider that in case IRIL < 10 dB-SPL the measurement is always impacted by the noise floor of the setup (mainly by the LNA on the ASPIC of the Hybrid or the PMOST on the microphone IC).

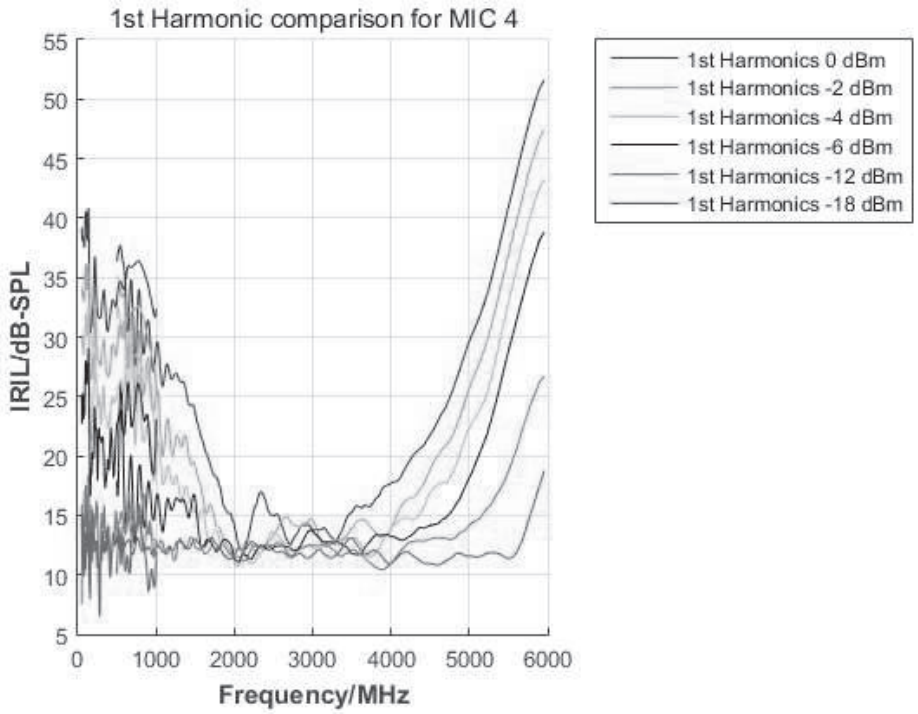


Fig.14. First harmonic output for changing RF power at Microphone input

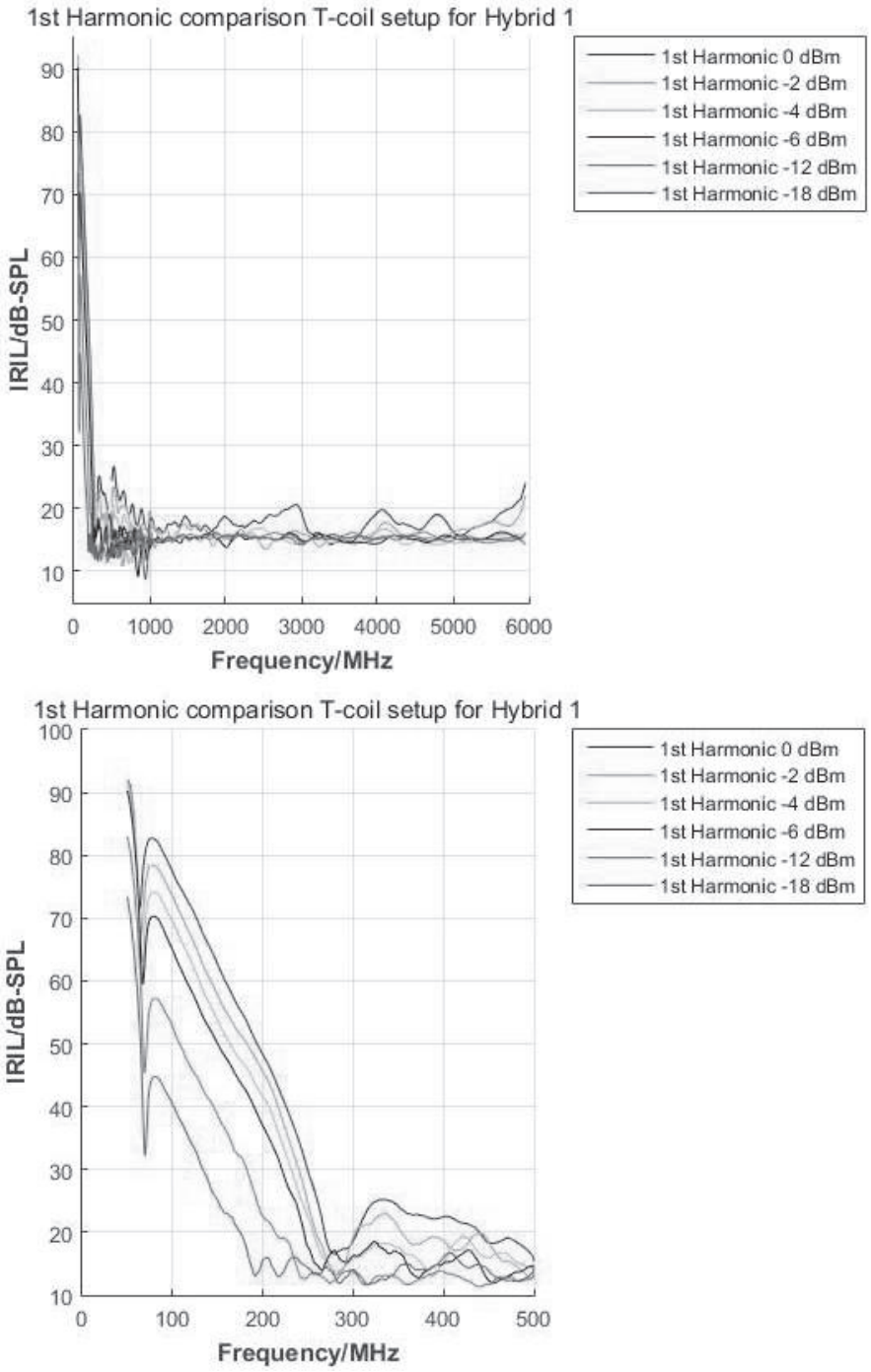


Fig.15. First harmonic output for changing RF power at Hybrid TCOILN&P input.

The acoustical behavior of the T-coil setup can be seen in Fig.15. For frequencies beyond 300 MHz we are close to the noise floor which does not bring any information. We added a second plot which it is similar to the first plot, but with a smaller frequency range for a better insight.

Examples of the first four harmonic measurements with the 3 test board setups "Hybrid MIC1 Input (ASPIC on Hybrid)", "Microphone (65JF62)" and "Hybrid TCOILN&P Input (ASPIC on Hybrid)" with input power -6dBm are given in Fig.16, Fig.17and Fig.18. The purpose of measuring the second, third and fourth harmonics is to detect strong distortion in the output signal. From the measurements we get a difference of > 8 dB between the 1st and the 2nd harmonic and > 6 dB between the 2nd and the 3rd harmonic (as long as the voltages of the 1st, 2nd and 3rd harmonic are not too close to the noise floor).

In theory you should get around 14 dB between the 1st and the 2nd harmonic for an ideal squarer used as demodulator. For more details about the max. difference between the harmonics please refer to [11].

Based on the measurement results for the harmonics we can conclude that

- our demodulators inside the ASPIC distort quite a lot.
- we should be careful with the result of the 1st harmonic if the dB-margins to the 2nd and 3rd harmonic decrease more than the figures given above.

The vertical axis of the first harmonic in Fig.13 is plotted in dBV(electrical output),whereas the acoustical output related to the input (IRIL) of the first harmonic is shown in Fig.14 and Fig.15

The IRIL values may only be used and referred to the first harmonic of the demodulated signal.

The noise floor for the figures, which are plotted in dBV, is around -85 … 80 dBV

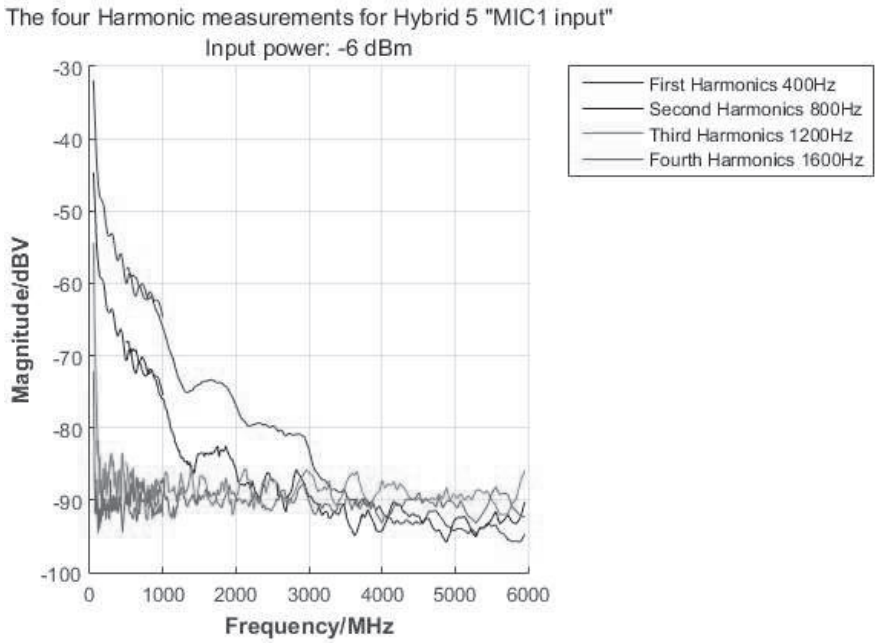


Fig.16.The first four harmonics for Hybrid 5 MIC1

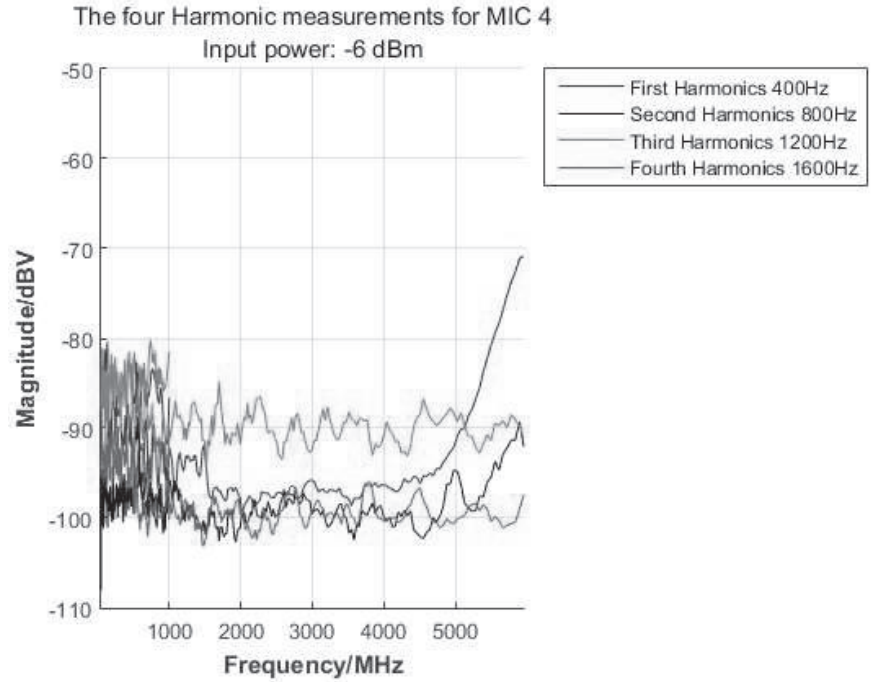


Fig.17.The first four harmonics for microphone 4 test board

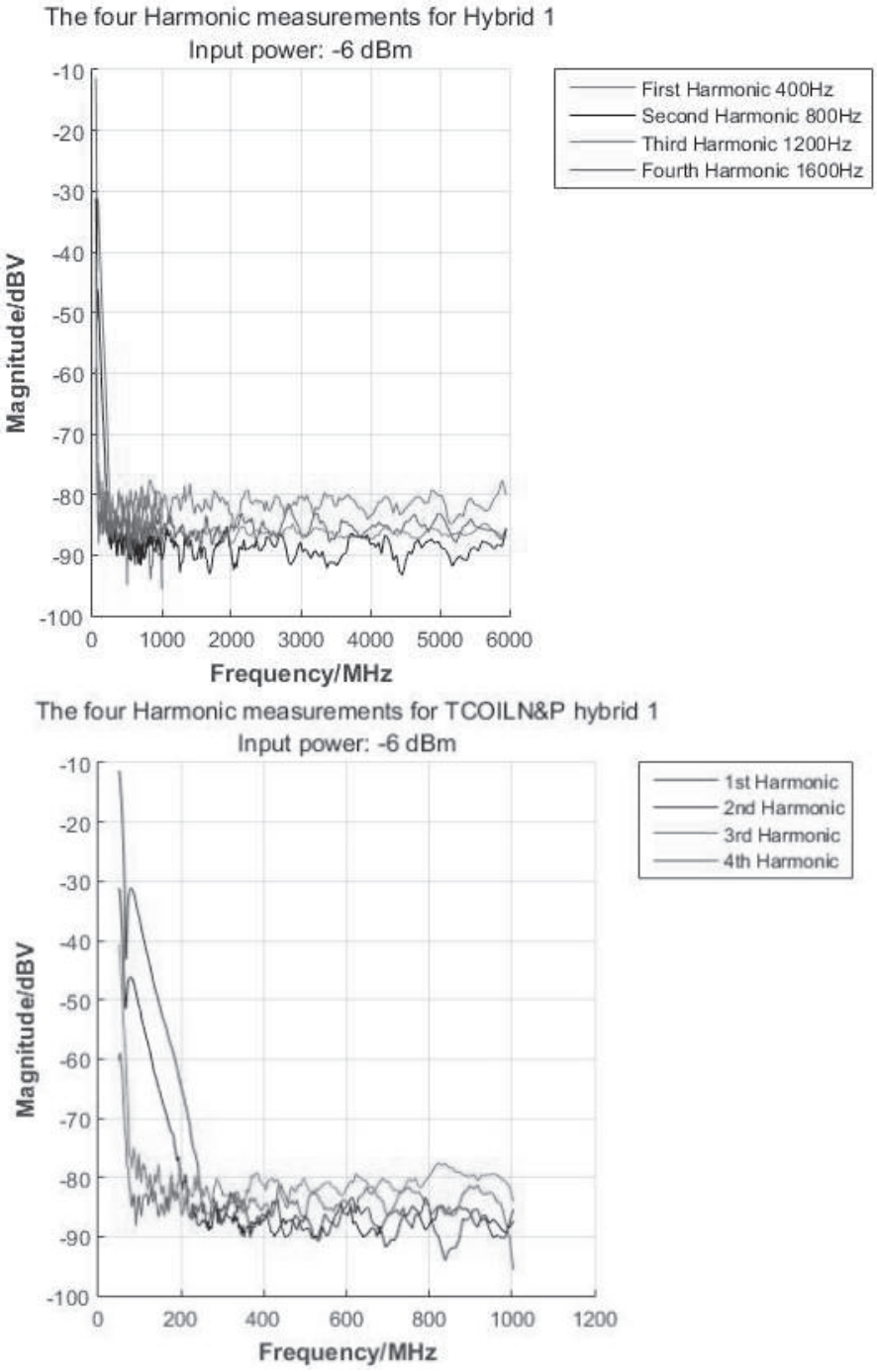


Fig.18. The first four harmonics for TCOILN&P Hybrid 1 test board.

Based on the results of Fig.13 - Fig.15 we may assume that the demodulator behavior of the LNAs inside the ASPIC and the PMOST in the microphone IC is quite close to the demodulator model roughly approximated by the equation $y = k_0(f) * x^2$ (with y: demodulated output voltage; x: RF input voltage; $k_0(f)$: frequency dependent demodulator constant). This approximation is valid as long as the RF input voltage does not turn on any ESD protection diodes - or in case of a too low RF input voltage - small demodulated output is not disturbed (hidden) by the noise floor of the measurement system.

4. Modeling of the Circuits

We mentioned in the introduction that we want to study two main parts of the HI. The studied parts are the HI Microphone and Hybrid.

The Hybrid consists of tiny and folded PCB (flexprint) with an analog/digital signal processing IC (ASPIC), a transceiver IC and a non-volatile memory IC. Beside these 3 ICs there are a few capacitors used for different chip-internal power supplies. All different functions and connections of the Hybrid are accessible via 23 pads. Among the important functions of the Hybrid are the microphone and telecoil audio channels. After some firmware configuration for the Hybrid, both audio channels are accessible via the input pads MIC1 and TCOILN&P and the output pads OUTN/OUTP. The signals of the latter pads are connected to a HI loudspeaker which outputs the acoustical signal.

The microphone is in a tiny metal case and converts the received acoustical signal to an electrical signal. During the study we analyzed only the 2-wire type 65JF62 from sonion. The microphone has to be powered with a DC current of about 8uA. The DC current is delivered by a current source on the ASPIC (of the Hybrid).

As it can be seen from Fig.35 the Hybrid was “RF-isolated” by ferrite beads from the remaining test board circuitry. The RF power was injected via a very short wire at the Hybrid pad MIC1 (or TCOILP or TCOILN). AGND of the Hybrid was also connected via a very short wire to RF-GND of the test board.
Fig.31 shows the test board for the microphone. Here the microphone was “RF-isolated” from the Hybrid by ferrite beads. The RF power was injected via a very short wire at the microphone pad MIC. AGND of the microphone was connected to RF-GND of the test board.

When using the telecoil channel a distinct telecoil type was soldered between the 2 Hybrid pads TCOILN and TCOILP. The RF power was then injected at TCOILN. AGND of the Hybrid was connected to RF-GND of the test board. Fig. 42shows the wire connections, the mounted telecoil.

We used the same strategy to model all the electrical circuits of our test boards. The steps are explained as follows:

1- For an accurate impedance (or S11-parameter) measurement, we calibrated our network analyzer in a way that it was close to our DPI measurement setup. See appendix Network Analyzer Calibration.
2- Measure the S11-parameter. It can be used later to perform the DPI measurement, as explained in chapter 3 above.
3- Perform the DPI measurements and plot the acoustical output.
4- Design the equivalent electrical circuit for each model. Each model had a design in LTSPICE and a similar model in AWR software programs, see Fig.29, Fig.37 and
5- Fig.47. The frequency range which we wanted to study was between 50 MHz – 6 GHz which was quite large. To get smaller errors in the electrical model it was necessary to split the frequency range into three smaller parts. In the end, we decided to have a separate model for each of the 3 frequency ranges which have been the following: 50 MHz – 1 GHz, 1 GHz – 3 GHz and 3 GHz – 6 GHz[2].
6- Use the same calibration setup mentioned in point 1 above to get impedance magnitude and phase measurements. (It is also possible to convert from the S-parameter measurements to impedance using conversion formulas, see appendix S-parameter to Impedance conversion.) The impedance magnitude and phase were used to match the behaviors of the simulated electrical circuit and DPI measurement curves. Based on a hypothetical circuit topology we first created an AWR model for the relevant test board connection, where an optimizer adjusted the variable components on the circuit until we got the correct impedance magnitude and phase behavior. We needed to build the same circuit in LTSPICE, where we used the same component values which had been calculated by AWR. The corrected model was used to study the transferred RF signal.

[2]Overlapping frequency ranges might bring eventually more accuracy during the impedance or s11 parameter fitting process.

7- An equivalent voltage source for the simulated models was needed at the circuit input. We had to create a special voltage source for our electrical model. It was derived from the input power data used during the DPI measurements. This point was important to get a more accurate match between the simulated and measured models.
We performed the DPI measurement with different transferred power levels. The transferred power levels we investigated were (-18, -12, -6, -4, -2, 0) dBm. Among these measurements, we chose the -6 dBm amplitude data for the DPI voltage AC source. See appendix DPI voltage source.

It was important to create some individual circuits of certain components and connections inside the test boards, for example the ferrite beads, the telecoil and the wire interconnections (e.g. AGND to RF-GND).

The Hybrid flexprint (PCB part with ASPIC and pad area flap) was modeled and simulated by J. Abadia (PHONAK Comm. Murten) with CST MW[3], a 3D-EM modeling and simulation tool. The interconnections from the solder bump pad to the real pads on the ASP IC were estimated by A. Tombeur (nxp)[4].
Because of the lack of data for the sonion microphone we had to estimate the PCB interconnections and their RLC-parasitics by ourselves. We based it on a functional schematic of the microphone and looked at the PCB of an opened microphone. See appendix for more detailed information about input circuit of microphone.

After applying all these steps, the electrical model for the transferred RF signal (or voltage) was ready to be compared with the DPI measurements.

4.1 Matching parameters

There are four parameters which can be used to match between the test boards and the equivalent electrical circuit. The possible parameters are the magnitude and phase of the complex impedance and the magnitude and phase of the complex S11-parameter.

In the beginning of the thesis, we recognized that it will be difficult to match the circuits manually because of the complexity of these circuits. Therefore, it was more convenient to create a program which optimized the circuit. However we could not get convincing results from only matching the impedance magnitude,

[3]Sonova cannot unveil more details here because of reasons of confidentiality.
[4]Here too, Sonova cannot unveil more details because of a non-disclosure agreement with nxp.

therefore we tried to match the phase too. For this matching of the complex impedance or S11-parameter we used Microwave office software. AWR provided a free student demo version.

Some parts of the test board circuit consist of special EMI suppressing components (like a ferrite bead). The RLC-values (of the lumped elements) of these EMI components were constant and did not contribute during the matching process. However, the number of lumped elements with constant RLC-values was quite large compared to those with variable values,. This limited the matching accuracy using Microwave office. An example is given in

Fig.47 which shows the TCOILN&P electrical circuit. In total we have 85 RLC-values for the hypothetical RLC circuit, but we can adjust only 10 RLC-values in Microwave office to match the circuit. Another part, which we can adjust and eventually match well, is e.g. the wire from Hybrid AGND to the RF-GND of the test board.
Other examples: The total number of RLC-values in the microphone test board circuit is 70 and the number of possible variables which can be adjusted by Microwave office are 20, see Fig.29.For the Hybrid MIC1 connection the total number of components are 41 and the number of the adjusted component are 11. Because of the restricted number of variable components, we could not create hypothetical RLC circuit models which match the 4 parameters (impedance (magnitude and phase) and S11-parameter (magnitude and phase)) well in each frequency range.

We could maximally match three parameters which is the impedance magnitude and phase with S11-parameter magnitude. At the same time, we also recognized that increasing the number of the matched parameters will not help us to get a better behavior, as we can see in the following examples where it was sufficient to match only the impedance magnitude and phase.

Fig.19 shows different matching circumstances. All these curves show the RF voltage drop over the last branch in the microphone integrated circuit, which we need to investigate. The first legend item “Impedance mag” in Fig.19 has been derived from a model which considered the impedance magnitude as the only matching parameter. The second legend item “Imp (mag + phase)” is the result of both impedance magnitude and phase matching. The third legend item “Imp (m+p) & S11(m)” is given by matching the impedance magnitude and phase, as well as the S11-parameter magnitude. The third legend item“S11 magnitude” uses the S11-parameter magnitude and phase match.

A comparison of all these four curves in Fig.19 with the first harmonic DPI measurement of the microphone with -6 dBm injected power can be found in Fig.17. We compared only the curve which represents the first harmonic with -6 dBm transferred power. We can observe that the best agreement is given by matching the impedance magnitude and phase.
Notice that the DPI measurements cover the frequency range between 50 MHz – 6 GHz, while the simulated model covers only the frequency range between 3 GHz – 6 GHz.

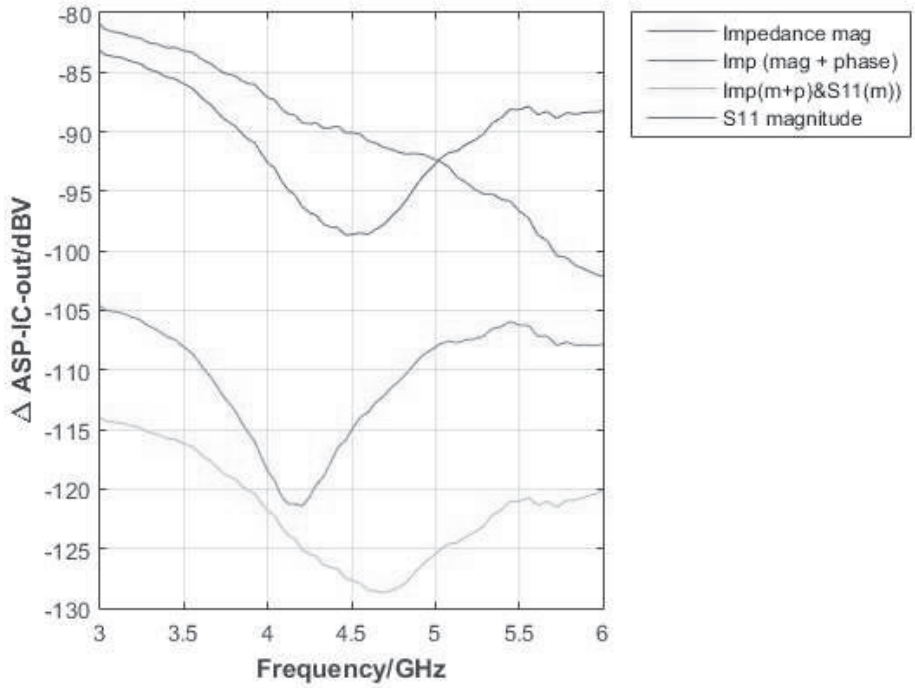


Fig.19. The RF signal of the microphone IC output.

The vertical axis of Fig.19 is defined as ΔASP-IC-out which represents the last branch in the microphone integrated circuit.

For the other circuit models, we matched only the impedance magnitude and phase. Comparing the best matched approach of the electrical circuit with the DPI measurement that we see that we are still away from a perfect solution. Check next section (Strange matching) to get an idea about how close we are. There could be

many reasons forthis mismatch.The most realistic one is that our microphone test board model for this frequency range (3 – 6 GHz) is not accurate enough.

Another explanation could be that the demodulator circuit model (with $y = k_0(f) * x^2$, e.g. for the LNA on ASPIC or the PMOST on the microphone IC) is too simple. Further probing in literature on page 246 of [11] showed that $k_0(f)$ for an OPAMP is not a constant over a large frequency range. $k_0(f)$ does not only damp the demodulator behavior with increasing frequency, it can even "boost" it. However, for a distinct carrier frequency, the squaring function seems to be quite a good approximation.

Strange matching

In this section we are going to study more closely the match between the simulated and measured voltages. We will concentrate on two things; the first one is voltage difference (in dB) between the start and stop frequency; the second one the behavior of the curve. Furthermore, we will only consider the first frequency range results for all models. These models are supposed to be the most accurate because of the lower impact of the RLC parasitics.

The acoustical output from the test boards is a demodulated signal which is compared with the electrical RF signal from the simulated models. Assuming a quadratic curve of the demodulator circuit the difference between them should be the double, which means that changes of the acoustical output from the DPI measurement should be the double of the RF voltage changes of the simulation model output.

The output voltage which we want to simulate in the Hybrid simulated model is the branch the branch after the microwave filter ("MWF_Vout"), see figures (Fig.37 and

Fig.47), and the output of the integrated circuit in the microphones test boards models, see Fig.29.

The abbreviation "ΔASP-IC-out" is used in the vertical axis to present the difference between "ASP-IC-Vout" and "ASP-IC-GND" in the integrated circuit of the Hybrid, see Fig.37.
"MWF-IC-Out" is used in the vertical axis to represent the difference between "MWF_Vout" and "MWF_Ground" in the integrated circuit of the Hybrid, see Fig.37.
"IC-M-Out"is used in the vertical axis to represent the difference between "IC_mid" and "IC_M_Ground" in the integrated circuit of the Hybrid, see Fig.29.

“IC-out”is used in the vertical axis to represent the difference between “IC_Vout” and “IC_out_Ground” in the integrated circuit of the Hybrid, see Fig.29.

Important: We tried to represent the squaring behavior of the demodulator in a single plot with aY1/Y2-axis range ratio of 1:2. However, the previous comment about non-constant $k_0(f)$ showed that it is not sufficient to do only this special 1:2-axis scaling to obtain a good matching between “RF input voltage [dBV]” vs. “IRIL DPI measurement[dB-SPL]”.

A good matching would deliver more or less parallel curves for “RF input voltage [dBV]” and “IRIL DPI measurement [dB-SPL]” with constant k_0 and the above Y1/Y2 scaling. With non-constant $k_0(f)$, the frequency transfer of the demodulator can show damping or even boosting behavior for increasing frequency and the 2 curves for “RF input voltage [dBV]” and“ IRIL DPI measurement [dB-SPL]” are no longer parallel to each other.

Starting the check with Hybrid MIC1:

Observe that the simulated version of this test board starts at 500 MHz and not from 50 MHz.

By comparing the two curves in Fig.20 below, you will find that the voltage difference in the ASPIC is almost the same as the DPI measurement, which does not really follow the expectation in the previous paragraph. We can also see some correlation between these curves.

In Fig.21, the voltage difference between the MWF output and DPI measurement is almost the double and the correlation is weaker compared with ASPIC output in Fig.20.

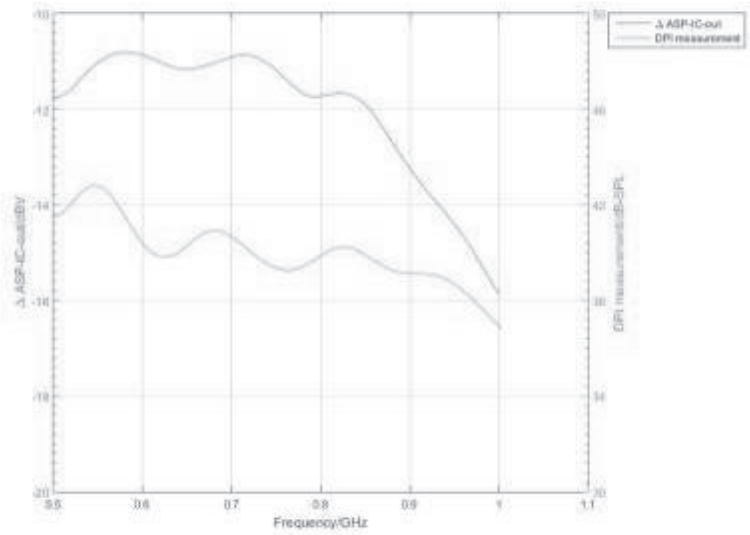


Fig.20. Comparing the RF signal at the ASPIC branch with the IRIL output (DPI measurement).

The MWF output of Hybrid is:

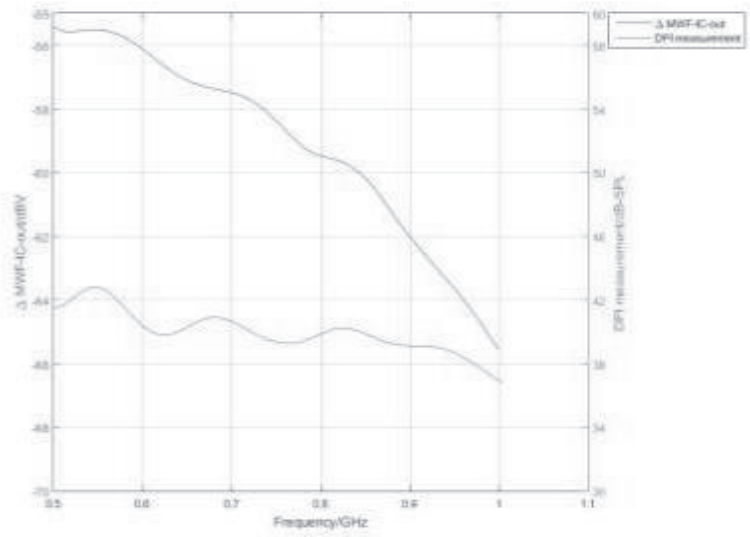


Fig.21. Comparing the MW filter output with the DPI measurement.

TCOILN&P connections:

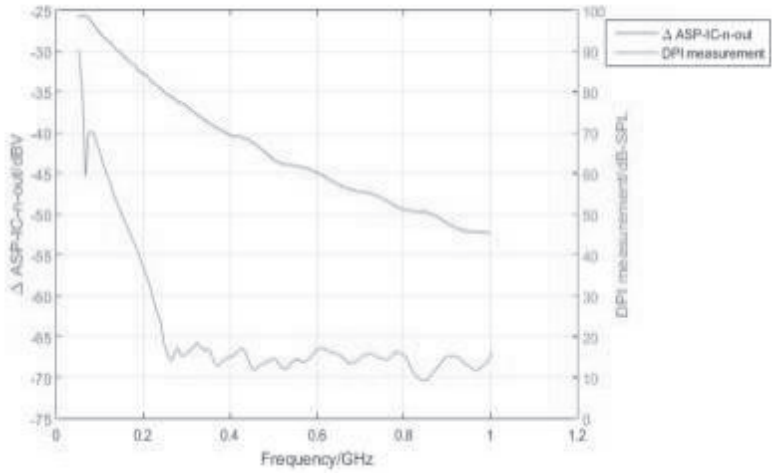


Fig.22. Comparing ASPICn Output of TCOILN&P connection with DPI measurement.

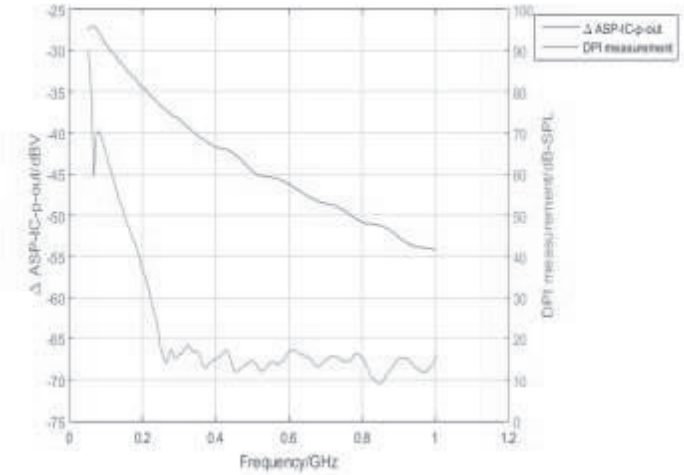


Fig.23. Comparing ASPICp Output of TCOILN&P connection with DPI measurement.

Microphone test board:
It's a bit difficult to explain the matching here, but there is a good agreement in most of the peaks, please check the next two figures (Fig.24, Fig.25):

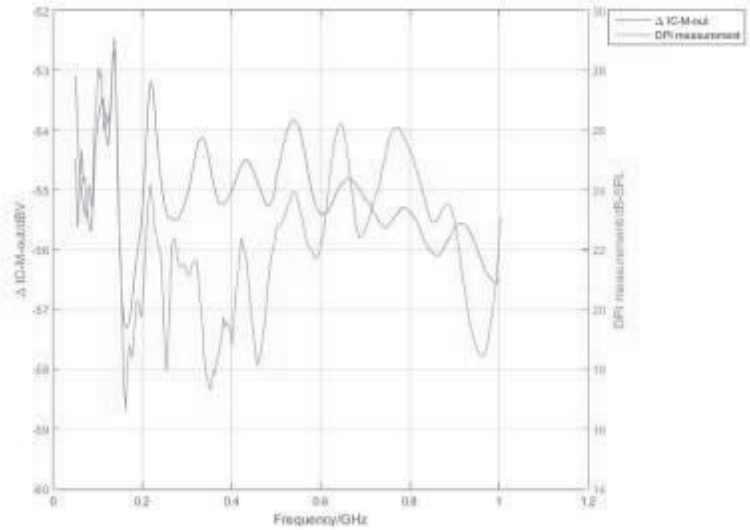


Fig.24. Comparing the RF signal from the middle branch in the microphone integrated circuit with the DPI measurement.

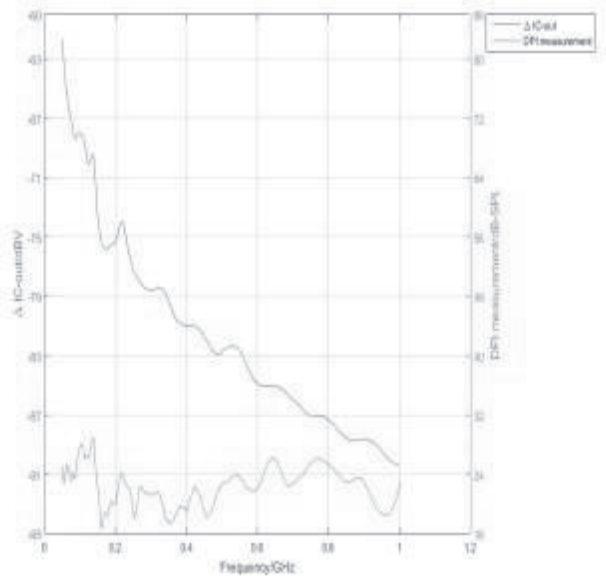


Fig.25. Shows the output voltage of the Microphone integrated circuit.

Vout is the RF voltage across the 20kOhm-resistor R14 in Fig.26 or Fig.29.

High frequency and demodulation

The calibration measurements we got from IT'IS foundation for our demodulator circuit showed a decrease in the demodulation behavior for higher frequencies. "The higher the frequency, the poorer the demodulator output" is a common property of most demodulator circuits if their circuit complexity is simple. But we have seen in [11] that as soon as the circuit complexity increases this simple behavior is no longer valid. This means that the demodulation behavior (of the LNA on the ASPIC or the PMOST in the microphone) cannot be predicted. That's also true even if we got a good agreement between the electrical simulation model and the DPI measurements.

To conclude, all demodulator circuits in the Hybrid or in the microphone remain "black boxes" for us.

Power Distribution inside circuits

To get a better idea about DPI in our circuits, we studied the power distribution inside some of these models.

In the next two figures (Fig.26, Fig.27), the dissipated power has been studied over certain parts in the microphone circuit. The studied parts are framed with the same color as the plotted power curves.

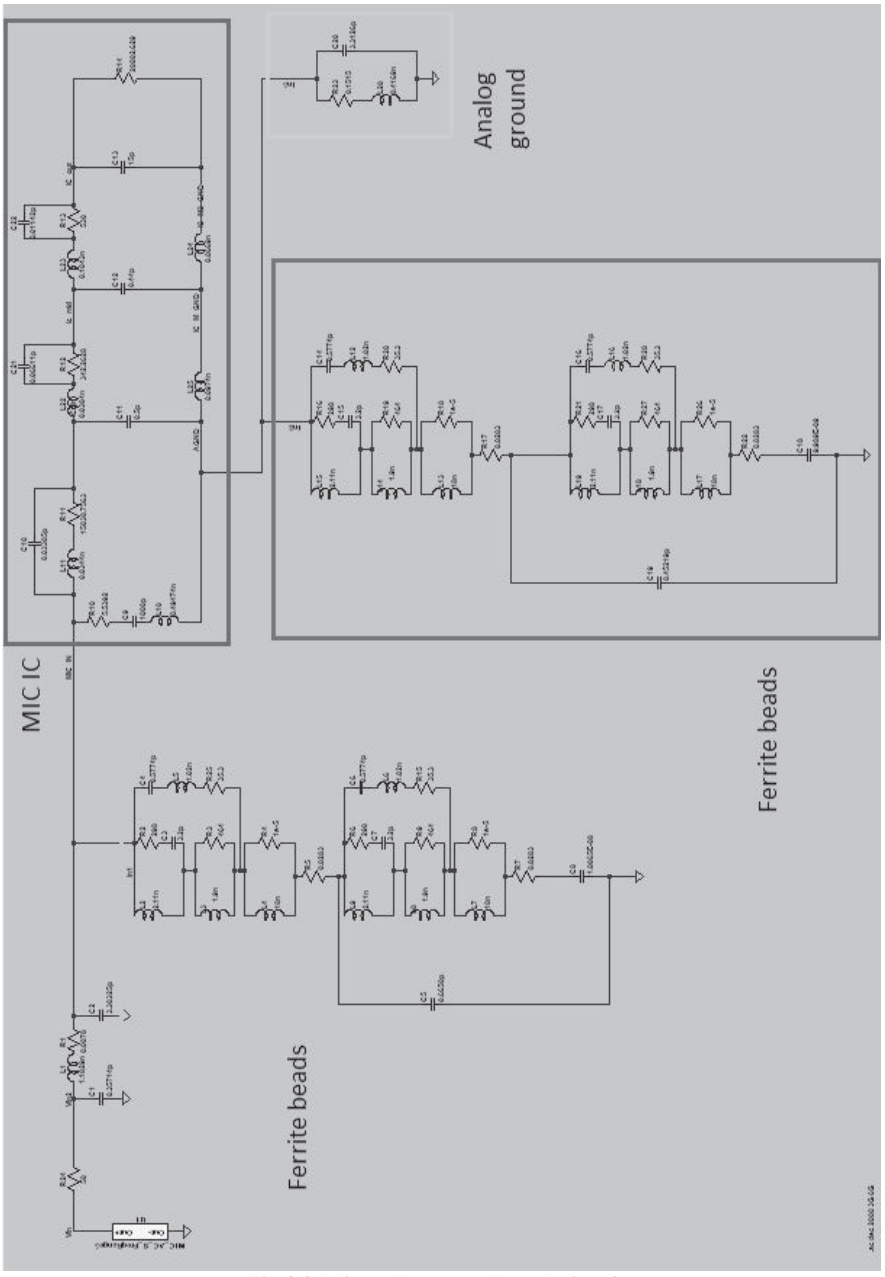


Fig.26. Microphone test board circuit

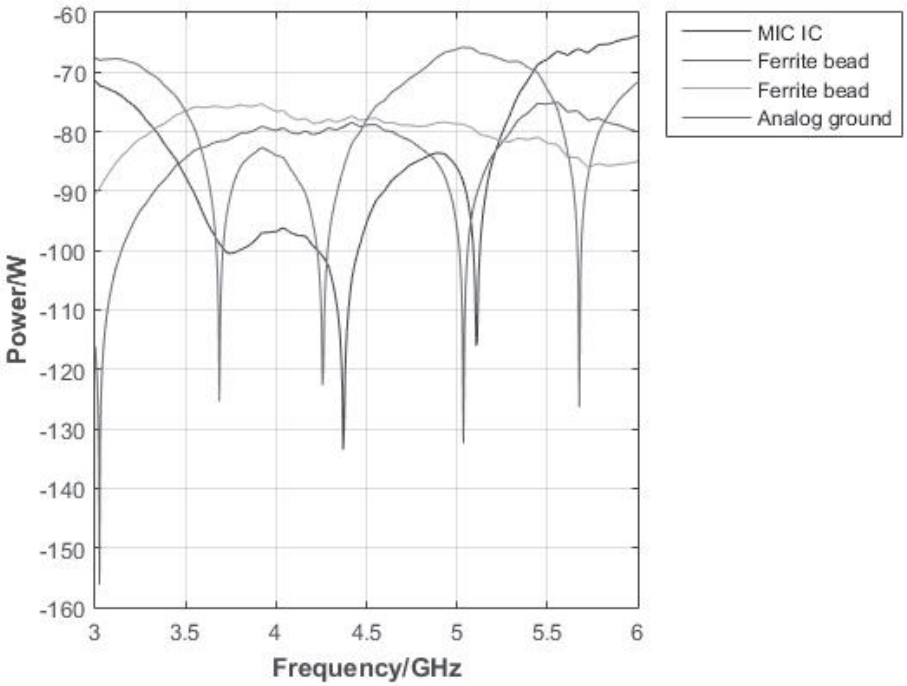


Fig.27. Real Power Distribution.

Note: The "real" power Pr in Watt is depicted in the chart above. (For the vertical axis: 0dB corresponds to 1W.) LTSPICE allows to calculate Pr = V*I*cos(phi) with Pr = Re{*V*I*} with *V, I*: vectors and phi: angle between *V* and *I*.

As you can see in the Fig.27above, the integrated circuit for the microphone gets almost the lowest amount of power in the frequency range 3 – 6 GHz, which is exactly the opposite of what we wanted. Now, we have the power distributed everywhere on the test board circuit and not concentrated in the microphone IC (as it is normally intended for the DPI measurements).

Our main understanding from the DPI measurements is that the RF or microwave (MW) power should be concentrated on regions of the electrical circuit where malfunctions could occur, which should be the microphone's integrated circuit in this case.

Looking at the circuit model above it is obvious that MW power is distributed into other branches than the integrated circuit, mainly because of the structure or network topology of our model.

To conclude, our model for the microphone is not good enough for DPI measurements.

It would be more accurate if the main amount of the MW power would be forced to the branch leading to the demodulator which we want to study. But for the given test boards or the network topology of the simulation model it is physically not possible to achieve such a power flow concentration. It will not be an easy task to improve the test boards with their biasing networks and special connections, e.g. by better mounting of the IC, on which the demodulation takes place. Even if we applied flip-chip technology on the test board to avoid the relatively long PCB traces of the Hybrid you would still get branches/paths on the IC itself which transfer the RF or MW signal or power to places where it is not demodulated. The larger amount of the RF or MW power leaks somehow away and is not concentrated in components in front of the demodulator or in the demodulator itself.

It turned out that we got a slightly better power distribution with the TCOILN&P model, see the TCOILNP section below. But in general, all our DPI test boards and the mounting of the Hybrid or HI Microphone on them heavily suffer from this type of power leakage.

We replaced the DPI voltage AC source by a regular constant voltage AC source, as you can see in the next Fig.28.

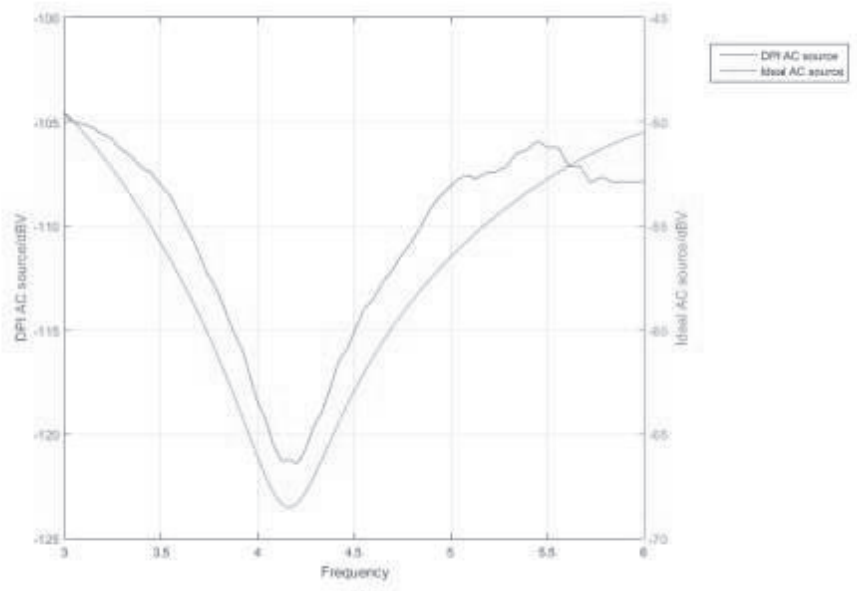


Fig.28. Microphone output with both DPI voltage source and regular AC voltage source curves.

It's clear that we can get a more accurate result with DPI AC voltage source, but as you see the difference in the behavior is more than 5dB.

To conclude: For all the modeling and measurements we did with the test boards, DPI is not a MUST. We can simply do it with a constant voltage AC source at the input. So, for our measurements it is not mandatory to have Ptrans = const.
It is more important to get good RF models of the biasing networks on the test board, the interconnections (on the test board, Hybrid PCB, IC (inside the microphone case and in the Hybrid as well)) and of the demodulating part (amplifiers and ESD protection diodes on the ICs somewhere along or at the end of the RF signal path).

4.2 Microphone test board circuit:

We have used five test boards which have a built-in microphone. These microphone test boards have been tested with DPI measurements to check their behavior. The results can be seen in Fig.14. The whole microphone circuit model is shown in Fig.26.

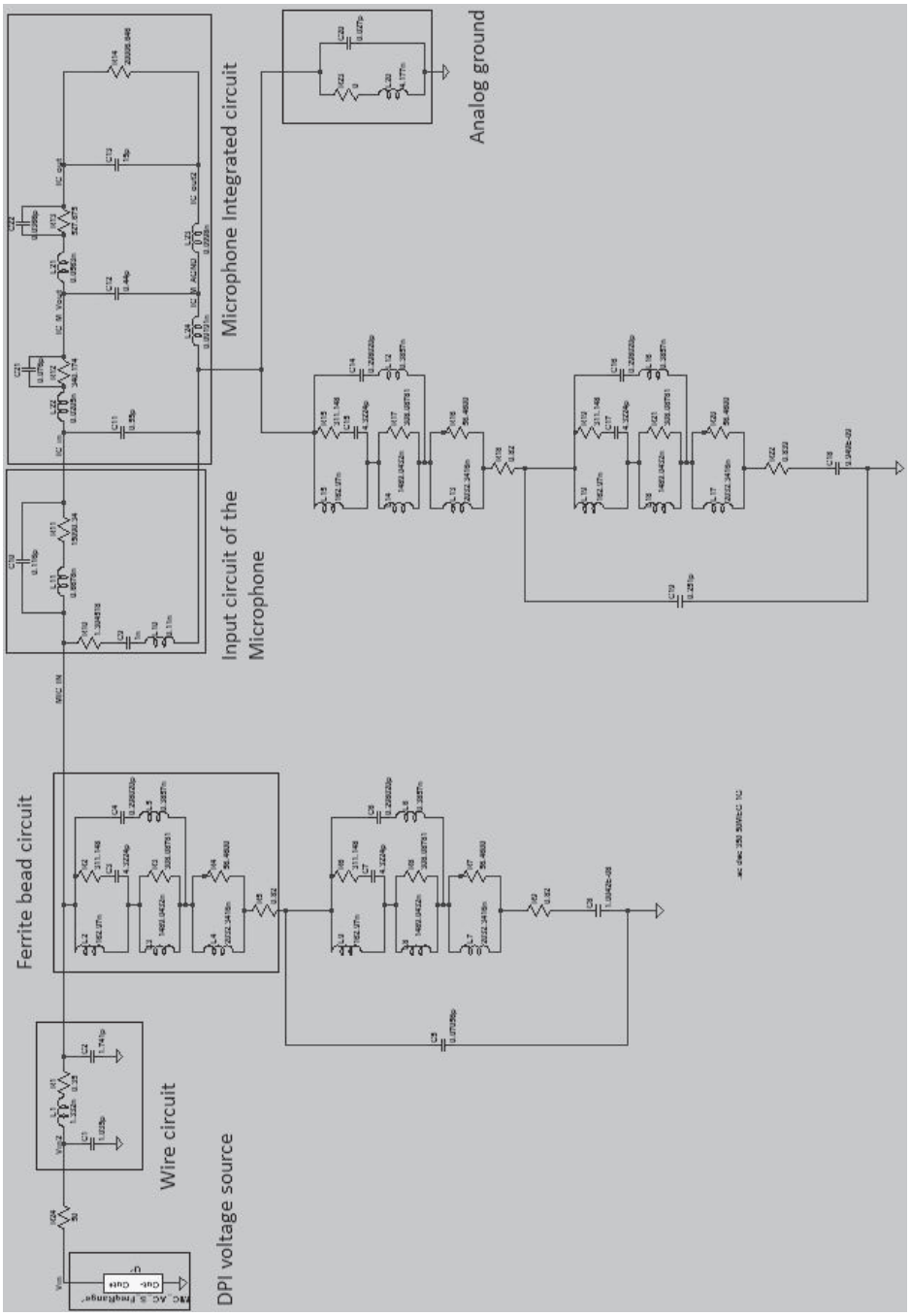


Fig.29.Electrical circuit model of the microphone test board

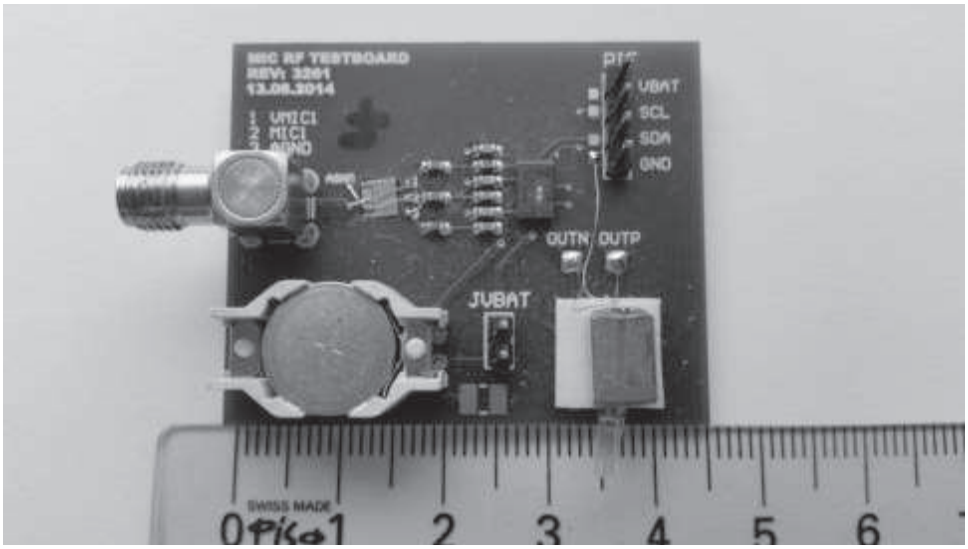


Fig.30. A picture for the microphone test board

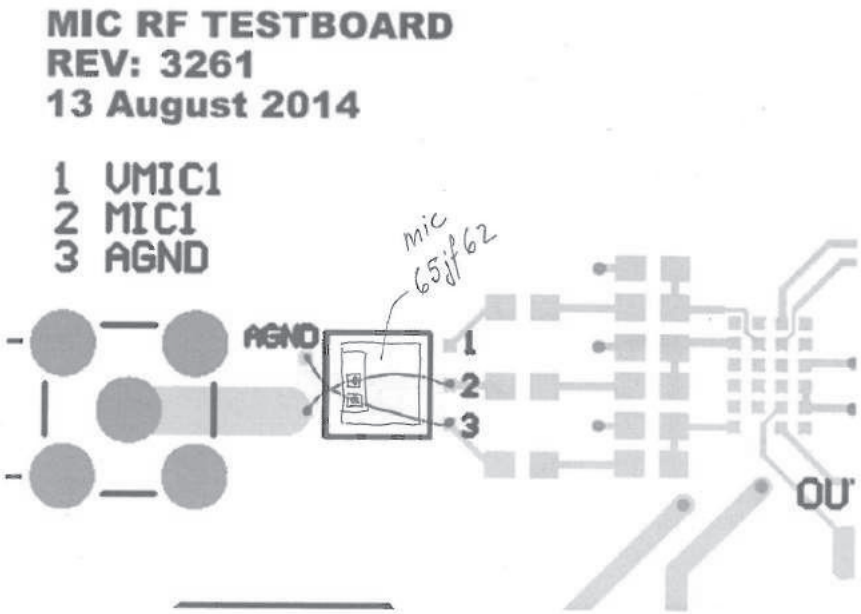


Fig.31. PCB layout showing the microphone test board connections on a PCB.

The main effort which followed this point was to create an electrical model of these test boards in order to compare their simulation result with the DPI measurement behavior. The first approach to model the circuit of the test board contained both passive (RLC elements from connections and ferrite beads) and active parts (integrated circuit). We took into consideration all the possible parasitics when we created this electrical model.

The Microphone circuit complexity has been increased during the thesis. The final model consisted of ferrite beads and RLC parasitic elements in front and around the microphone integrated circuit. The topology of the microphone test board was changed a few times from a simple to a more complex model, but we think that the final model is still not complex enough.

The main parts of the microphone electrical model are the connector to the DPI voltage source, thin wire connection for the RF signal, ferrite bead, analog ground connection, input circuit of the microphone and microphone integrated circuit, see Fig.29.

DPI voltage source: the idea of this special AC voltage source is to use the same injected power as during the DPI measurement in order to create a better match between the simulated and measured models, see appendix DPI voltage source.

Connecting wire for analog ground: we have some wires connected between the test board's input and the rest of the circuit, see Fig.31. An equivalent RLC circuit was created for these wires depending on the wire dimension and shape of the connection.

Ferrite bead: the main part of the electrical model of this component was taken from Murata [8] After measuring the impedance of this component (see appendix Ferrite bead model BLM18AG471SN1D), an AWR program has been created to match between the proposed (or theoretical) RLC circuit and the component measurements.

Input circuit of the microphone: the inner circuit of the microphone consists of both passive components and the microphone integrated circuit. The passive part consists of some metal traces on a tiny 2-metal layer PCB, a 15 KOhm-SMD-resistor and a 1nF-SMD-capacitor. Both SMD components have the EIA size 01005. For more details see Input circuit of microphone in the appendix.

Microphone integrated circuit: Up to this point we were interested only in the linear and passive part of the circuit. The schematic[5] we obtained from manufacturer of the microphone (Sonion) does neither reveal the RLC parasitic elements inside the microphone nor of the microphone IC itself. Unfortunately we could not get a better model from Sonion.

The following parts shows the transferred RF signal behavior for 3 different frequency ranges, see Fig.32, Fig.33 and Fig.34. The simulated branches are from the middle and output of the microphone integrated circuit.

The first frequency range result (50 MHz – 1 GHz):

As mentioned before we have a good match between the measured and simulated models up to 1 GHz, see the explanation above at section (Strange matching).

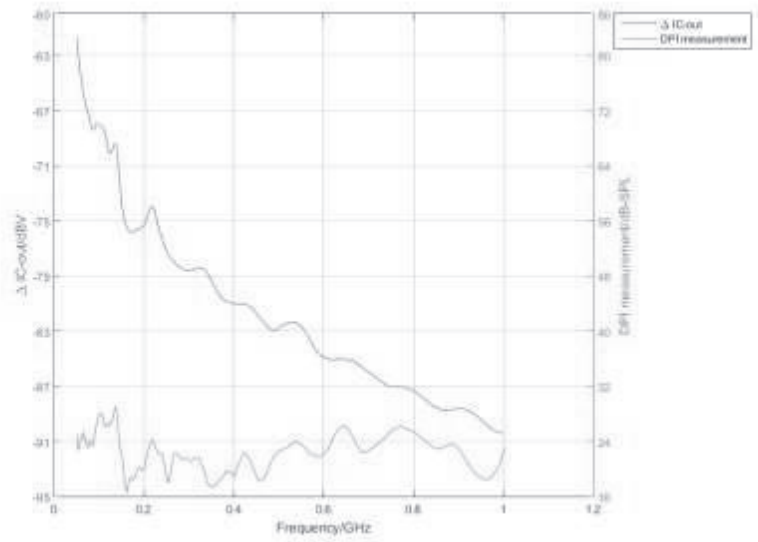


Fig.32. First frequency range results for microphone test board.

[5]We could not unveil this schematic because it is confidential.

The second frequency range result (1 GHz – 3 GHz):

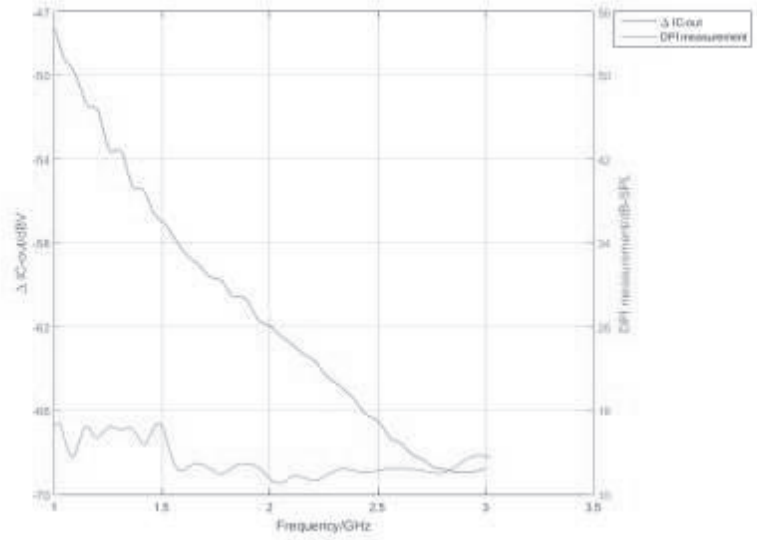


Fig.33. Second frequency range results for microphone test board.

The third frequency range result (3 GHz – 6 GHz):

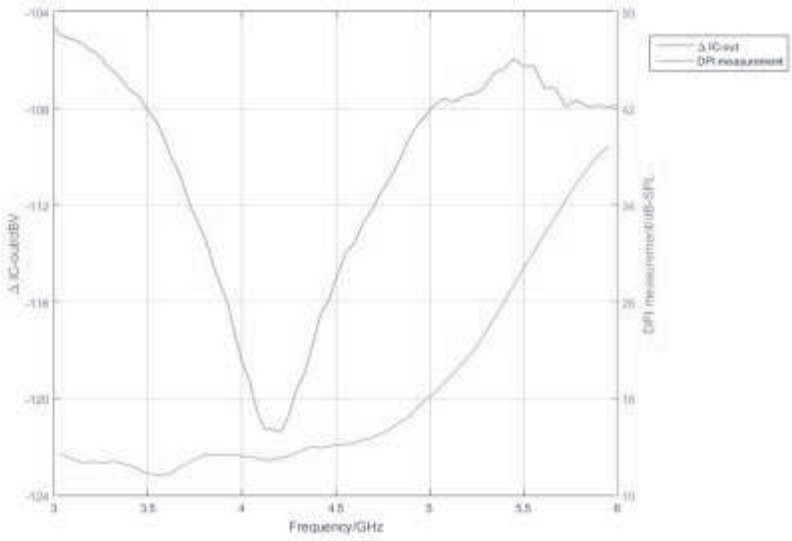


Fig.34. The third frequency range results for microphone test board.

Here we have a partial matching in the frequency range between 4.2 and 5.4 GHz. The rest gives a different behavior.

Fig.32, Fig.33 and Fig.34 show a small correlation in some frequency ranges, but in general the correlation is very poor.

Check the appendix "Full frequency range" to see the plot for the full frequency range (50 MHz - 6 GHz).

4.3 Hybrid MIC1 circuit:

The first Hybrid connection (MIC1) consist of an external circuit, ferrite bead, the Hybrid PCB (3D-EM simulation model made by Javier Abadia Phonak Comm. Murten and the interconnections on the ASPIC (or chip), see Fig.37. The interconnections on the ASPIC were estimated by NXP.

As we mentioned before we tested the Hybrid with different connections. Under this part we used MIC1 connection which is illustrated in the schematic in Fig.35. The physical view of the Hybrid itself is shown in Fig.36.

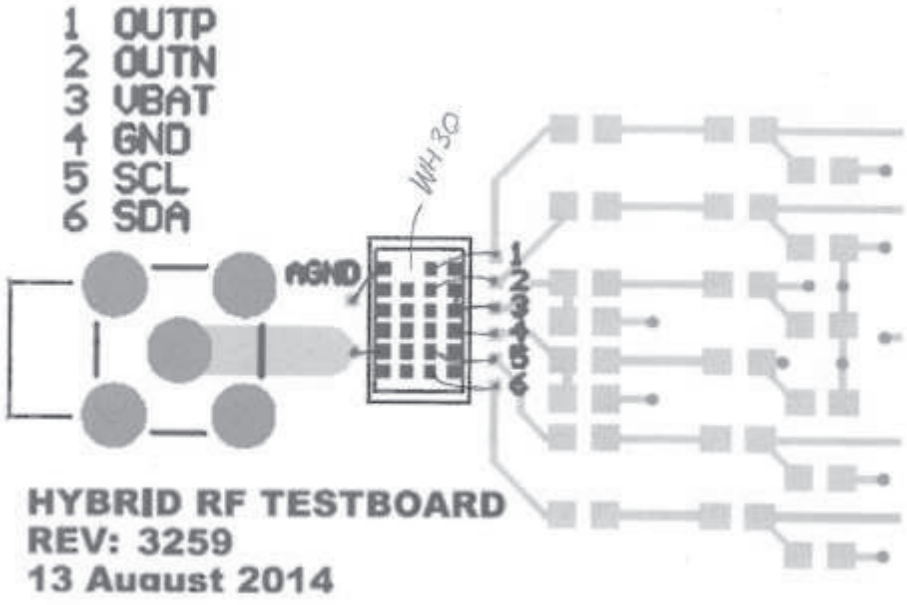


Fig.35. The PCB layout of Hybrid test boards with MIC1 connection on PCB layout.

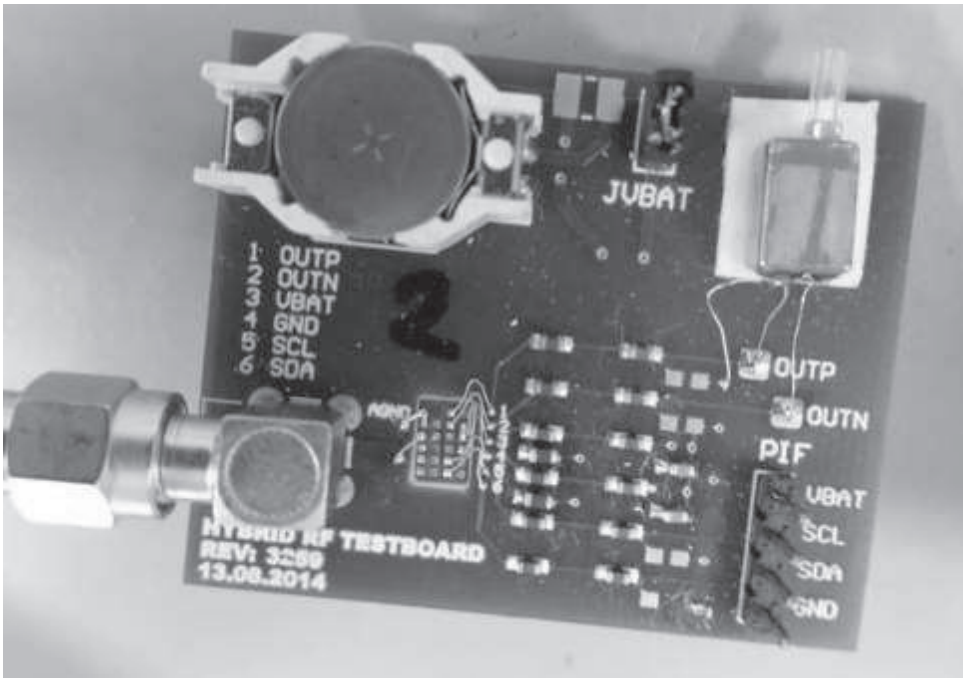


Fig.36. Hybrid test board fully assembled.

Note: The picture shows a wire connection made to TCOILN. For the measurements it was connected to MIC1.

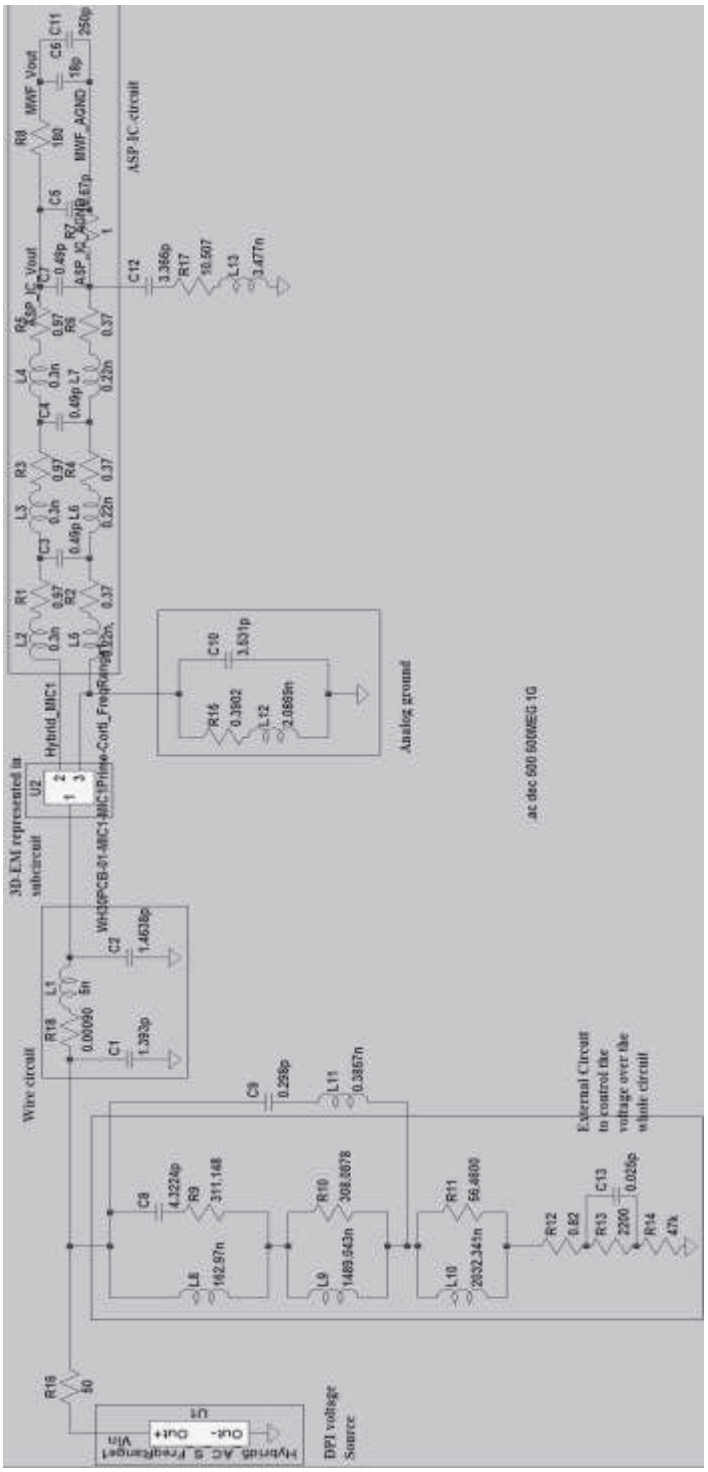


Fig.37. Hybrid test board electrical model with MIC1 connection.

The component U2 in Fig.37, is a SPICE sub-circuit which was extracted from s-parameter results obtained by 3D-EM simulations of the Hybrid PCB. The input for the 3D-EM simulations which were done by Phonak Communication Murten is described in the appendix 3D-EM models for Hybrid PCB.

The component U1 is also a SPICE sub-circuit, but it was extracted from the generator output used during the DPI measurements.

Comparing the results of the simulated electrical circuit with the measured parts, we can see that there is a good match for the first frequency (500 MHz - 1GHz) model but a weaker matching for the frequency ranges (1-6 GHz).

RF voltage and IRIL matching for the 1st frequency range (500 MHz – 1 GHz):

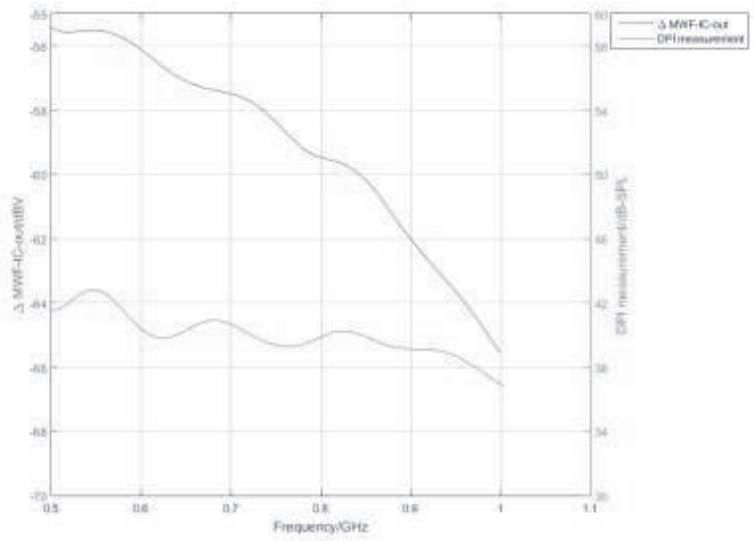


Fig.38. The first frequency range results for Hybrid MIC1 input test board.

RF voltage and IRIL matching for the 2nd frequency range (1GHz – 3 GHz):

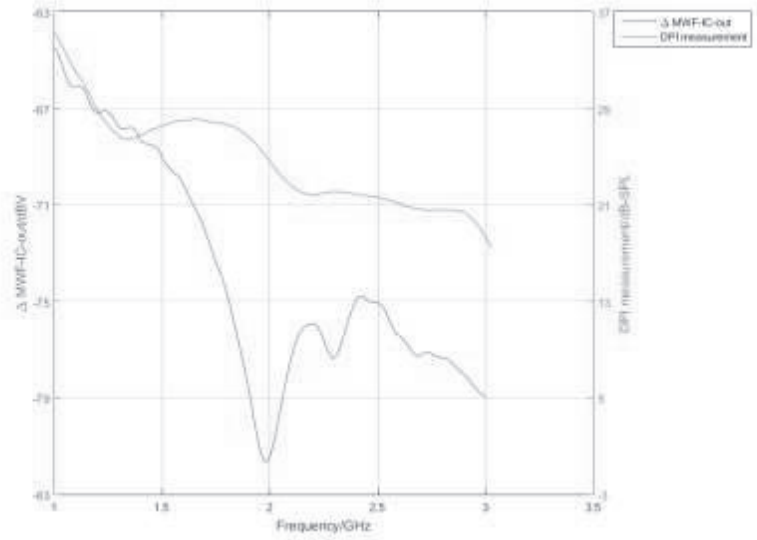


Fig.39. The second frequency range results for MIC1 test board.

RF voltage and IRIL matching for the 3rd frequency range (3GHz – 6GHz):

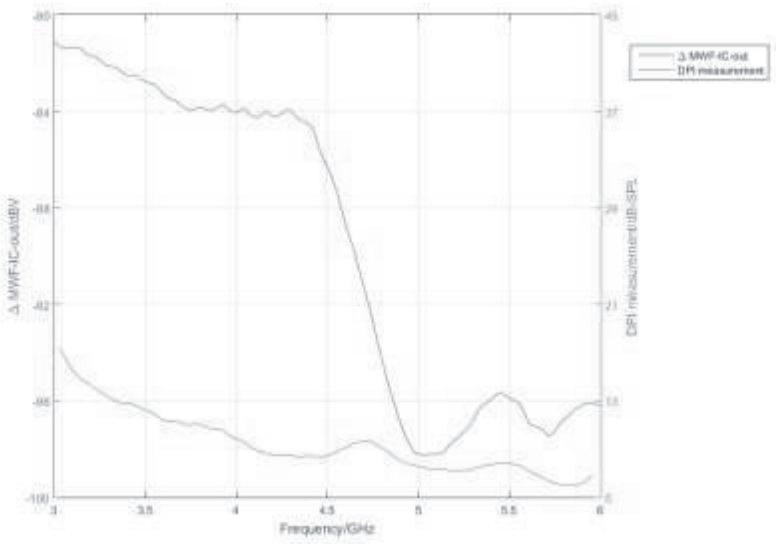


Fig.40. The third frequency range results for MIC1 test board.

4.4 Hybrid TCOILN&P circuit:

The second connection (TCOILN&P) consists of the telecoil (see appendix Tcoil), a wire circuit and 3D-EM simulated model for the Hybrid (see appendix 3D-EM models and interconnections).

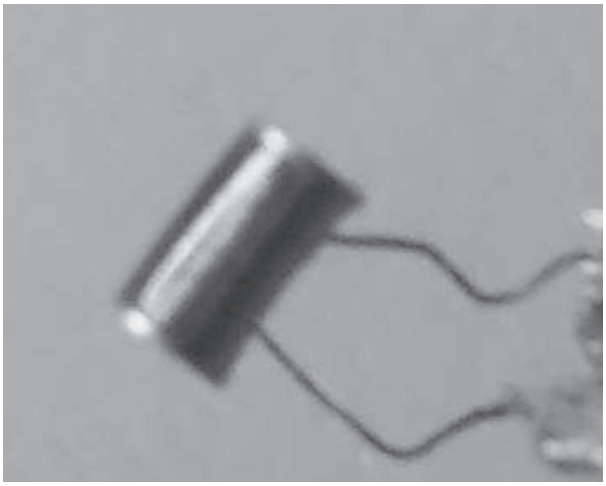


Fig.41. TCoil component.

The measurement required the use of a special component called a tcoil, see Fig.41. This component was connected to the Hybrid pads TCOILN & TCOILP as shown in Fig.43. This component was measured and the equivalent circuit was created so that we can simulate it as a LTSPICE model. (See appendix Tcoil).

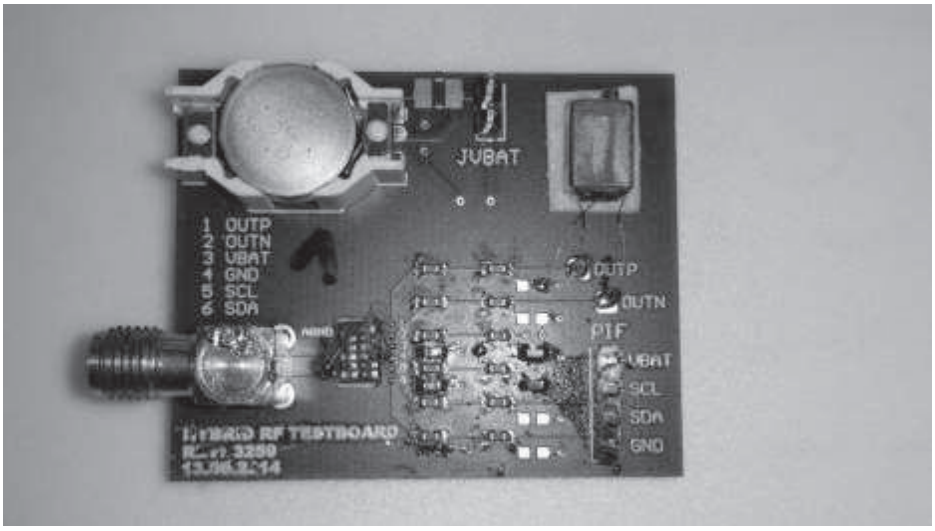


Fig. 42. TCoil Hybrid Testboard.

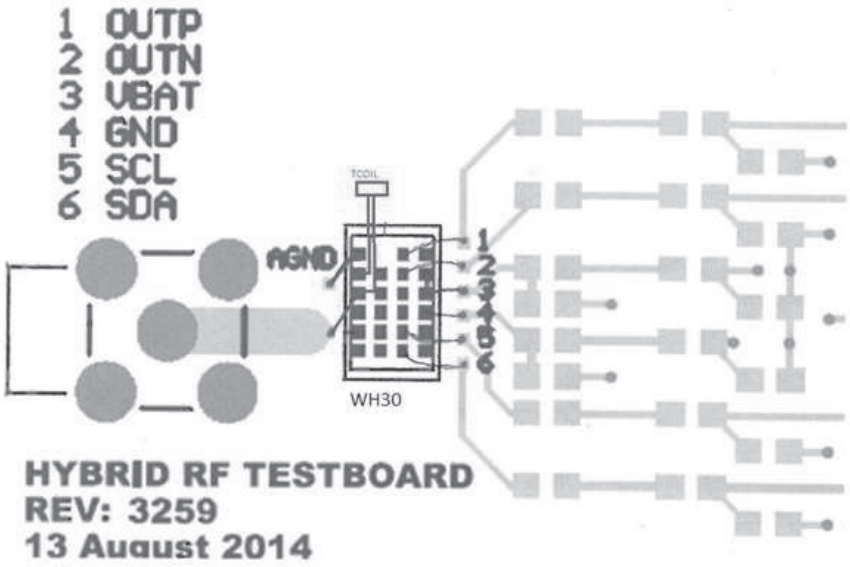


Fig.43. Hybrid test board with TCOILN&P connection on PCB layout.

Comparing the results of the simulated electrical circuit with the measured parts, we can see a good match for the first frequency range (500 MHz - 1GHz) model, but a weaker matching for the frequency ranges (1-3 GHz and 3-6 GHz).

Results of the first frequency range (50 MHz – 1 GHz):

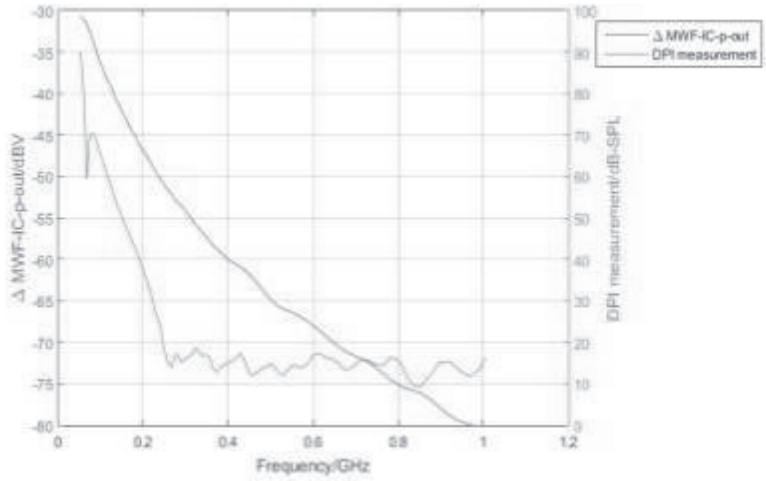


Fig.44. The first frequency range results for Hybrid test board with TCOILN&P connection

Results of the second frequency range (1 GHz – 3 GHz):

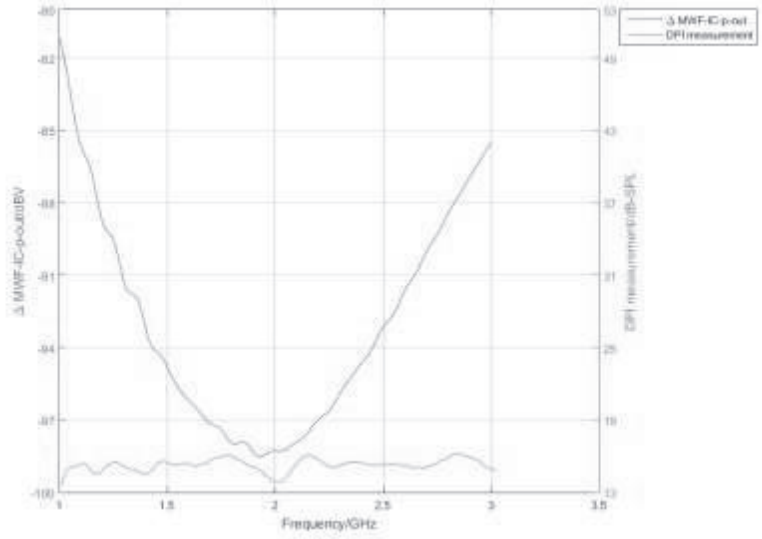


Fig.45. The second frequency range results for Hybrid test board with TCOILN&P connection.

Results of the third frequency range (3 GHz – 6 GHz):

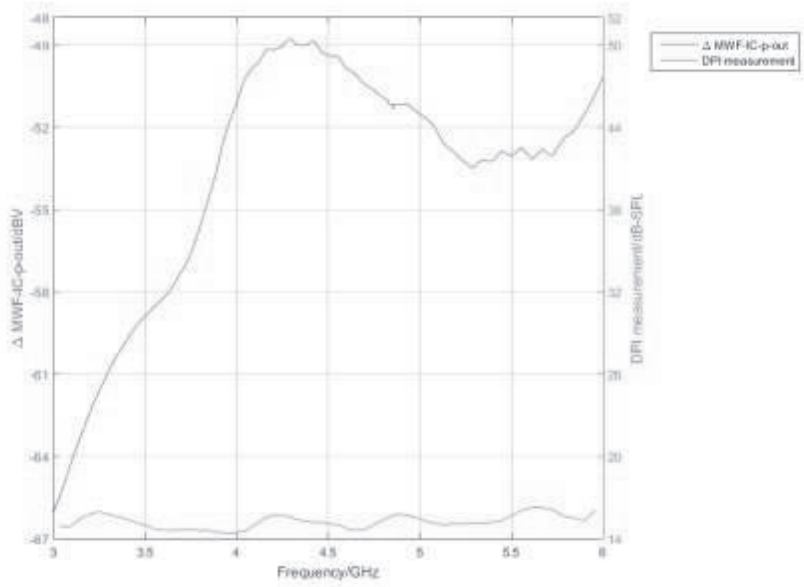


Fig.46. The third frequency range results for Hybrid test board with TCOILN&P connection.

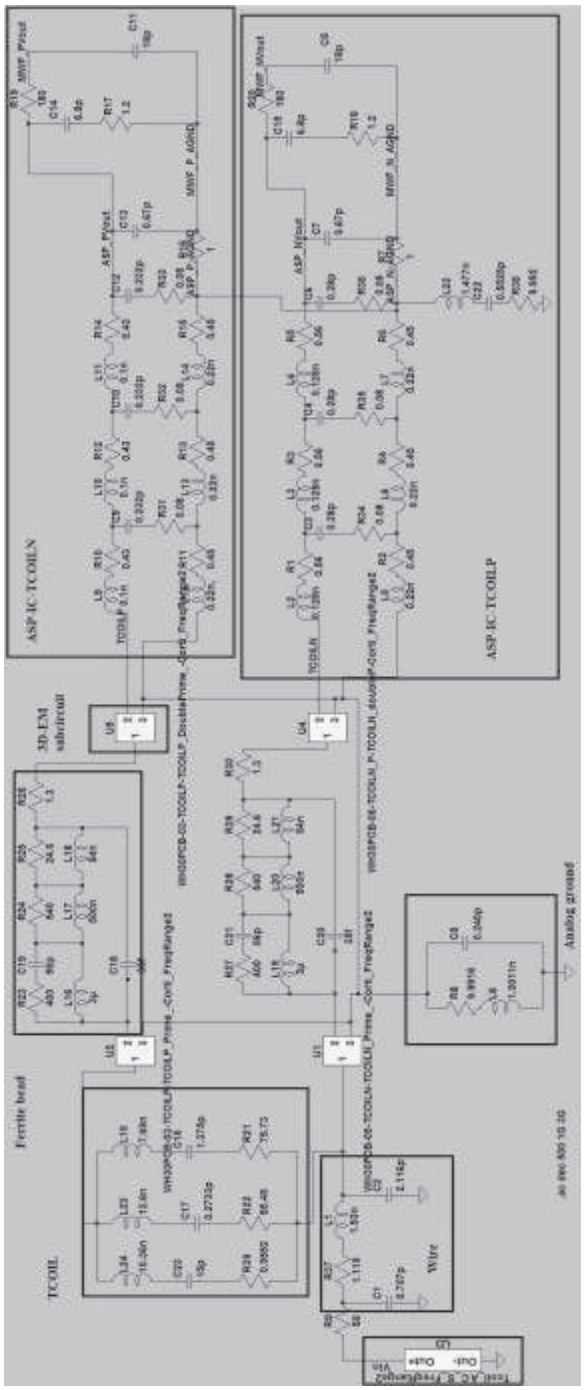

ASP-IC-TCOILN
ASP-IC-TCOILP
3D-EM
substrate
Ferrite bead
TCOIL
Analog ground
Wire

Fig.47.Hybrid test board with TCOILN&P connection

Notes: We used the previous schematic to model the TCOILN&P connection. The important blocks have been named. The components U1-U4 are SPICE sub-circuits extracted from s-parameter results obtained by 3D-EM simulations of Hybrid PCB parts. The input for the 3D-EM simulations is described in the appendix.

The impedance magnitude and phase matching was a very important part of the thesis work. This part has been mainly done by AWR software, where we created the equivalent LTSPICE circuit for each model.
The AWR has an optimizer which can optimize a specific circuit depending on the mask that you create. The optimizer adjusts only the components which are marked as variable components. In our case, we created a mask for both the impedance magnitude and phase, see Fig.48.

Sometimes it was not easy to get a very accurate matching for both parameters.

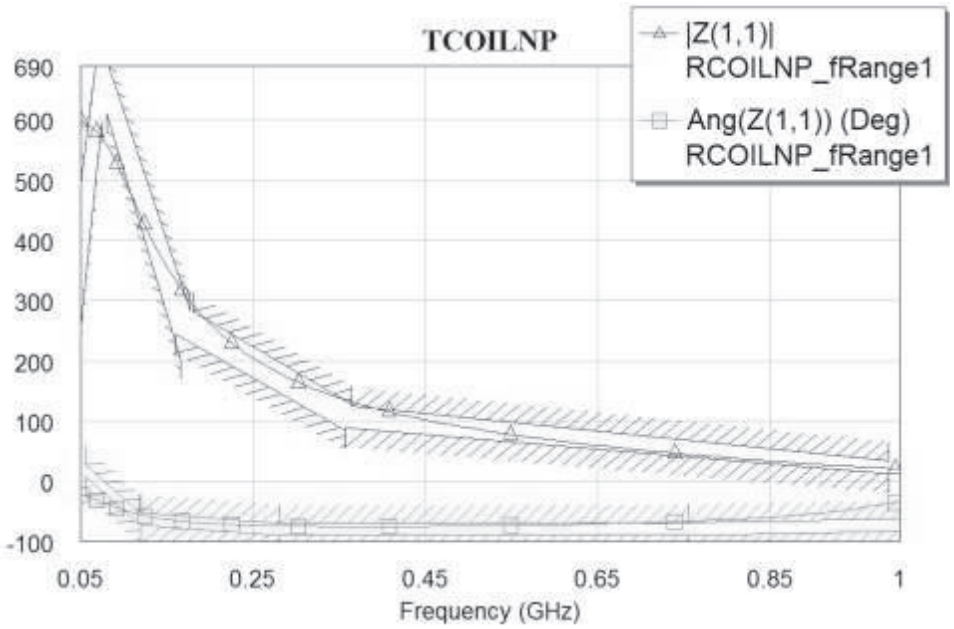


Fig.48. Impedance magnitude and phase matching for the first frequency range for the Hybrid test board TCOILNP.

5. Measurements of parasitic microwave antennas (PWMA)

5.1) The IT'IS foundation demodulator circuit

With the help of IT'IS foundation, we created a demodulator circuit with two different connections to a dummy hearing instrument to be tested in the GTEM cell. The dummy HI consisted of a normal HI, but without the Hybrid. Instead of the Hybrid the IT'IS demodulator circuit was mounted. Please see picture below, Fig.50.

The goal of the investigation was twofold.

A) to use these measurement to compare with the demodulator circuits on the test boards we used during the DPI measurement.
B) to get an impression of the *unloaded* PMWA foot point voltage for 3 different sets of PMWAs (MIC1/AGND, TCOILP/AGND and TCOILP/TCOILN).

For the measurement of the *unloaded* PMWA foot point voltages we had constant field strength of 20V/m in the GTEM cell over the f-range 50 MHz - 4 GHz.

For the PMWA impedance we hadn't got an idea.

The main purpose of this measurement was to show that *unloaded* PMWA foot point voltage can go up to +5 dBV (or +18 dBm). It means that the ESD protection diodes on the ASPIC in the HI Hybrid (and eventually also on the microphone IC) can easily be turned on even for a PMWA loaded by the Hybrid (or the microphone).

In the beginning we could not draw any further conclusions with the demodulator circuit because we did not have any real load and we could not calculate the antenna's impedance. Later on, we realized that it would be possible to make a guess of the *PMWA impedance by a simple measurement with a network analyzer* (eg. at the MIC1/AGND solder pads pad in Hybrid region of the HI PCB) and then to compensate (by open/short NWA measurements) the connection between NWA and connected solder pads. This procedure would enable much more investigations: it would then be possible to model the PMWA (Vemf_hyb and Zant_hyb) for a distinct solder pad connection and with a good simulation model of the Hybrid, you would be able to combine PMWA and Hybrid. This combined model - PMWA with Hybrid – could be quite realistic and allows good guesses of the RF voltages inside the Hybrid up to the location on the IC where the ESD protection diodes or the audio LNA sit.

A similar procedure could be applied for the demodulation of the HI microphone only. In this case the Hybrid would be mounted on the HI PCB, but the HI microphone removed. The PMWA (Vemf_mic and Zant_mic) seen from the microphone pads on the HI PCB could then be measured and used for simulations. (Note: For this measurement the demodulator circuit from IT'IS foundation must be moved from the Hybrid to the microphone place.) During the simulations the "far-end side" of the PMWA should be loaded by the Hybrid input, the "near-end side" of the PMWA should be loaded with the microphone input/output.

In order to get an idea of the overall EMI of both PMWAs (seen from the microphone and Hybrid side), the 2 RF power contributions can be calculated and compared. The microphone and the Hybrid most likely have different demodulator behavior. Therefore, the two RF power contributions may not be added to estimate the overall demodulated output.

See the demodulator circuit schematic in the Fig.49 below:

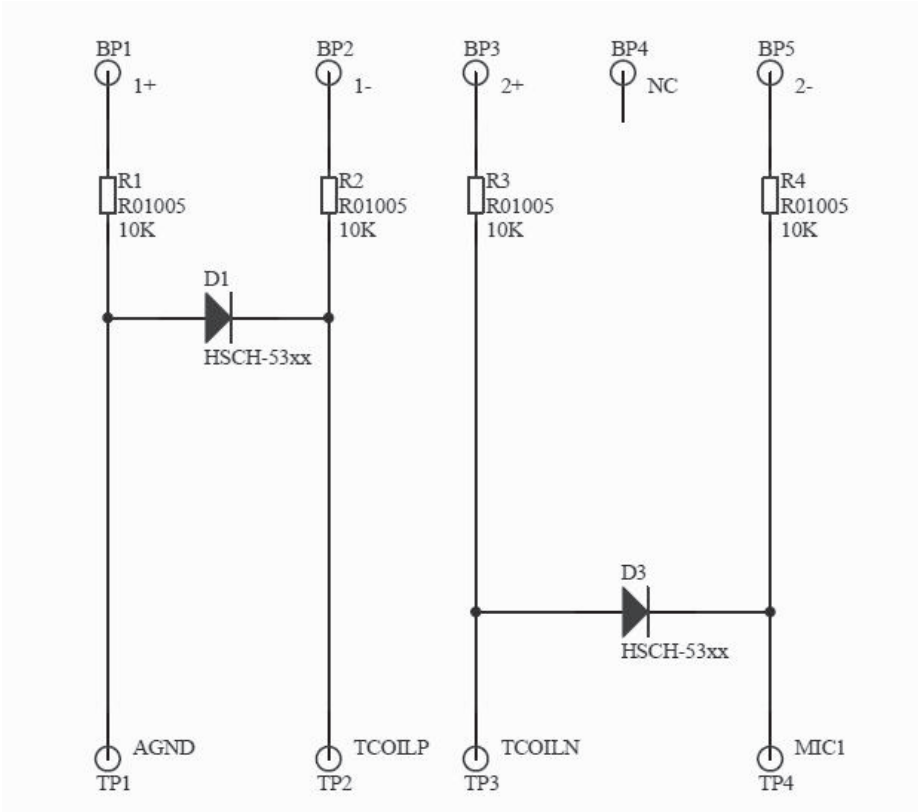


Fig.49. Schematic of IT'IS Foundation demodulator circuit.

Note: BP1-BP5 was connected on distinct solder pads of the Hybrid region on the HI PCB. TP1-TP2 and TP3-TP4 were connected to the carbon fibers which lead the demodulated 80Hz-signal to the preamplifier input outside of the GTEM cell. The carbon fibers are high ohmic resistive material (about 2 MΩ/m) and avoid that the EM-fields inside the GTEM cell are distorted.

In the picture below Fig.50, we can see the demodulated circuit connected to the dummy HI. A rectangular glass plate is used as a stress relief to protect the circuit physically. The demodulator circuit itself consists mainly of resistors and Schottky diodes.

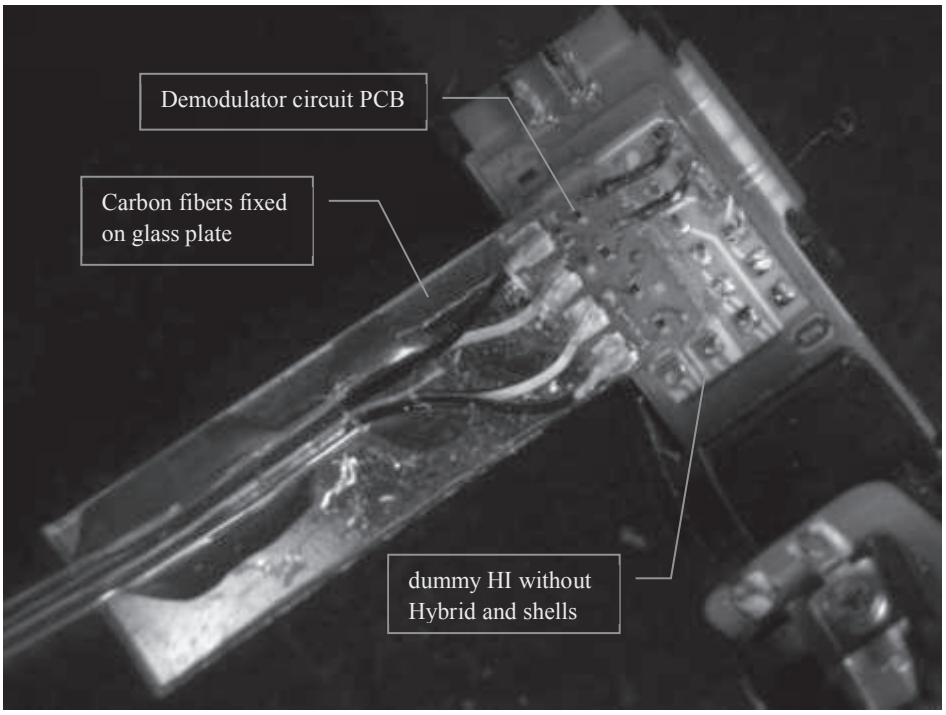


Fig.50. IT'IS Foundation demodulator circuit mounted on a dummy HI.

Applying these measurements allowed us to test the benefits of the Julstrom method. The measurement results of different orientations are given in Fig.51 and Fig.53 and with the Julstrom calculation in Fig.52 and Fig.54 for the same measurements. You can observe that we get a higher output value when we apply the Julstrom method.

Comparing the peaks at a frequency around 3 GHz between Julstrom method and the normal measurements Fig.52, you will observe that Julstrom peak is higher by a few dBs. This is a more accurate result because the Julstrom method takes the maximum sum of all the measured orientations.

These peaks give also an idea about the voltage level in the HI. Considering the peaks again at around 3 GHz, which have a very high level, it makes clear that at this voltage the ESD protection diodes start to conduct.

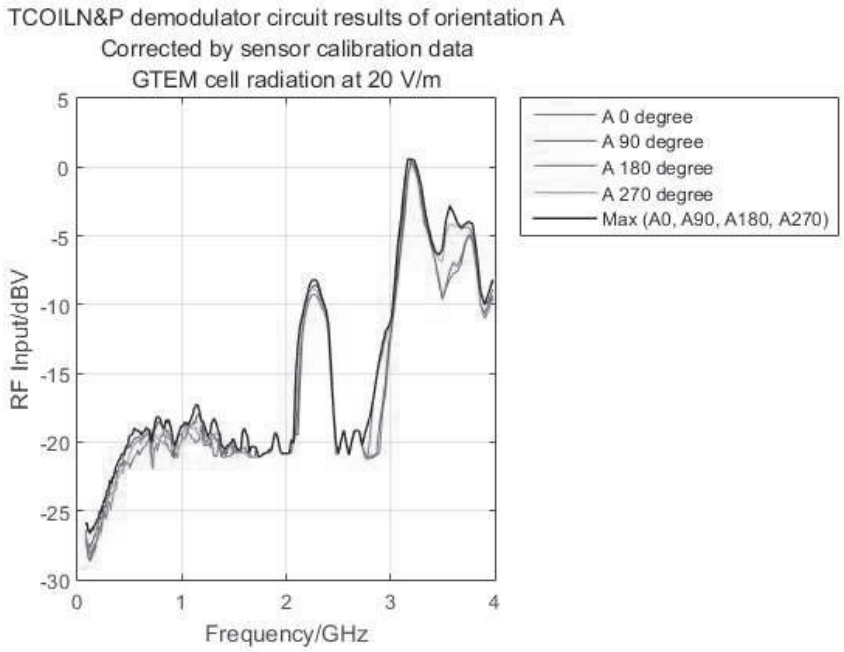


Fig.51. TCOILN&P demodulator circuit results of orientation A

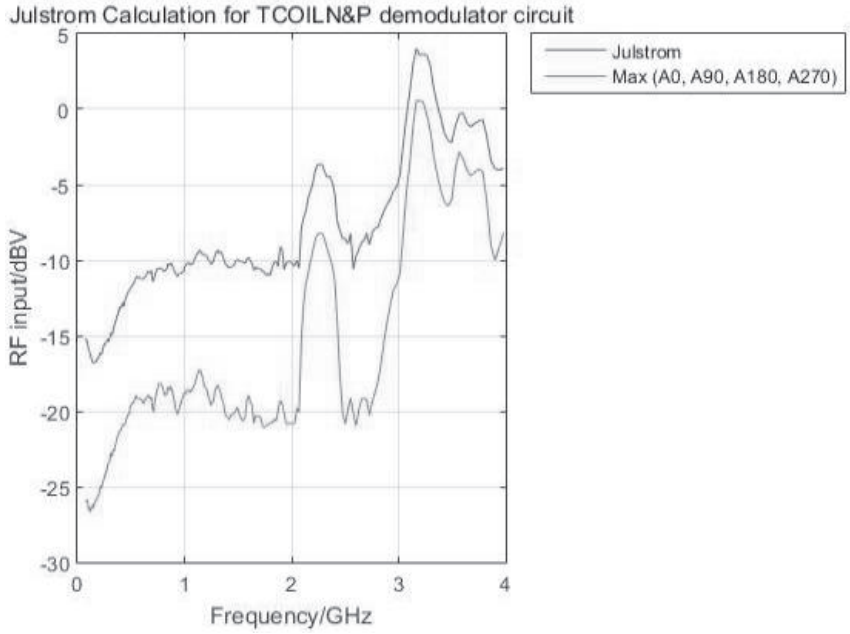


Fig.52. Julstrom calculation for TCOILN&P demodulator circuit.

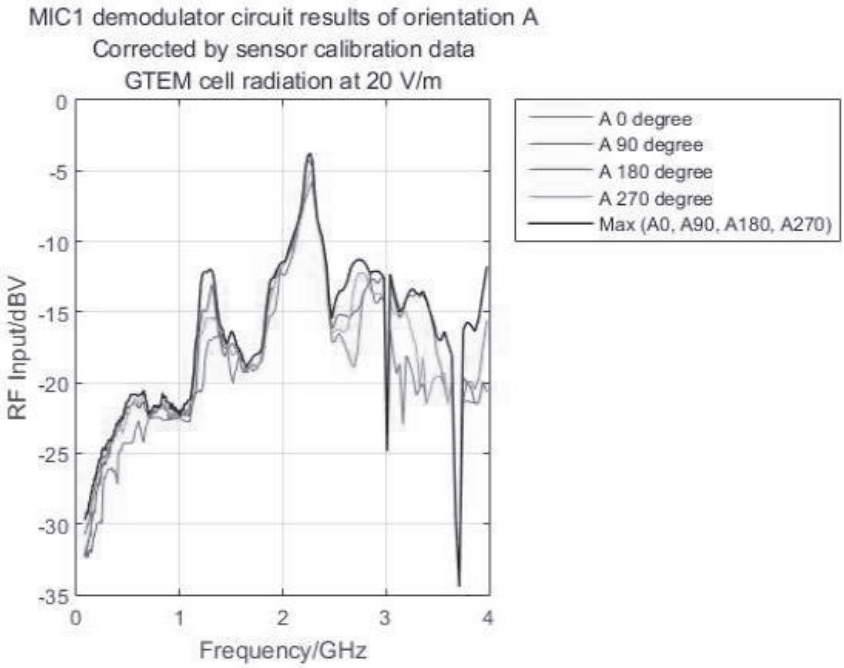


Fig.53. MIC1 demodulator circuit results of orientation A

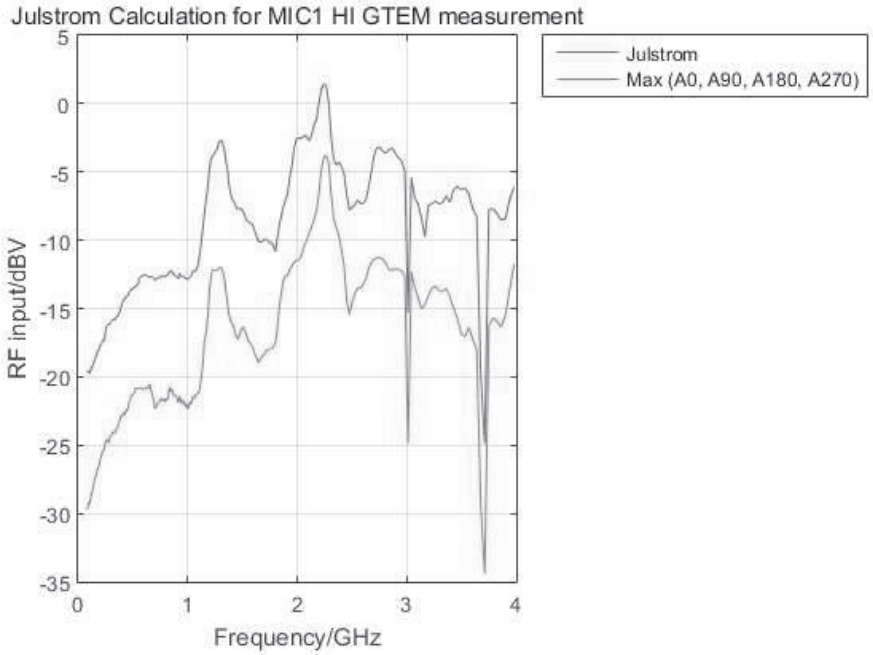


Fig.54. Julstrom calculation for MIC1 demodulator circuit.

5.2) Real HI measurements

We applied GTEM cell measurements for three Golden Unit HI samples. HI manufacturers normally perform IRIL measurement for HI in 4 orientations according to the IEC 60118-13 standard. The idea of the measurements here is to show that it is important to extend the number of the measured orientations to 6 because there is still some higher output level which is not included when doing only a single orientation, 4 rotation angle measurement.

For the measurement results of the golden unit HI samples please see Fig.55 & Fig.56 for a HI Tcoil and Fig.57 & Fig.58 for a HI Omni Microphone.

Findings: We got an idea of the demodulated output (IRIL/ORIL) of the *loaded* PMWA foot point voltage for a real or normal HI (with constant field strength of 50V/m over the frequency range 80 MHz - 6 GHz). The maximum IRIL/ORIL output is quite dependent on the HI orientation in the GTEM cell. The Julstrom method considers this dependency well.
However, we could not get any information about the PMWA impedances and their loading by the Hybrid circuit and the remaining parts of the HI. The measurements only showed that these 3 HIs are well below the IRIL limit (that is

at +55 dB-SPL according to the standard IEC 60118-13). This HI design seems to be well done with respect to RF immunity. Obviously the small ferrite beads in the TCOILN/P lines on the Hybrid PCB must be quite effective (together with a small capacitance at the ASPIC input pad).

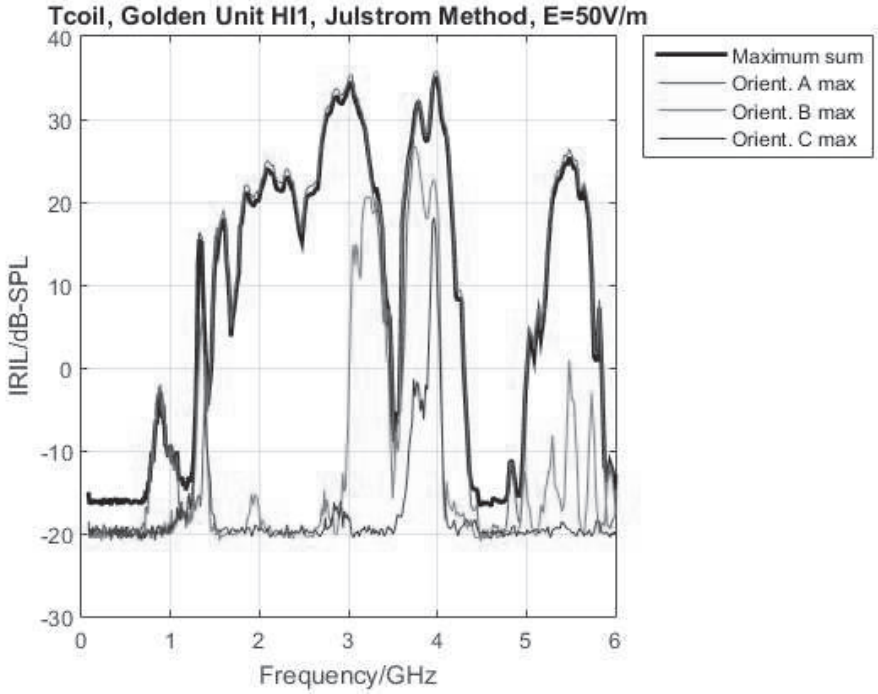


Fig.55. Golden Unit HI1 with Tcoil, GTEM cell measurement.

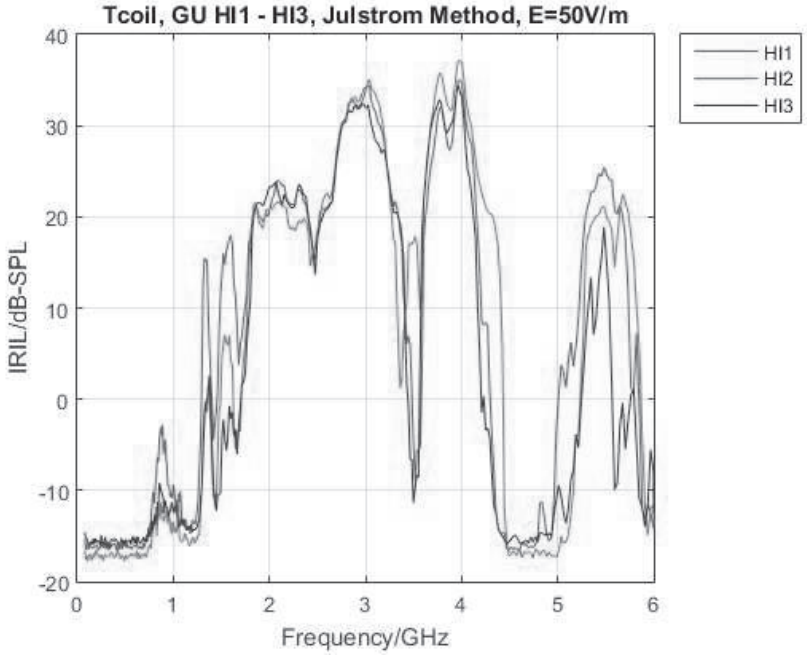


Fig.56. Golden Unit HI1-HI3 with Tcoil, GTEM cell measurement.

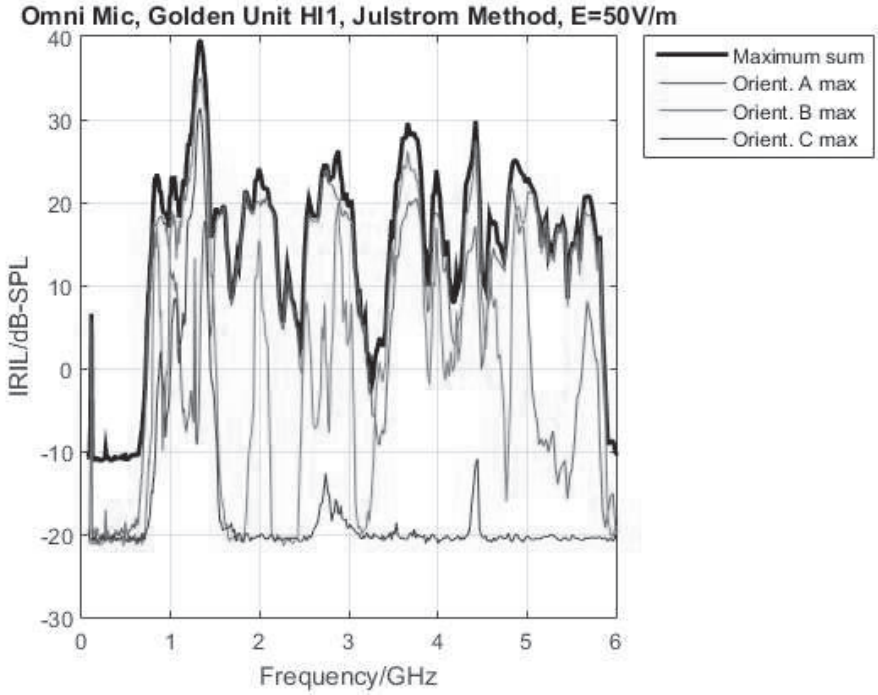


Fig.57. Golden Unit HI1 with Omni Mic, GTEM cell measurement.

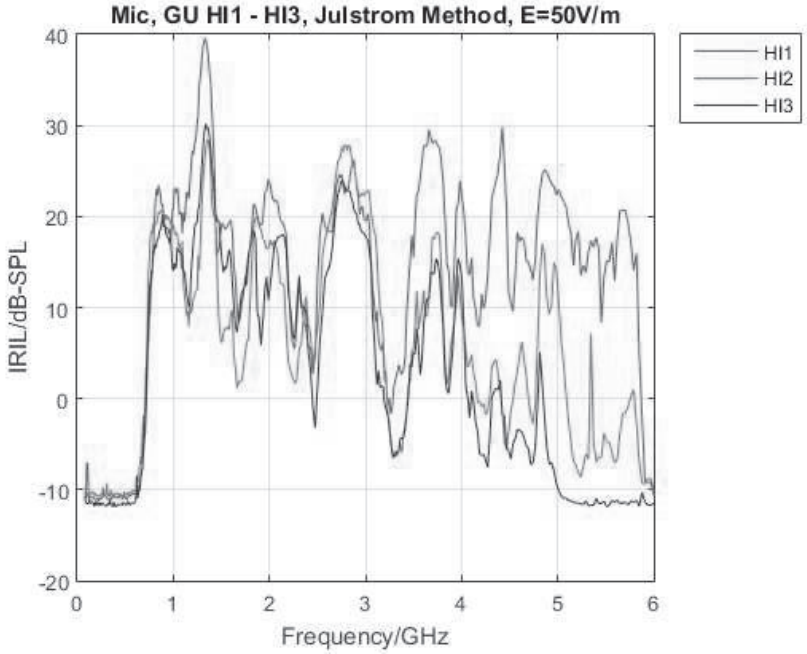


Fig.58. Golden Unit HI1-HI3 with Omni Mic.

Based on the latest findings for PMWA impedance (which can be obtained by a simple NWA measurement under 5.1) The IT'IS foundation demodulator circuit), we can use the measurement results of 3A) and 3B) for a new simulation of a whole HI and then compare these simulated results with the measured results of 5.2) Real HI measurements. But, here again, the missing links for a good comparison of RF input voltage and DPI output will be the demodulator circuits on the microphone IC and Hybrid ASPIC.

5.3) L-shape and monopole antenna

We performed measurement for a monopole and L-shape antennas with different bending by using the GTEM cell



Fig.59. Measured monopole antenna.



Fig.60. Measured L-shape antenna with 2 cm bending.

First ideas to measure these "artificial" antennas in GTEM cells were taken from [5]. We modified the procedures we found there to our own requirements.

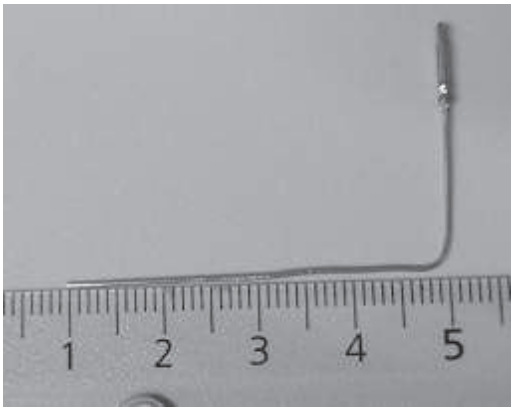


Fig.61. Measured L-shape antenna with 4 cm bending.

With these measurements we got an idea of the artificial monopole and L-shape antenna foot point voltages (loaded by 50 Ohms) irradiated in the GTEM cell with a constant E-field strength of 50V/m and the impedances of these artificial antennas over the frequency range 50 MHz - 6 GHz. However, we did not obtain real HI PMWA impedance and its loading (by the Hybrid circuit and the remaining parts of the HI). At least, with this new model we can calculate - almost reasonable - RF voltage transfers inside the HI.

We further investigated these measurements by using the measurement data of the L-shape antenna (foot point voltage loaded by 50 Ohm and antenna impedance) combined with the input impedance of a Hybrid MIC1 circuit.
See Fig.62 on the next page.

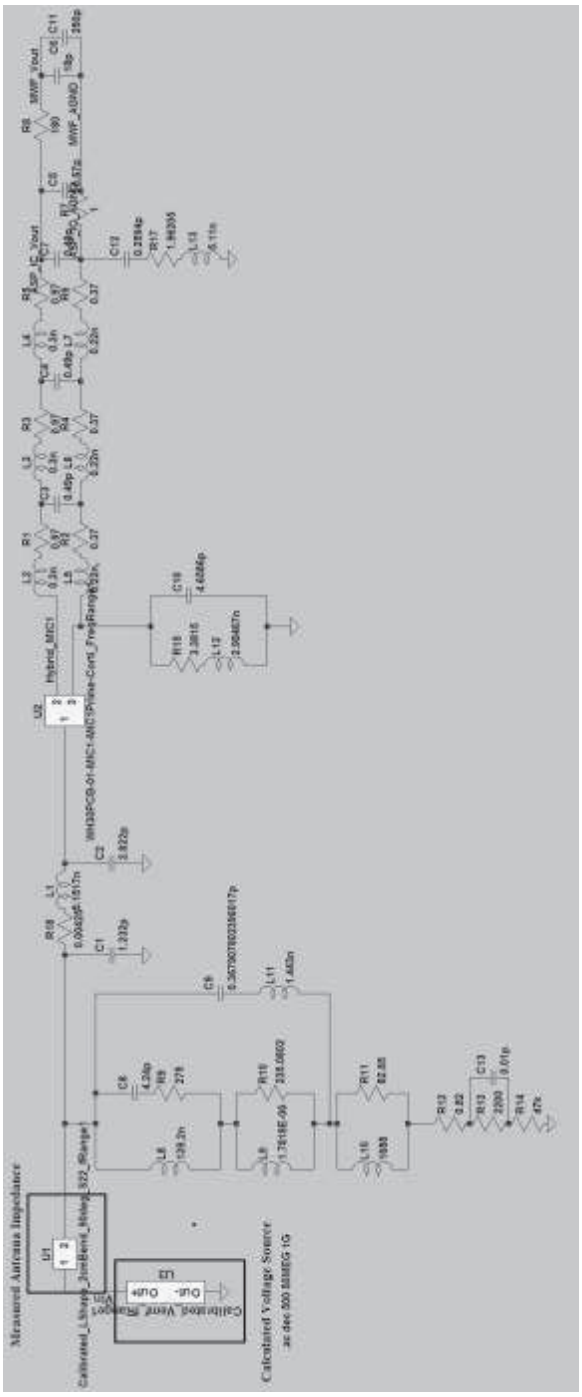


Fig.62. Schematic of loaded, artificial antenna.

Regarding the AC voltage source in the schematic above, we made a special calculation to get the same RF power provided by the L-shape antenna at its output during a GTEM cell measurement with E = 50 V/m over the whole frequency range from 50MHz to 6GHz. With these calculations we could also compensate the E-field error, see in the appendix Voltage AC source of the artificial antenna circuit.

The main idea here was to show the voltage transfer inside the HI.

Results for the 1st frequency range (50 MHz – 1 GHz):

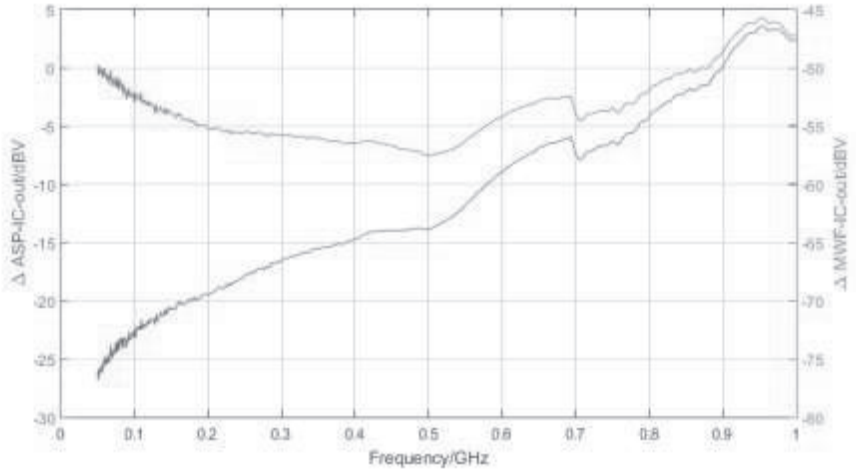


Fig.63. HI with L-shape antenna RF voltage transfer inside HI for frequency Range1.

Results for the 2nd frequency range (1 GHz – 3 GHz):

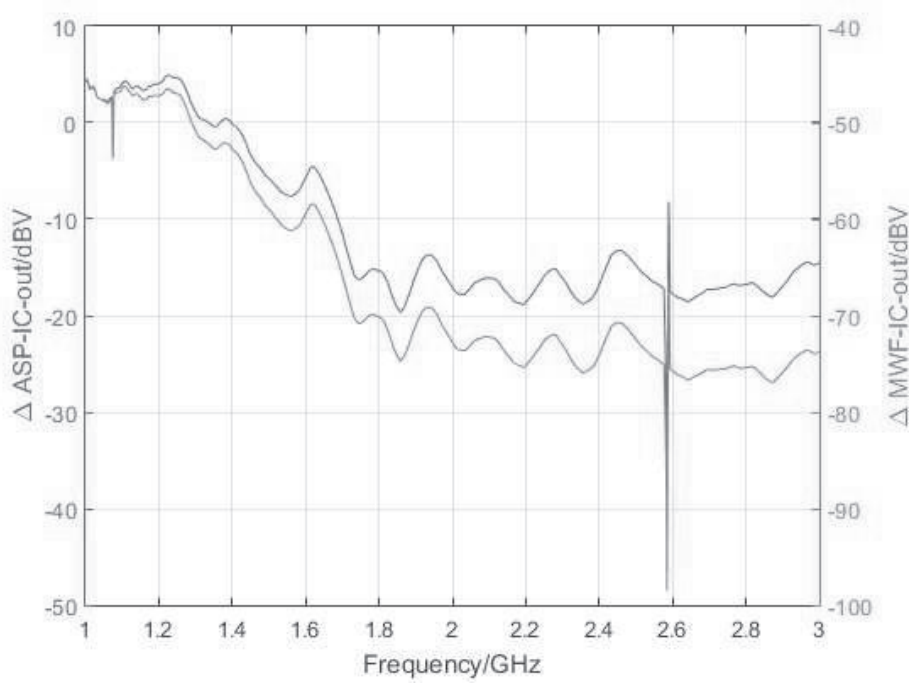


Fig.64. HI with L-shape antenna RF voltage transfer inside HI for frequency Range 2

Note: The peaks and drops at around 1.07 GHz and 2.58GHz of the curves above are approximation artifacts of LTSPICE.

Results for the 3rd frequency range (3 GHz – 6 GHz):

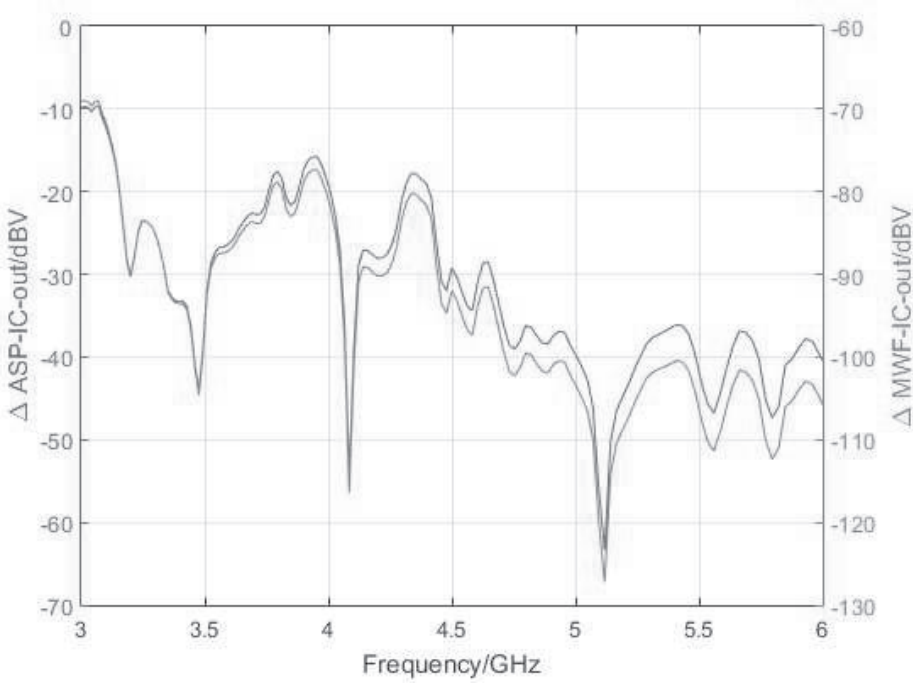


Fig.65. The HI with L-shape antenna RF voltage transfer inside HI for frequency Range 3.

According to the simple ESD diode demodulation model for MIC1 (from A. Jakob, please see appendix section), the demodulation by the ESD protection diodes starts with an RF level of about > - 4 dBm (or > -17 dBV) across the ESD diode.

From Fig.63, Fig.64 and Fig.65 we can see that the RF voltage across the ESD diodes (V(aspic_vout)-V(aspic_agnd)) is high enough to be demodulated in the frequency range 0.3 – 1.7 GHz, around 3 GHz and 3.9 GHz.

6. General Findings and Conclusions, Future Improvements

As the title of the master thesis says, all our effort aimed to "Understand(ing) the Parasitic Effects on the Microwave Interferences at Hearing Instrument Level up to 6GHz"

In the beginning of the work PHONAK thought that this goal might be achieved by

1) a new immunity measurement method different to the common and standardized one (irradiated HI in a GTEM cell with the HI acoustical output as EMI response). The new measurement method should avoid the drawback of HI inherent parasitic microwave antennas (PMWAs). The method should also be applicable for both HI Hybrids and microphones.
2) modeling of the EMI sources and the RF propagation paths in the microphone and the HI amplifier inputs.
   The modeling of the electrical circuit should be based on input impedance (or s11-parameter) measurements, RLC circuit estimates for wired connections, s-parameter models for the Hybrid PCB and circuit estimates for interconnections and front-end circuits on the integrated circuits of the HI amplifier and microphone.
3) modeling of the different RF signal propagation paths in the microphone and the HI amplifier inputs and comparing with the output results obtained with the new immunity measurement method.
4) Measurement of PMWAs in dummy and real HIs. (Application of the Julstrom approach, in either case for VRF_in and IRIL)
   The L-shaped antenna was used as a distinct realization of a PMWA …

Some goals could be achieved, some only partially and some not.
Based on the different findings in the 3 previous chapters and in the appendix we can say the following:

- The effort to get good RF models for the test boards, the interconnections on PCBs and on the ICs themselves was underestimated. The current RF model, which we could build, is only valid up to 1 GHz.
  We split the whole frequency range of 50 MHz – 6 GHz into 3 parts to lower the complexity of the RLC circuit models and to obtain a reasonable input impedance match between measurement and simulation. After combining the 3 frequency range results we got large errors at the borders of adjacent frequency ranges. For a better impedance match adjacent

frequency ranges should overlap.
To get a better RF model which is valid up to 6GHz, the test board (with its wire connections and auxiliary components used for supply and biasing), the HybridPCB, the microphone and eventually also the ASPIC and microphone IC must further be analyzed and better modeled, e.g. with a 3D-EM simulation tool.

- There has been a considerable lack of knowledge of the different RF demodulators (behavior of the amplifier inputs/outputs, ESD protection diodes on the ICs, etc). The ASPIC and microphone IC-designers and manufacturers cannot provide such RF models.
- To make the ASPIC, the Microphone and its IC, the Hybrid and the HI PCB compatible with demanding RF and MW requirements, the design and manufacturing cost would increase by a considerable amount. In the worst case the HI design is not feasible because fulfilling the RF requirements would ask for a much larger IC (chip area) and with that also a larger HI.
- The use of the DPI method on the microphone and the Hybrid (with input MIC1 and TCOILN/P) is questionable, since the dissipation of considerable amount of RF (or MW) power in other branches of the test board, the Hybrid, and other interconnecting circuits or even in the IC itself cannot be avoided. So, only a small portion of the transferred RF power at the test board input would arrives at the demodulating parts (deep inside the HI electronics). It will not help to redesign the test board and interconnections. The current limitations given by the different signal branches in the IC remain.
  It turned out that DPI with constant RF input voltage -instead of constant transferred RF input power - at the Hybrid or the microphone input would also do the task if we only consider the transferred RF voltage.
  In spite of its drawbacks, the DPI method with constant transferred RF input power can be used to compare the RF immunity of Hybrids and microphones.
- The 2-wire microphone, sonion 65JF62, shows a very good RF (or MW) immunity up to 4 GHz. This is mainly due to the 15KOhm-resistor of the off-chip RC-filter which avoids high RF voltages across the ESD protection diodes of the microphone IC and further increases RF damping in front of the demodulating part, i.e. the PMOST.
  For frequencies beyond 5 GHz, the EM immunity of the microphone is

limited by its PCB technology, the off-chip RC-filter components and slots between the metal housing of the microphone and it's PCB.

- Because of lack of time it was not possible to measure the efficiency of "real" HI PMWAs (e.g. their unloaded foot point voltage and impedance). However, we got an idea about the foot point voltages and antenna impedances by measuring "artificial" PMWAs (L-shape and monopole antennas).
  In order to get a full RF model of "real" PMWAs with their loading by the Hybrid or microphone, a more accurate RF model of the Hybrid (S11-parameter or complex impedance up to 6GHz) is needed.
- Other measurements we performed with the GTEM cell and the IT'IS demodulator circuit mounted in a dummy HI showed that it is possible that ESD protection diodes at the ASPIC inputs can demodulate or rectify the RF signal. The RF power delivered by the PMWA to the ASPIC input can drive the ESD protection diodes in their conductive mode and they become a source of EMI. In a simple Spice model we could show that the combination of the demodulation contributions of the LNA and the ESD protection diodes can lead to demodulation ratios much bigger than 2:1 (interference output voltage change [dB] / RF input voltage change [dB]). The findings on the ESD protection diodes confirmed results of former EMI investigations performed by Sonova.
- To get a successful damping of RF or MW power at the ASPIC input a 2-stage low-pass (LP) filter is needed. The 1st LP filter stage consists of an off-chip ferrite bead in series with the signal line and an on-chip capacitor (of small capacitance and small series resistance) bypassing the remaining RF power to "ground".
  The 2nd LPfilter stage consists of an on-chip 1st order RC-filter to further damp the RF or MW power and avoid demodulation by the LNA on the ASPIC (or by the PMOST on the microphone IC).
  If the design of the 1st stage of the LP-filter is well done the ESD protection diodes cannot demodulate the RF signal and the2nd LP filter stage is effective.
  To make a really good 1ststage LP-filter design it is mandatory to know more about the RLC parasitic circuits of the Hybrid, the ASPIC (or microphone IC) IO-pads and about the PMWA output impedance. The latter can be roughly measured over a coaxial cable with a NWA. (The effect of the coaxial cable and its connections to the Hybrid pads must be

taken into account by applying the de-embedding method we used throughout this work.)

Reference

[1] Wikipedia contributors. "Electromagnetic compatibility." Wikipedia, The Free Encyclopedia. Wikipedia, The Free Encyclopedia, 11 Feb. 2016. Web. 15 Mar. 2016.

[2] Julstrom, S. D., L. K. Kozma-Spytek, and B. B. Beard. "Radio frequency immunity testing of hearing aids." *Electromagnetic Compatibility Magazine, IEEE* 2.2: 69-81.

[3] HI EMC standards IEC 60118-13 ed. 3 (by https://webstore.iec.ch/) and ANSI C63.19-2011 (by https://webstore.ansi.org/)

[4] European Hearing Instrument Manufacturer Association. "Electromagnetic Compatibility; Hearing Instrument RF Interference Analysis, Annual Technical Report, V2.2." EHIMA/HIA, Mar. 2010.

[5] Circuits, Integrated. "Measurement of Electromagnetic Immunity, 150 kHz 1 GHz, Part 4: Direct RF Power Injection Method." *International Electrotechnical Commission Standard IEC* (2006): 62132-4.

[6] Hui, Ping. "Application of GTEM cells to wireless communication transceiver designs." *Microwave Journal* 46.9 (2003): 168-170.

[7] Alaeldine, Ali, et al. "A direct power injection model for immunity prediction in integrated circuits." *Electromagnetic Compatibility, IEEE Transactions on EMC,* 50.1 (2008): 52-62.

[8] Keskinen, Kai. "Modeling a Ferrite Bead on High Speed Serial Links." (n.d.): n. pag. Ferrite Bead on HSSL Links. Coresim, 14 Apr. 2004. Web. 31 Jan. 2015.

[9] Rostamzadeh, C., F. Grassi, and F. Kashefi. "Modeling SMT ferrite beads for SPICE simulation." *Electromagnetic Compatibility (EMC), 2011 IEEE International Symposium on*. IEEE, 2011.

[10] "Microwave Office" RF/Microwave Circuit Design Software. National Instruments.

[11] Goedbloed, Jasper J. *Electromagnetic compatibility*. Vol. 1. 1992.

Appendix

A. Cubicle and manipulator setup

In this section we show some pictures of the tools which were used to perform the measurements accuracy. of the Julstrom method. Please see Fig.66, Fig.67 and Fig.68.

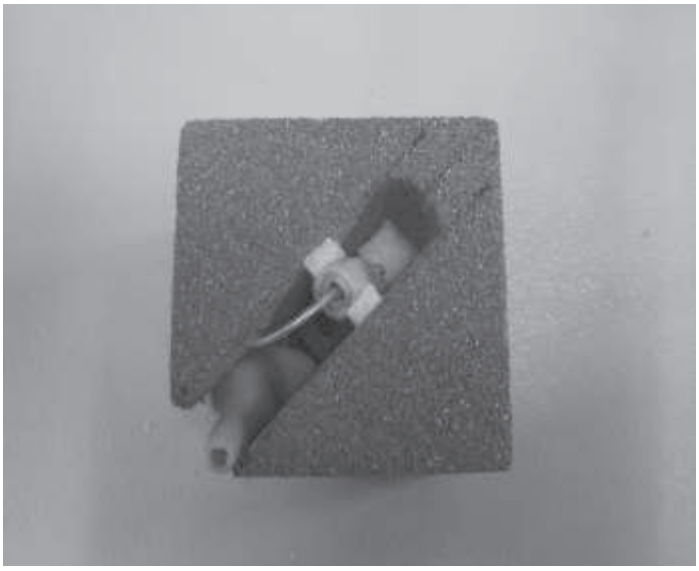


Fig.66. Golden Unit HI mounted inside a cubicle



Fig.67. Cubicle orientations

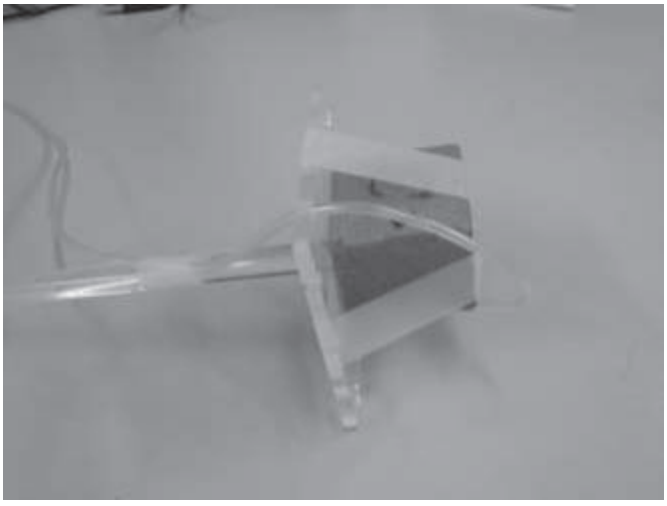


Fig.68. Cubicle mounted on a plexiglass plate with manipulator rod

B. Input circuit of microphone

We needed to extract the simulated microphone input circuit from its physical structure. As we mentioned before, sonion were not able to provide detailed

information about the microphone schematic and its parasitic behavior. Therefore, as a work around, the used microphone was opened in order to get an idea about the physical structure of the circuit inside. For details see Fig.69, Fig.70 and Fig.71.

The physical structure and the used components have been subsequently modeled and simulated as shown in the third and fourth chapter.

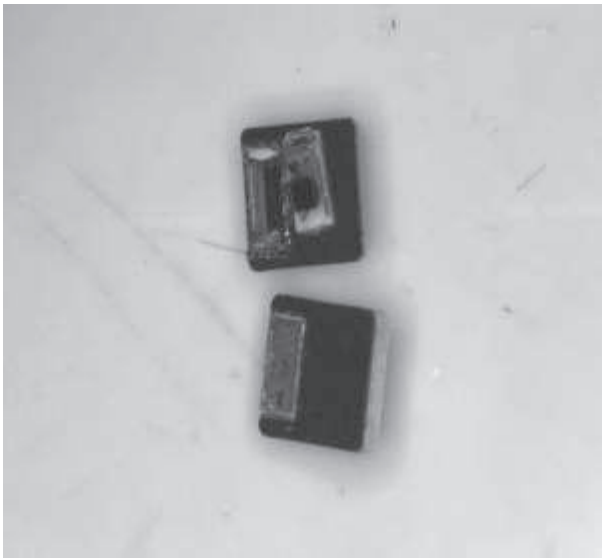


Fig.69. Opened microphone

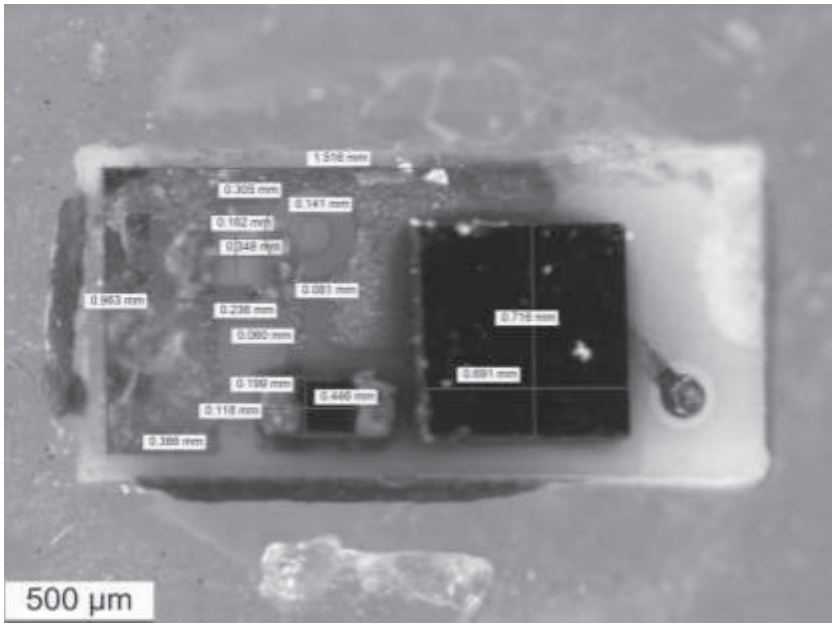


Fig.70. Microphone PCB layer 1

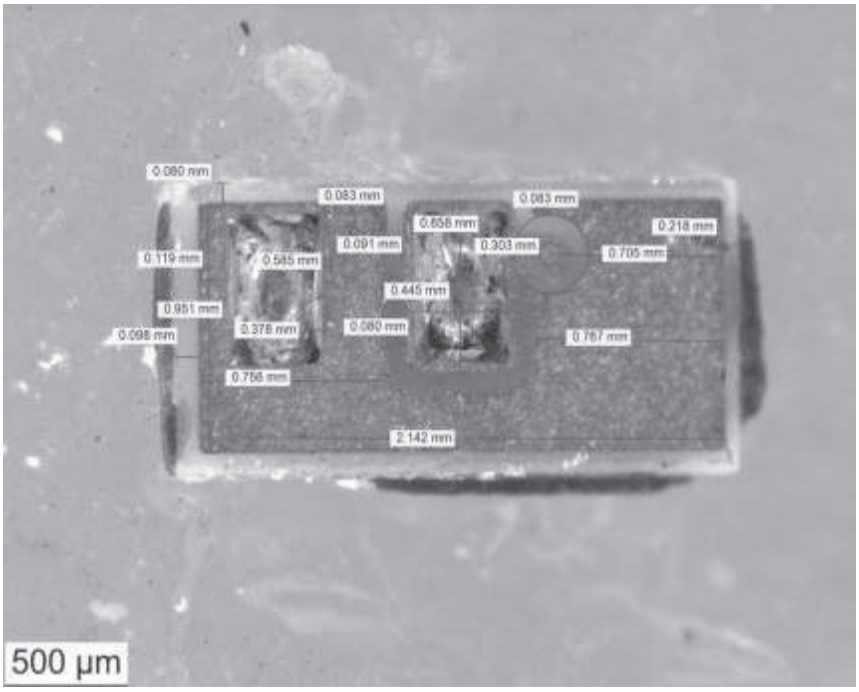


Fig.71. Microphone PCB layer 2

C. Voltage AC source of the artificial antenna circuit

The following steps were taken to calculate the voltage source AC component:

- Calculate the pure power on the antenna by using S21 with the GTEM calibration data.
- Calculate the complex generator voltage by using the following formula:

$$V_{emf}[V] = \left(\frac{Zo + Z_ant}{Zo}\right) * \sqrt{Zo * 10^{-3} * 10^{p_{corr}[dBm]/10}}$$

Where Z_ant is the measured antenna impedance, Zo is 50 Ω and p_{corr} is the corrected output power of the L-shape antenna delivered into a 50Ohm load.

The L-shape antenna is irradiated in the GTEM cell with an E-field of 50V/m.p_{corr} was corrected to this E-field value. For the correction please see the section “R. GTEM Cell Input Power Corrections:”.

D. ESD protection diodes

As it can be seen in Fig.72 we have ESD diodes in the integrated circuits. It is normal that these diodes start to conduct at high injected power. The conduction of these diodes can add some EMI noise to the original signal which appears at the output of the test boards. This can be seen in Fig.13 where the curve acts abnormally for injected power above - 2dBm. In the appendix "E. Simple ESD diode demodulation model for MIC1", the demodulation of ESD protection diode is explained in details. This type of demodulation also generates harmonics (i.e. the demodulated output is no longer a pure sinusoidal signal and a DC component as it can be seen in Fig.73. In this simple model for ESD diode demodulation only the 1st harmonic was considered. The DC component will be blocked in front of the LNA by an additional biasing network. Furthermore a transient simulation was done in LTSPICE. Fig.73 does not show the steady state response. It is superimposed by a slow transient caused by the large DC decoupling caps.

E. Simple ESD diode demodulation model for MIC1

Simulation model for MIC1 ASPIC input pad, created by A. Jakob (Sonova):

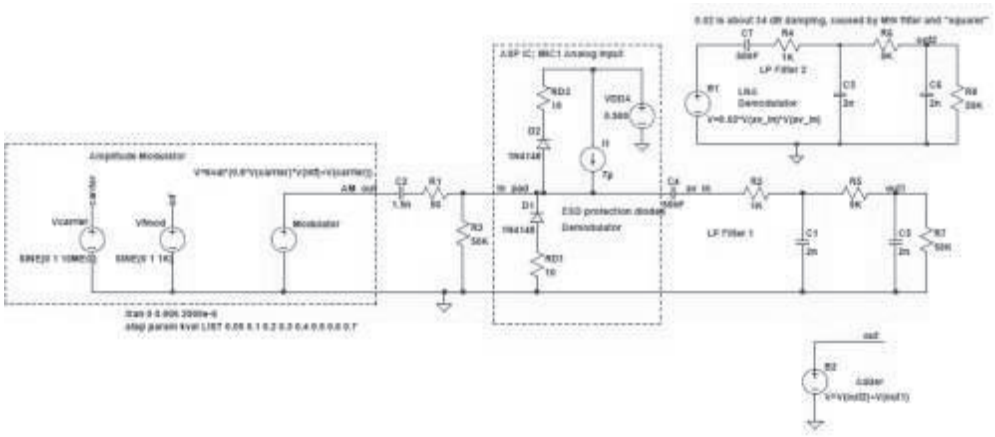


Fig.72. Demodulation caused by the ESD diodes together with a squarer

Note: I1 (= Id) is the DC biasing source.

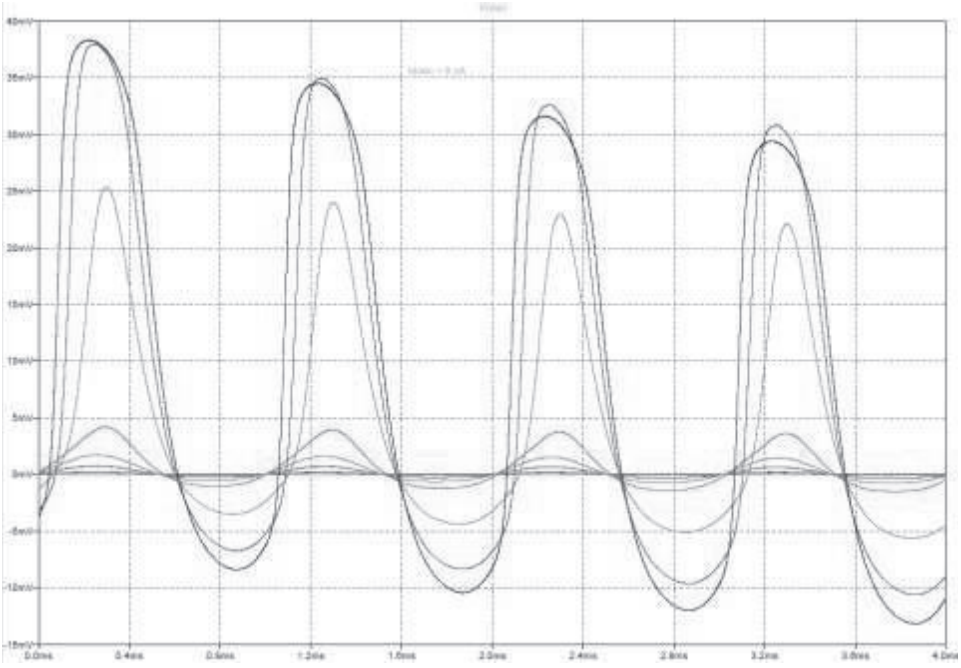


Fig.73.Vout, biasing with 8uA

In the above model (with schematic “asic_MIC1_input_pad_UHF_v23_Id_8uA”), the carrier input parameter “kval“ was stepped from 0.05 to 0.7. (or kval = -26 … -3 dB; with kval = 0dB the generator output RF carrier is equal to 707 mVrms or +10 dBm). In the 1st simulation run, I1 was chosen as 8uA and in the 2nd run, I1 was 7uA.
The 1KHz harmonics of the demodulated output for both vales of Idrain were plotted in a spread sheet. The results are given in Fig.74. In addition, the damping of the MW filter and the squarer were assumed to be 34 and 54 dB.

Conclusions: This rough demodulator model for the ESD diodes and the LNA show that the “demodulation ratio” of the ESD diodes combined with the LNA demodulator can change from 2:1 up to 10:1 when the ESD diodes start to conduct! That is exactly what we wanted to show.
Furthermore we can see that ESD diode demodulation starts with an RF level of about > - 4 dBm (or > -17 dBV).
This is in quite good agreement with the DPI output measurements where we got large distortion for an RF input level of > - 4 dBm.

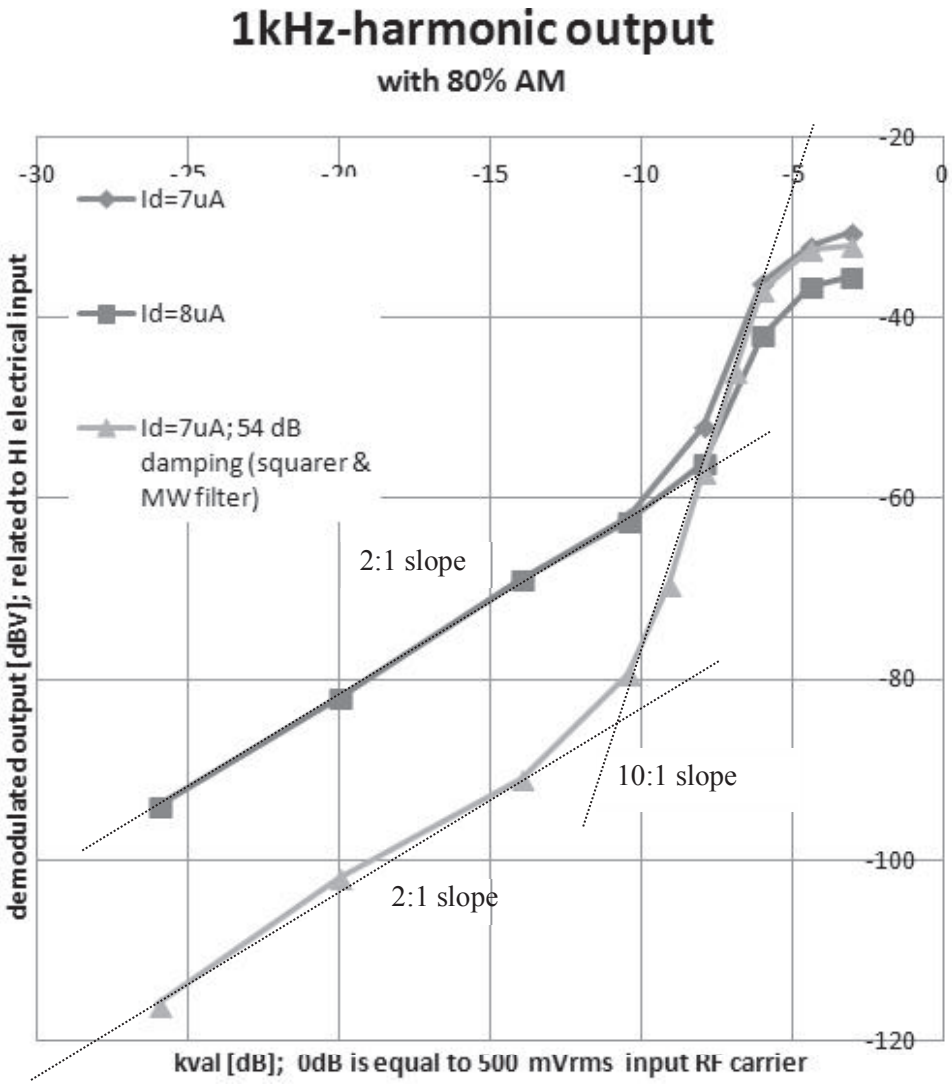


Fig.74. 1KHz-harmonic output

F. Network Analyzer Calibration

We observed some unexpected results after applying the R&S Calibration Kit ZV-Z132, 3.5mm, 50 Ω, female.

After finishing the calibration, we expected a single point in the center of the Smith Chart when we connect the match port of the calibration kit, and a point in the farthest left to the center point when we connect the short port of the calibration kit. We should also get a point at the farthest right from the center point, when we connect the open port of the calibration kit.

In our case, we got a strange behavior when we connect the open or short port of the calibration kit. As you can observe from the picture below (Fig.75), the Smith Chart shows a line instead of a point.

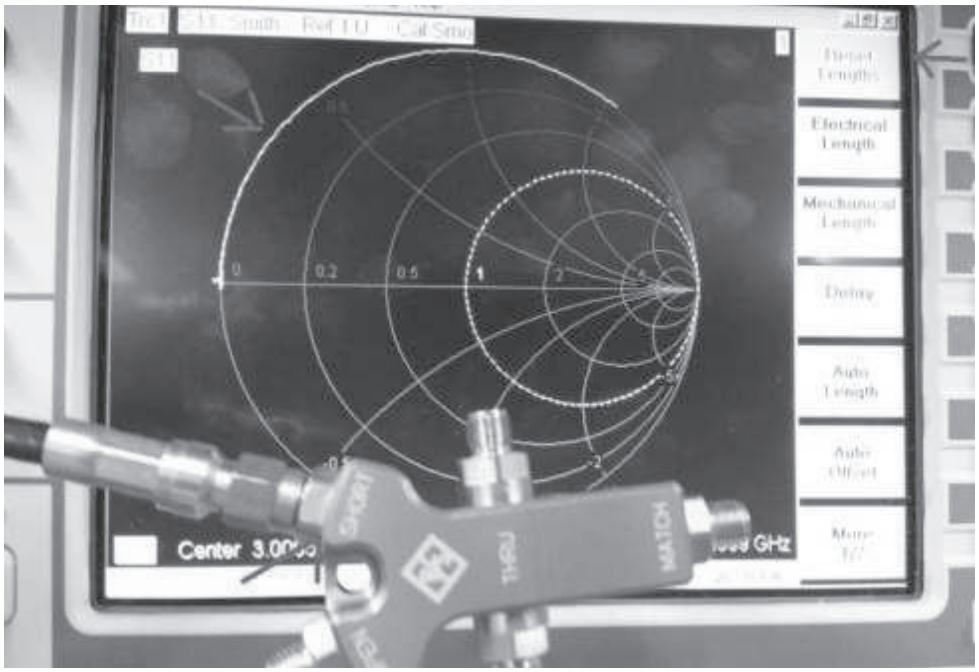


Fig.75. Checking the Smith Chart directly after the calibration.

We corrected this result by port extension or by correcting the length of the calibration.

The port extension is done by pressing the “Auto Length” button on Fig.76 below. The improvement (compared to the above picture) can be seen in the picture below (Fig.76), which shows a normal short circuit connection.

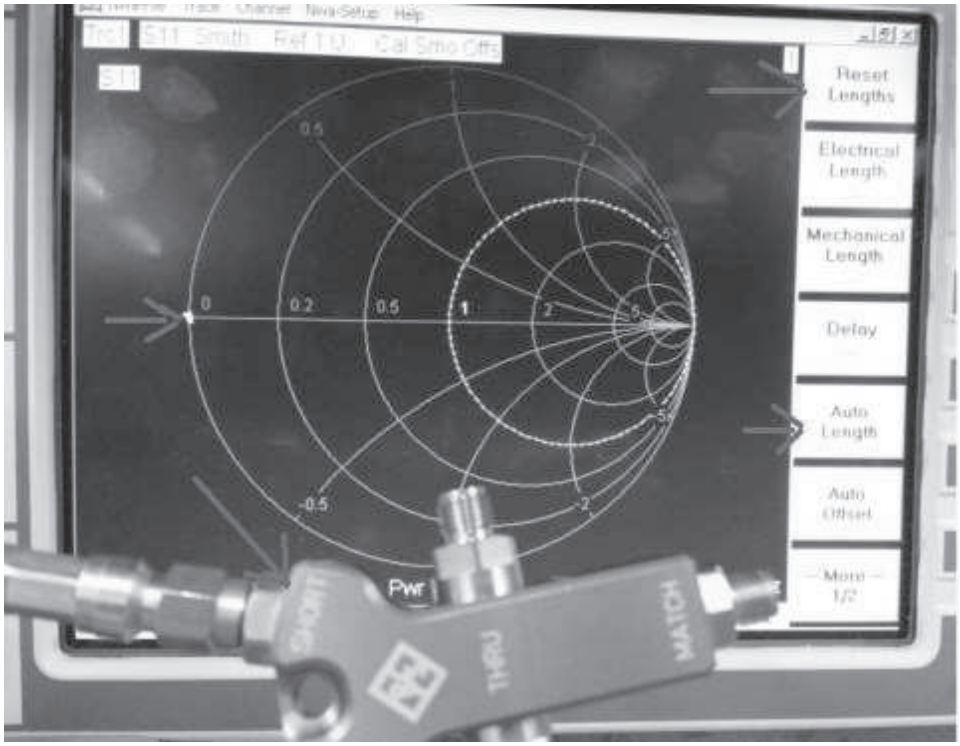


Fig.76. Port extensions

G. Tcoil (or Telecoil)

This HI component was used in a distinct Hybrid connection called TCOILN&P. The Hybrid connection was measured by the DPI method and the next step was to create an electrical model of this connection which in turn, required finding a suitable electrical model for the Tcoil component.

The component was studied by taking impedance and S11-parameter measurement and then an equivalent circuit was proposed. It was not enough to only use one circuit for this component because the complexity of the circuit increased with frequency.

We created two matched circuits. The simpler topology was used for the first frequency range (50 MHz - 1 GHz), see Fig.77. For higher frequencies, a more complex topology was required, see Fig.78.

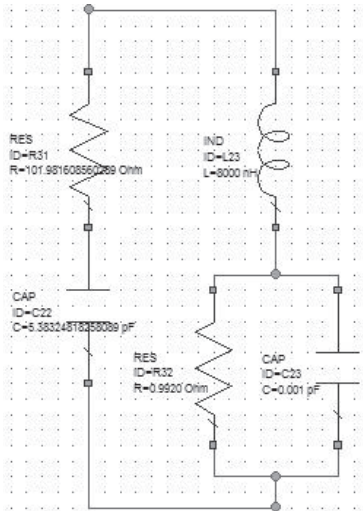


Fig.77. Simple Tcoil topology for frequency range between 50 MHz - 1 GHz.

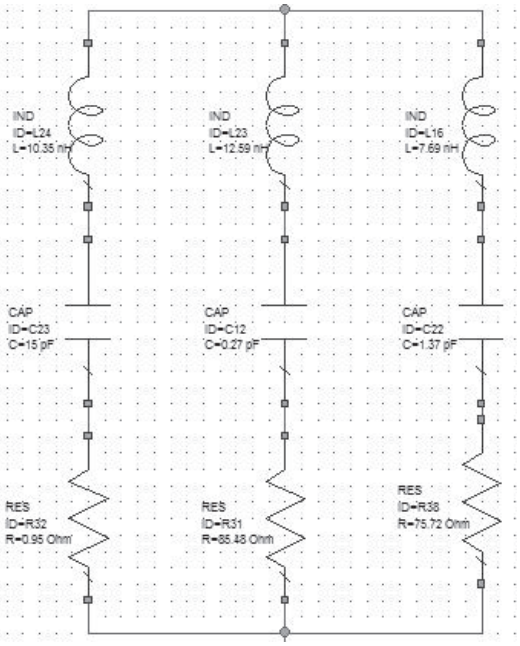


Fig.78. A more complex Tcoil topology for frequency range between 1-6 GHz.

We used AWR software to match the measured impedance magnitude and phase with the proposed electrical circuit. In Fig.79, you can see an example of how the matching was done using AWR.

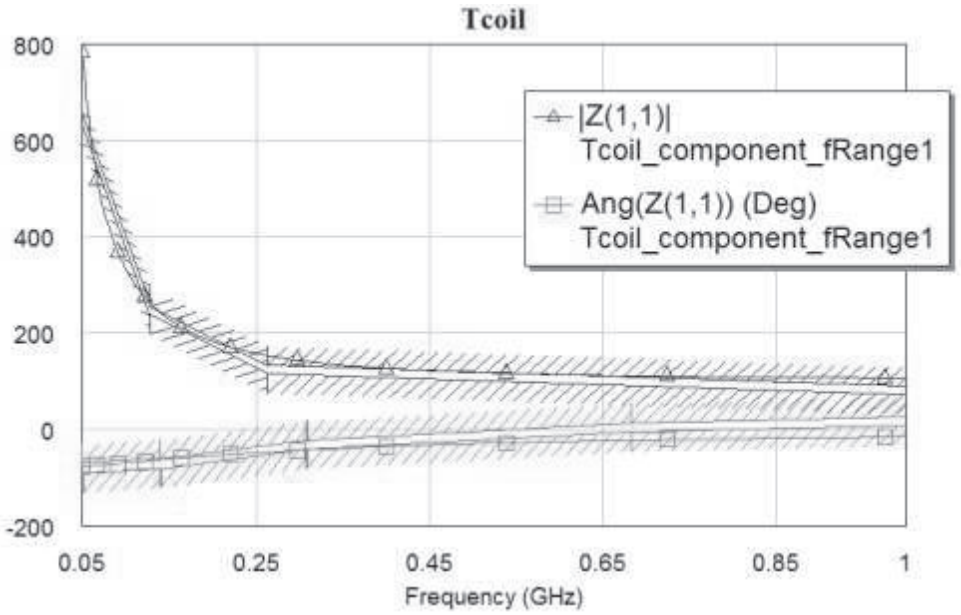


Fig.79. Matching of the Tcoil impedance for f-Range1.

Note: The matching of the impedance magnitude and phase of the Tcoil component for frequency range 1 (between 50 MHz - 1 GHz) is shown above

H. 3D-EM models and interconnections

It was difficult to represent certain parts of the Hybrid PCB as a lumped element RLC circuit because of the folded structure which makes parasitic estimation impossible. Therefore, it was more convenient and accurate to create a 3D model and then implementing it as a sub circuit in the LTSPICE model. The 3D-EM model was created and simulated in CST MW by Javier Abadia (Phonak Comm. Murten). The simulation output consisted of S-parameter files for all requested ports on the Hybrid PCB.

The Fig.80 shows the structure of the 3D- model which was used for the simulations in CST MW implementation.

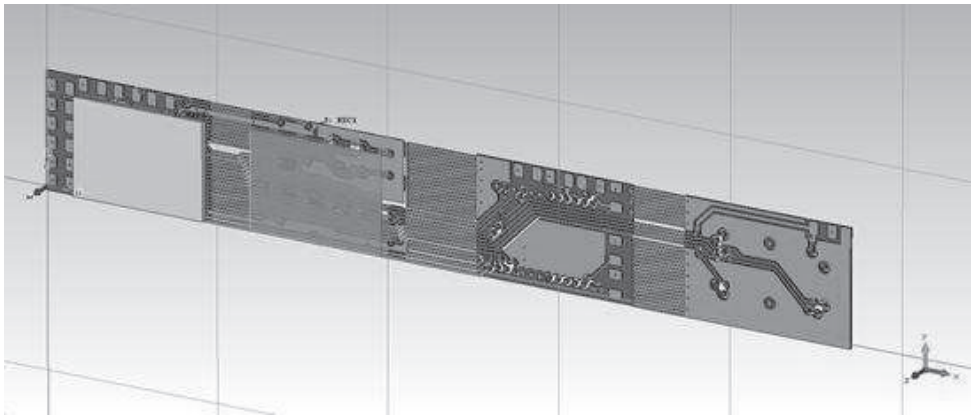


Fig.80. 3-D model of part in the Hybrid test board

I. Converting from S11 parameter to impedance

We can start with the equation which relates S11(S_{11}) to input impedance.

$$S_{11} = \frac{Z_{in} - Z_0}{Z_{in} + Z_0}$$

Where Z_{in} is the input impedance and Z_0 is usually 50 Ω.

Solve Z_{in} equation:

$$Z_{in} = Z_0(\frac{1 + S_{11}}{1 - S_{11}})$$

Define the real and imaginary parts of the input return loss parameter:

$$Z_{in} = Z_0(\frac{1 + R + jX}{1 - R - jX})$$

R represents the real component and X represents the imaginary component.

Define the conjugate and then multiply it with the original equation:

$$Z_{in} = Z_0(\frac{1 + R + jX}{1 - R - jX})(\frac{1 - R + jX}{1 - R + jX})$$

$$Z_{in} = Z_0(\frac{1 - R^2 - X^2 + j2X}{(1 - R)^2 + X^2})$$

The real component of the input impedance becomes:

$$Z_{in}(Real) = Z_0(\frac{1 - R^2 - X^2}{(1-R)^2 + X^2})$$

The imaginary component of the impedance becomes:

$$Z_{in}(Imaginary) = Z_0(\frac{j2X}{(1-R)^2 + X^2})$$

J. Creating the DPI voltage AC source

The main idea is to create for the electrical RLC (or LTSPICE) models a similar environment as we have in our DPI measurements. Therefore, we used the same input power as in DPI measurement after applying some correction to it.

In our study we used 10 test boards, 5 of them are used for Hybrid measurements and 5 for microphone measurements. The DPI measurements were applied for each test board with six different amplitudes. The amplitudes, which we used in our measurements, were [-18, -12, -6, -4, -2, 0] dBm.
From these amplitudes, we chose the DPI measurement with-6 dBm amplitude to be the input in our simulated model with LTSPICE. The RF output (in front of the demodulator on the IC) of our simulated circuit was compared with the acoustical output of our -6 dBm DPI measurements.

The formula to calculate the input voltage of the electrical models is:
CircuitInputVoltage [dBV] = PowerGenerator [dBm] - LossyCable [dB] - DirectionalCouplerInsertionLoss [dB] – CouplerCapacitor [dB] + 6 dB – 13 dB

Defining each term in the equation above:

Generated power: is saved during the DPI measurement and the data can be retrieved from the saved measurement file.

LossyCable : An equation which calculates the lossy coaxial cable (S_04212_B) attenuation can be found in the cable datasheet. The formula is as follows:

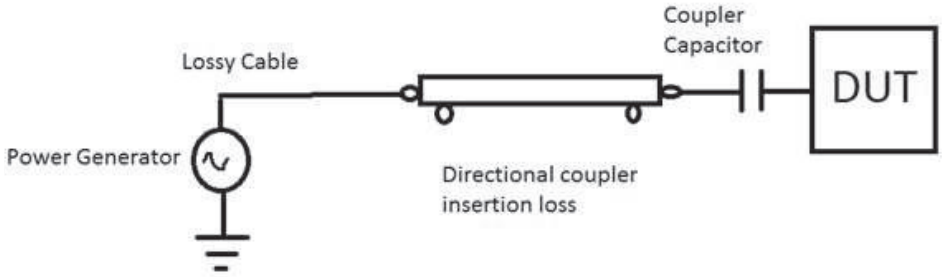
$$Attenuation = a * \sqrt{f} + b * f$$

Where a and b are coefficients, and their values is a = 0.197 and b = 0.045.

DirectionalCouplerInsertionLoss: we can measure the insertion loss of directional coupler using a network analyzer, see appendix (Directional coupler measurement).

CouplerCapacitor: From the datasheet of the coupling capacitor (Agilent 11742A), they have mentioned the maximum power loss in the frequency range between (45MHz to 12.4 GHz) is 0.35 dB. The frequency range we use in our measurement is between 50MHz to 6 GHz. We took 0.25 dB as average constant loss for our coupler capacitor.

Please see the illustration picture below:



Term (– 13 dB): We use this constant value to convert the unit of the calculated value from the power and voltage unit dBm (referred of 50 Ω) to voltage unit dBV(referred of "zero" Ω) . To do this conversion we only need to subtract the value of 13. Because:

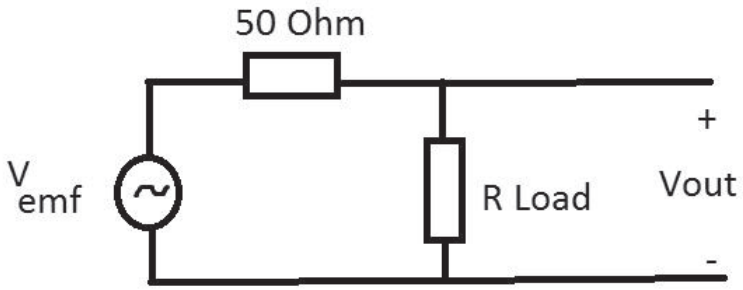
$$0\ dBm = -13\ dBV\ at\ 50\Omega$$

Term (+ 6 dB): We should also include the electromotive force in our calculation. Which conclude that we have to add 6 dB to our output voltage, when we have the same source and load resistance.

The formula which represents the electromotive force is:

$$V_{out} = V_{emf} - 6\ dB$$

The next picture represents the circuit situation:



Now, the calculated data can be used to create LTSPICE sub circuit for Vemf which works as voltage source.

K. Directional coupler measurements

The S-Parameters of two Directional Couplers were measured by using a Network Analyzer. The measured S-Parameters were: $S_{11}, S_{12}, S_{21}, S_{22}, S_{13}, S_{24}, S_{33}, S_{44}$

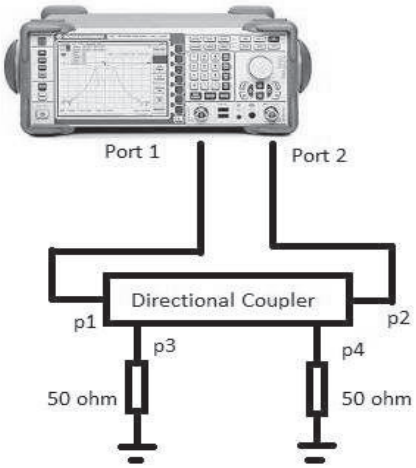
The directional coupler is a very important component for performing DPI measurements. With this component you can measure the forward and reflected power.

To perform the DPI measurement, the program (both methods, see chapter 3) needs to do some calculation for the transmitted power. Therefore, the program needs information about the power loss between the different directional coupler ports.

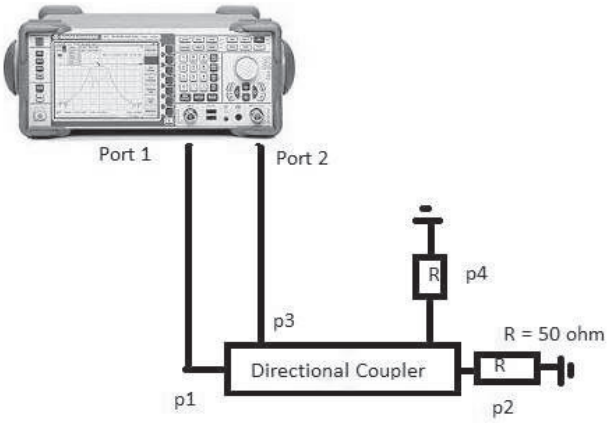
The network analyzer was used to measure the coupling/damping between the needed ports and the saved data was used later to calculate this transmitted power after measuring the forward or reflected power.

Taking measurement for different ports in the directional coupler required different connection/setup. The following diagrams show how the connections should be to get different port measurements.

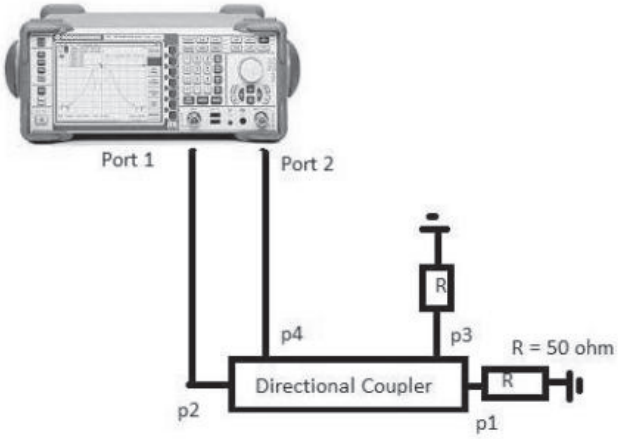
Setup for $S_{11}, S_{12}, S_{21}, S_{22}$ measurements



Setup for S_{13}, S_{33} measurement:



The setup for S_{24}, S_{44}measurement:



The following figures show the S-parameter measurement results of directional coupler MC 05122-20.

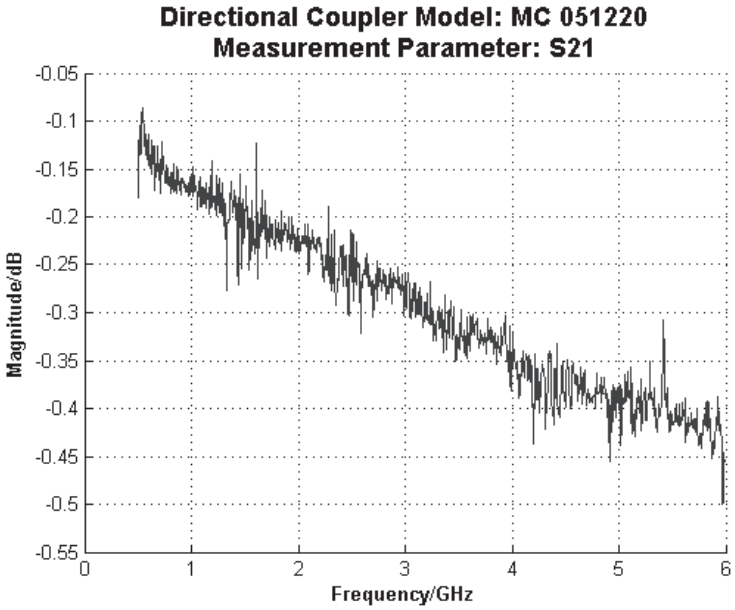


Fig.81. S21 parameter of the directional coupler

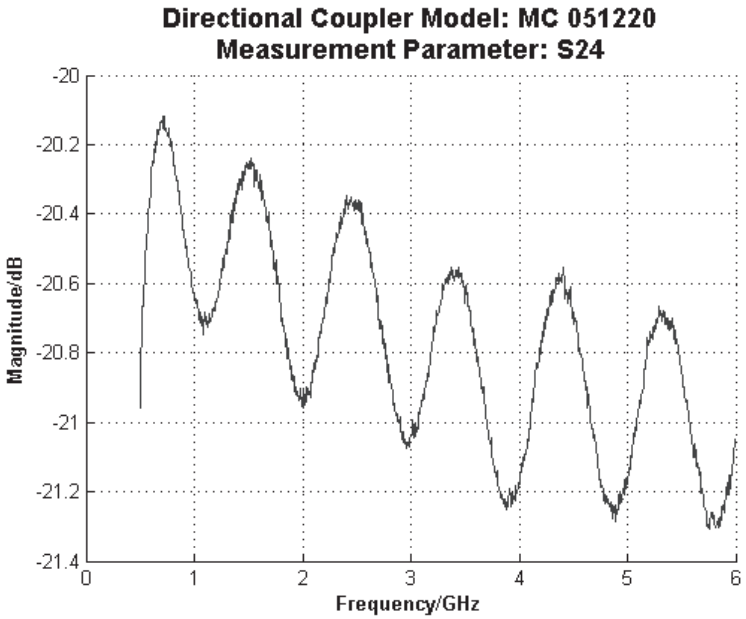


Fig.82. S24 parameter of the directional coupler

L. Ferrite bead model BLM18AG471SN1D:

The ferrite bead component was used to suppress high frequency noise in our test boards. The ferrite bead, which we studied, is BLM18AG471SN1D. These ferrite beads were used to model the microphone test board.

These components can have a complex circuit model, especially for high frequencies. Thus, it is important to investigate these components in more details to get an accurate final model for our test boards.

The following explains the way of measuring a ferrite bead (or any similar component) up to 6 GHz. We also show how to match a proposed circuit representing this component.

The study consists of three parts:

Part 1: Accurate impedance measurements

Measuring small components for high frequency can be very critical and challenging. Therefore, we tried to be as accurate as possible to get the best result.

In [9] a method is introduced to measure the impedance of a ferrite bead or any other similar component. To perform this method, we have to measure the impedance of an open SMA-connector (see Fig.85), short circuit SMA-connector (see Fig.84) and SMA-connector with the ferrite bead (see Fig.88).

Two formulas have been introduced in the article to calculate the component values for the proposed SMA-connector circuit, the formulas are as follows:

$$C_c \cong \frac{1}{2\pi f \,|\, Z_{in}^{open} \,|}. \qquad L_c \cong \frac{|\, Z_{in}^{short} \,|}{4\pi f}.$$

Where C_c and L_c represent the SMA-connector circuit components, f for frequency, Z_{in}^{open} and Z_{in}^{short} is the choosen values of the open and short circuit measured impedance. Choosing the right Z_{in}^{open} and Z_{in}^{short} depends on the following condition:

$$f << \frac{1}{2\pi\sqrt{L_c C_c}}$$

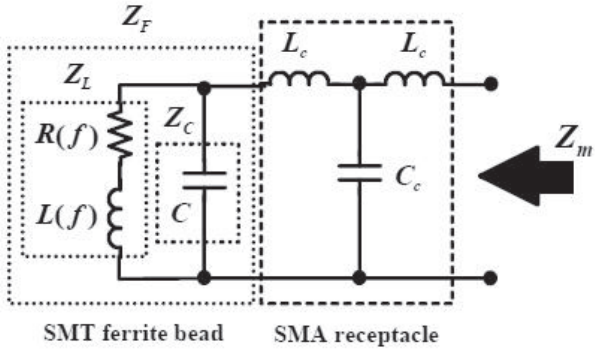


Fig.83. Circuit for a SMA connector with a simple ferrite bead.

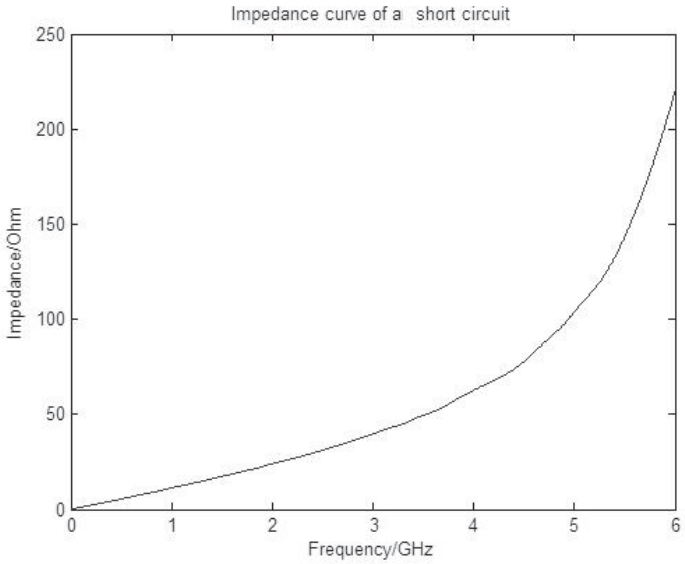


Fig.84. Impedance of a short circuit

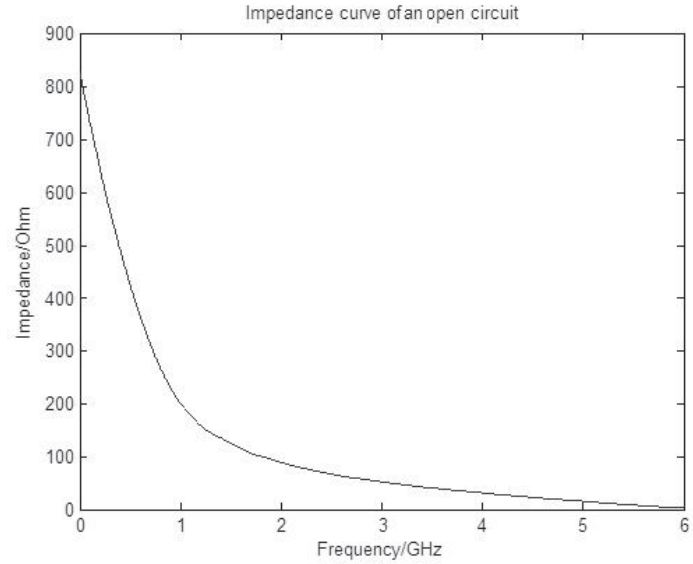


Fig.85. Impedance of an open circuit.

The calculated component values of the SMA-connector are used later on in another formula to calculate the impedance of the ferrite bead by extracting the effect of the SMA-connector impedance.

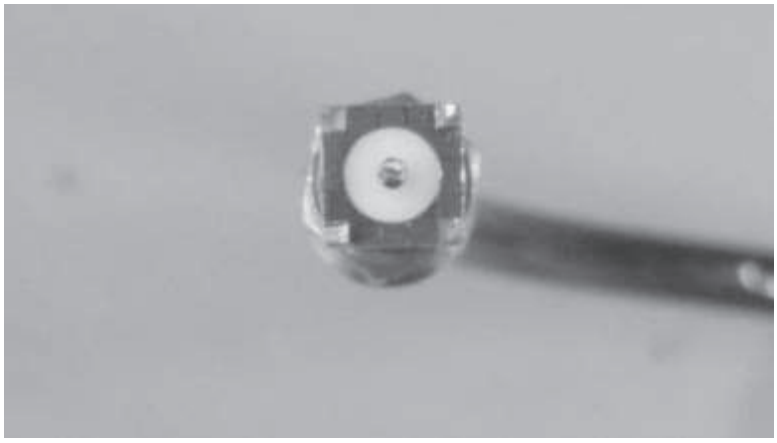


Fig.86. Open SMA-connector

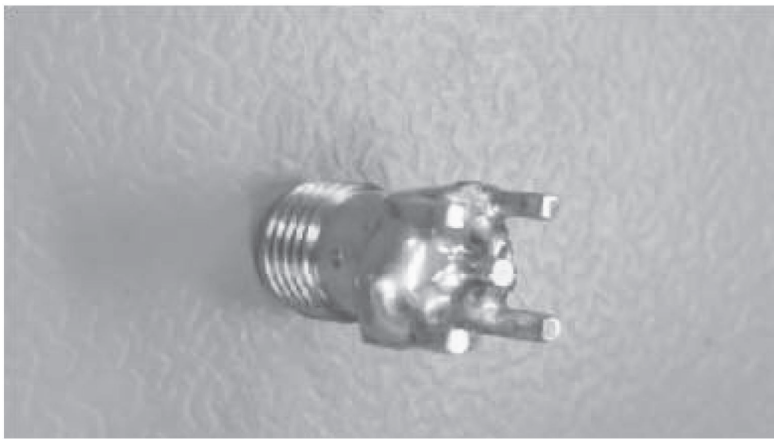


Fig.87. Shorted SMA-connctor

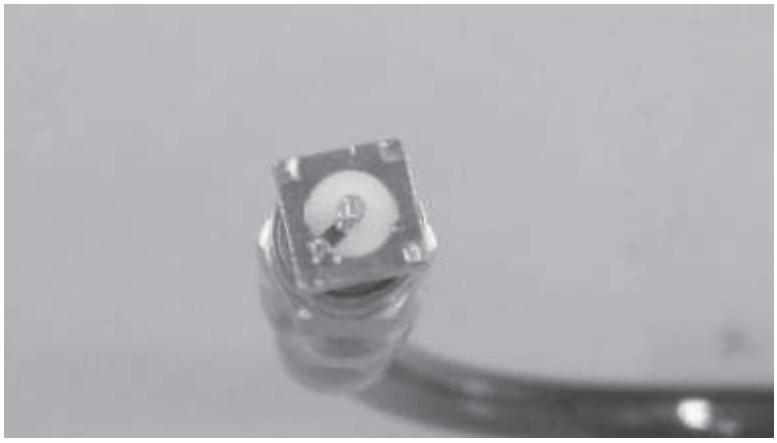


Fig.88. A ferrite connected to a SMA-connector

Using the SMA-connector to measure only one component can be a bit critical because of the signal absorption that can occur, see appendix (M. SMA-connector short circuit measurements).
For a further improvement and check, the de-embedding method was used. This method is called one-port de-embedding method.

This method uses S-parameter data to perform its calculations. We applied this method by creating a 2-port S-parameter file from the simulated SMA-connector circuit. We could estimate the component values of the SMA-connector, using the method described in [9]. Using these values, we can create a simulated model using LTSPICE, AWR[10] or any other equivalent software to retrieve an S2p file for this circuit. To extract the impedance of the connected circuit to the SMA-connector, we will also need to have the total impedance as S1p data format. Subsequently we apply the de-embedding by extracting the ferrite bead impedance from the two inputs above. The method is briefly illustrated in Fig.89.

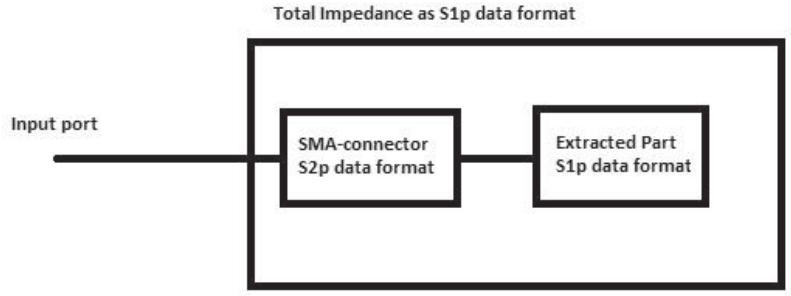
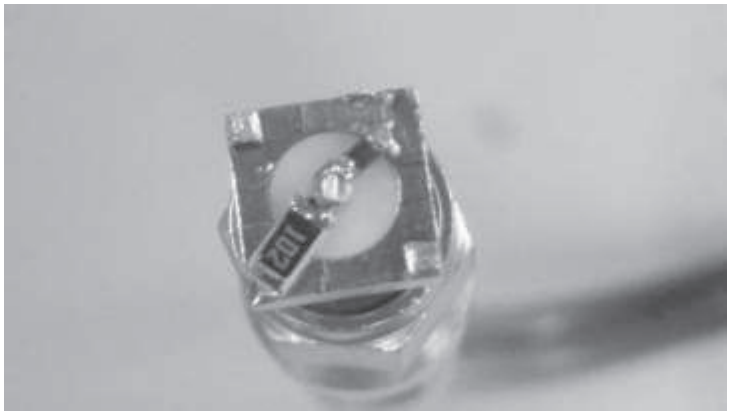


Fig.89. One port de-embedding idea

We mentioned before that measuring one component with SMA-connector is a bit critical. To get a higher accuracy, we added another component which is a resistor with 1 KΩ value, see the picture below.



After measuring the impedance of the connection above, we de-embedded the effect of the non-ideal resistor and the SMA-connector to get the ferrite bead impedance.

In the picture below (Fig.91), you will find the comparison between the ideal impedance of the ferrite bead (given in the data sheet) and the measured ferrite bead.

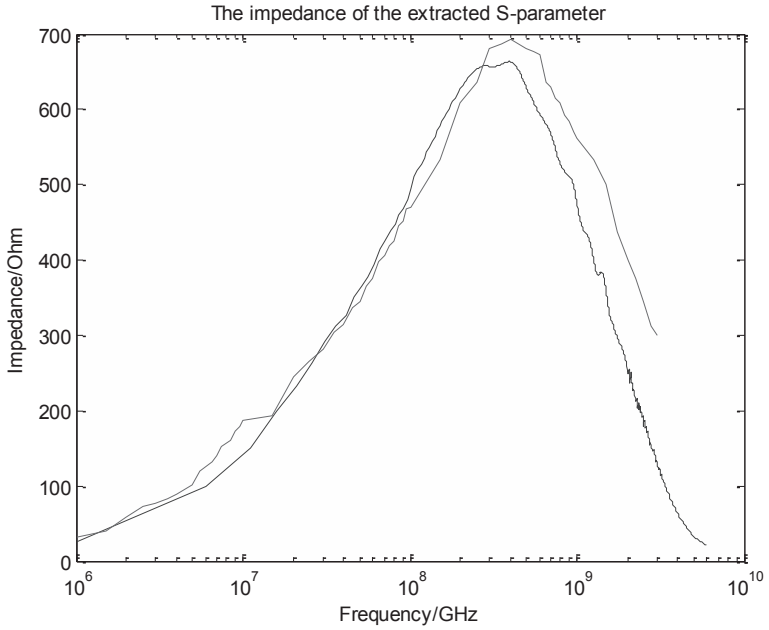


Fig.90. Comparison of ideal and extracted impedance of the ferrite bead

Note: The blue curve represents the simulated data, the red curve represents the data retrieved from the data sheet.

Part 2: Electrical circuit topology

A suitable circuit topology is important to give the same behavior as the measured impedance. At the same time, different topologies can give the same impedance behavior. However, it is safer to find a circuit topology which is close to our measured component. The best approach that we could find for our ferrite bead is a schematic diagram with lumped elements which was provided by Murata [8].

The complexity of the estimated ferrite bead circuit was not enough to give the best match. Therefore, we have added more components to the circuit in order to get a better impedance match. As a consequence the circuit complexity increases with frequency.

Part 3: Matching between measured and simulated ferrite bead

We need to choose the correct component values for the simulated circuit in order to get the right impedance behavior. Applying this task manually can be both difficult and time consuming, especially for large circuits.

As you will see in the next partitions we are using large and complex RLC circuits. Therefore, it was important to find an easier solution to perform the impedance matching for the used circuits.
To facilitate our work, we programmed an optimizer which had the ability to match between the impedance magnitude of the measured and simulated circuit. This program had some benefits in the beginning of the thesis to give an accurate impedance magnitude matching.

In the beginning, we thought we can make models which cover the whole frequency range which we studied, but later on, we found that it was impossible to get a matching for the large frequency range (50 MHz – 6 GHz). Therefore, we divided the frequency into three ranges. The new frequency ranges for the circuit models were: 50MHz – 1GHz, 1 GHz – 3 GHz and 3 GHz – 6GHz.

Fig.91 shows a good matching result.

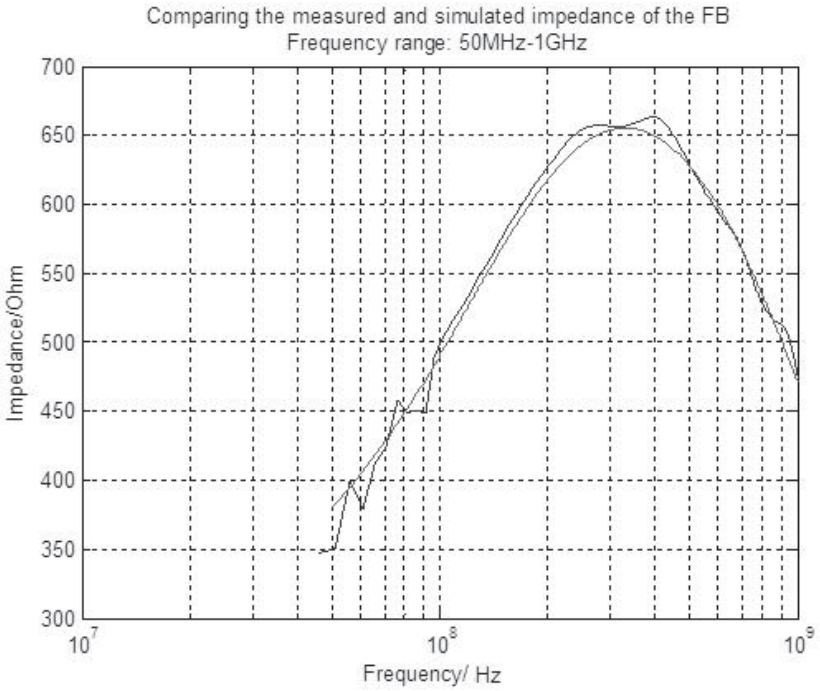


Fig.91. Impedance match of measured and simulated ferrite bead data, frequency range 50 MHz - 1 GHz.
Measured: blue curve, simulated: red curve

After simulating some final test board circuits, we did not get the results we expected. As a further improvement and investigation, we tried to find other parameters to improve the electrical circuits. Two more parameters were included later on; the impedance phase and the magnitude of the S11. We performed the S11 magnitude matching only for some of the test board models.

As we mentioned before, the program we created could only match the magnitude of the impedance. It was time consuming to create a program which did this job. As an alternative, we found a program which was able to perform circuit optimization for the impedance magnitude AND phase AND S11 magnitude, the program is called AWR. AWR provided us with a free demo version for students.

The next figures show the new matching with both magnitude and phase of the measured impedance:

We first needed to measure the impedance magnitude, see Fig.92 and then the impedance phase, see Fig.93. A mask was created in AWR for these measurements (impedance of the magnitude and phase), see Fig.94.

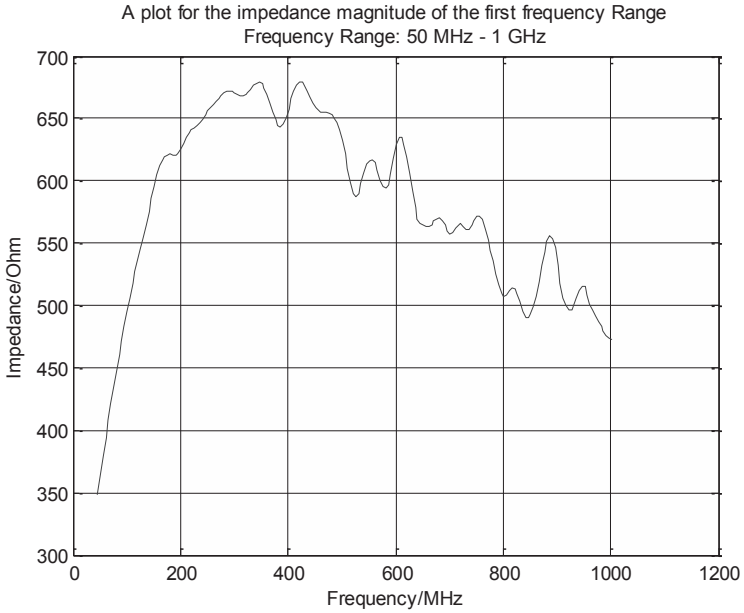


Fig.92. Impedance magnitude

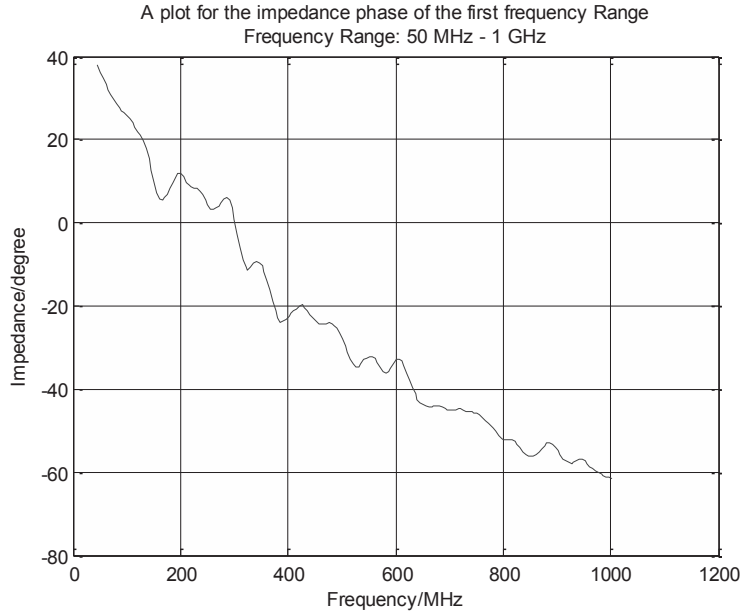


Fig.93. Impedance phase

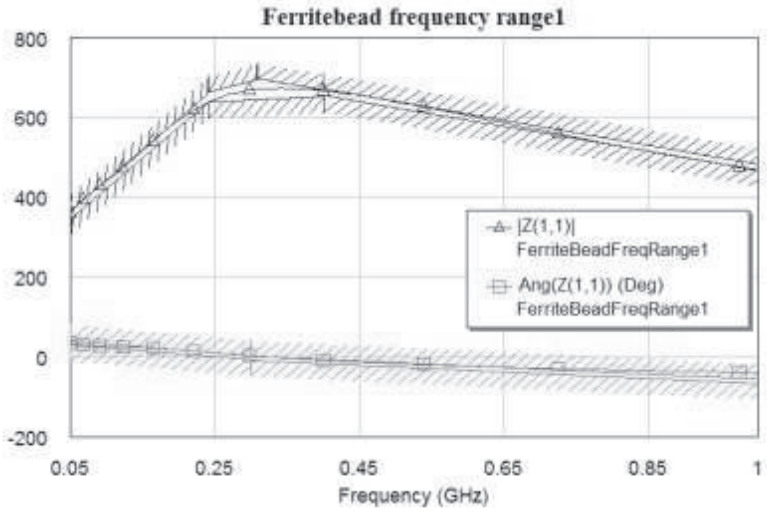


Fig.94. Adjusting the impedance magnitude and phase

The optimized circuit of the ferrite bead is shown in Fig.95.

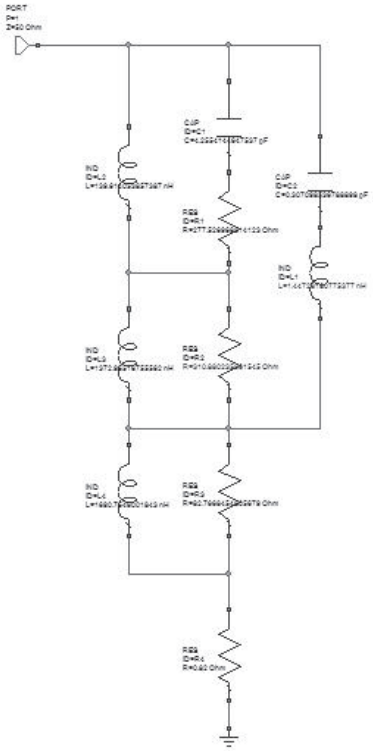


Fig.95. Ferrite bead circuit

M. SMA-connector short circuit measurements

It is important to have an accurate electrical model. Therefore, we need to get a better estimation for the impedance of the ferrite bead we are using in a larger frequency range. This will help to achieve a better circuit model with more accurate component values.

We use a SMA-connector to measure the ferrite bead. According to [9] "Modeling SMT Ferrite Beads for SPICE Simulation", we need to measure the short circuit version of the SMA-connector, which is used to calculate the inductor inside the SMA-connector.

We tried to establish three different types of short circuits. See Fig.97, Fig.99 and Fig.101. The best result has been accomplished by the full conductive plane short circuit, in Fig.102. The reason for the better impedance curve with this model is because we are blocking any radiation or absorption that could occur between the center and the ground of the SMA-connector.

The worst accomplished result was measured by the one pin short circuit model in Fig.98. The main reason is the non-damped electromagnetic waves which are absorbed from outside in the place where no conductive object is connected, see Fig.97. As you can see from the Fig.96, better results were accomplished with two pins, because of the extra connected pin in Fig.99.

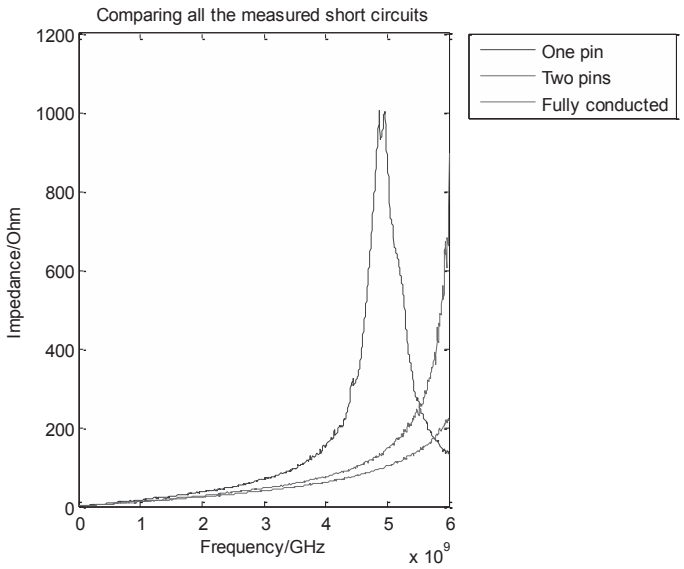


Fig.96. Different short circuit measurements

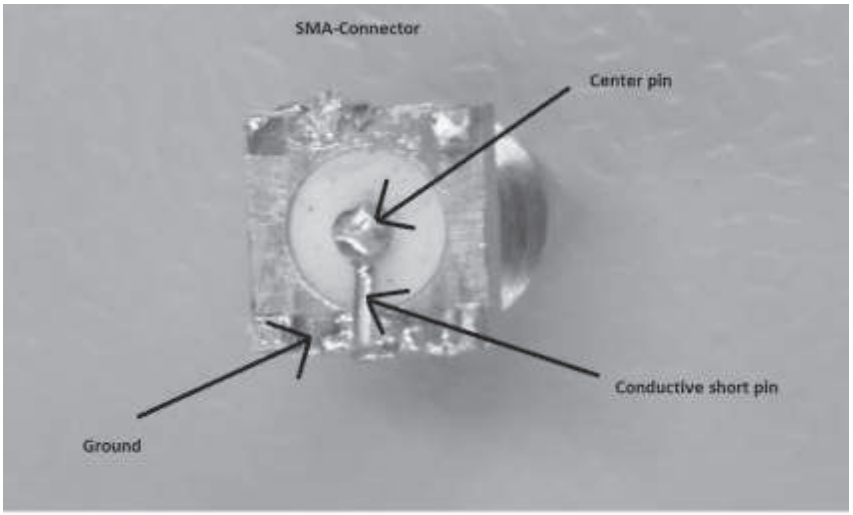


Fig.97. One conductive short circuit pin

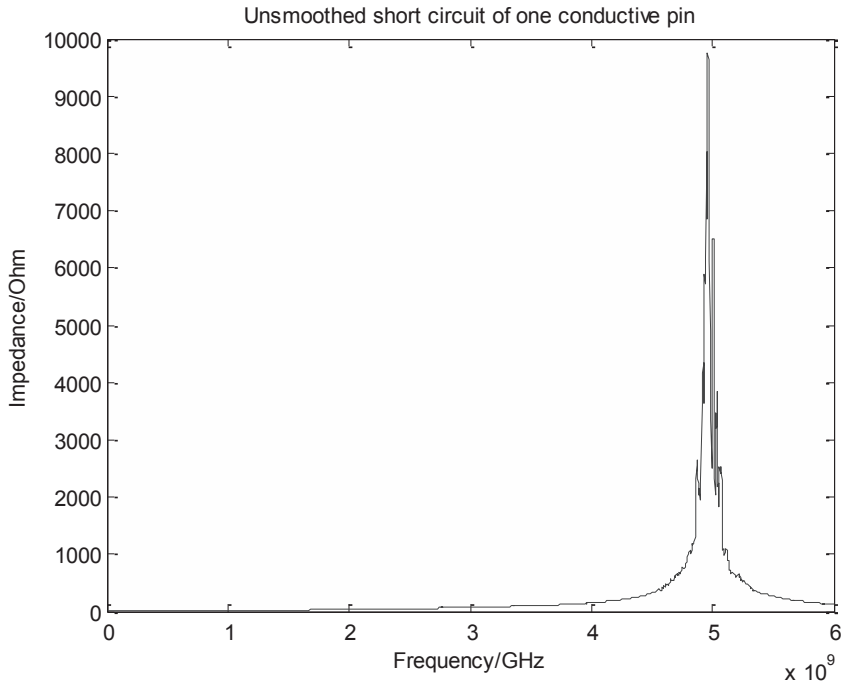


Fig.98. Impedance for a short circuit with one conductive pin

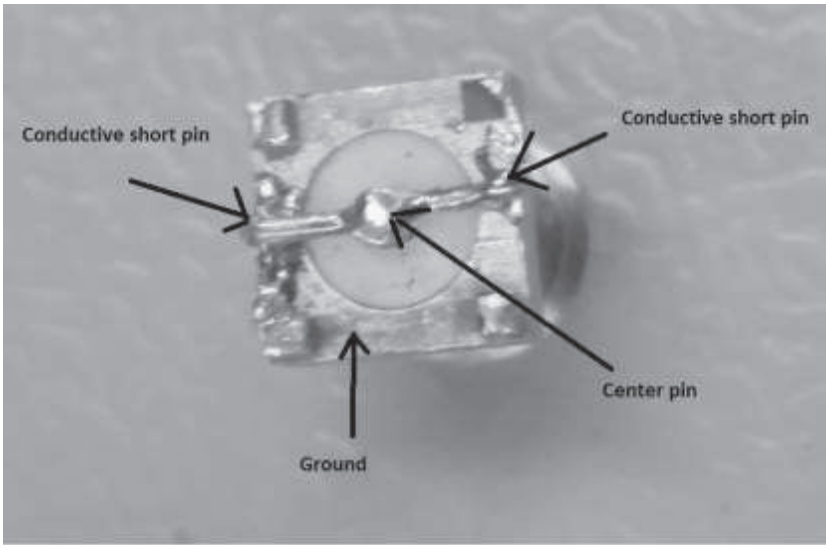


Fig.99. Two conductive pin short circuit.

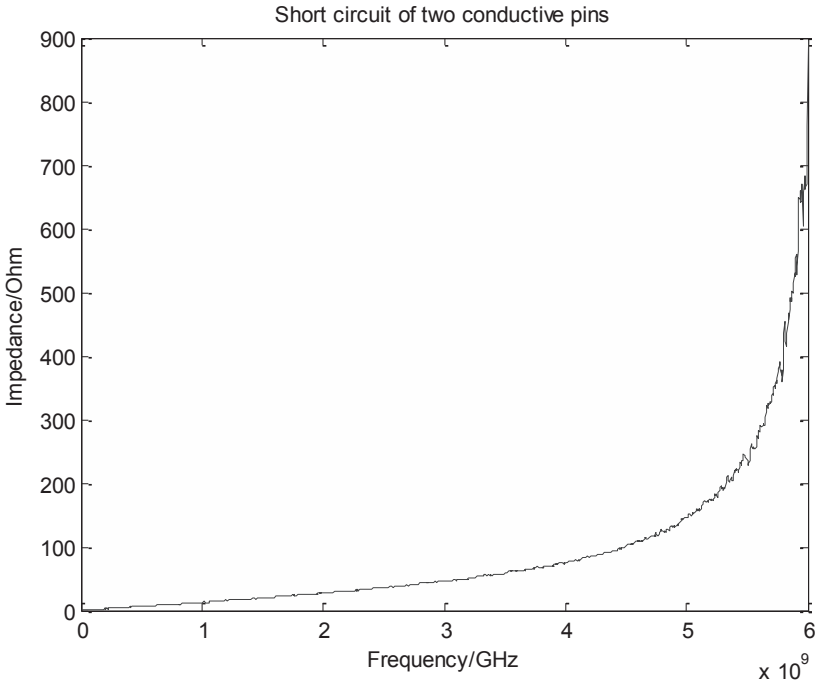


Fig.100. Impedance of a short circuit with two conductive pins



Fig.101. A very good short circuit for SMA-connector.

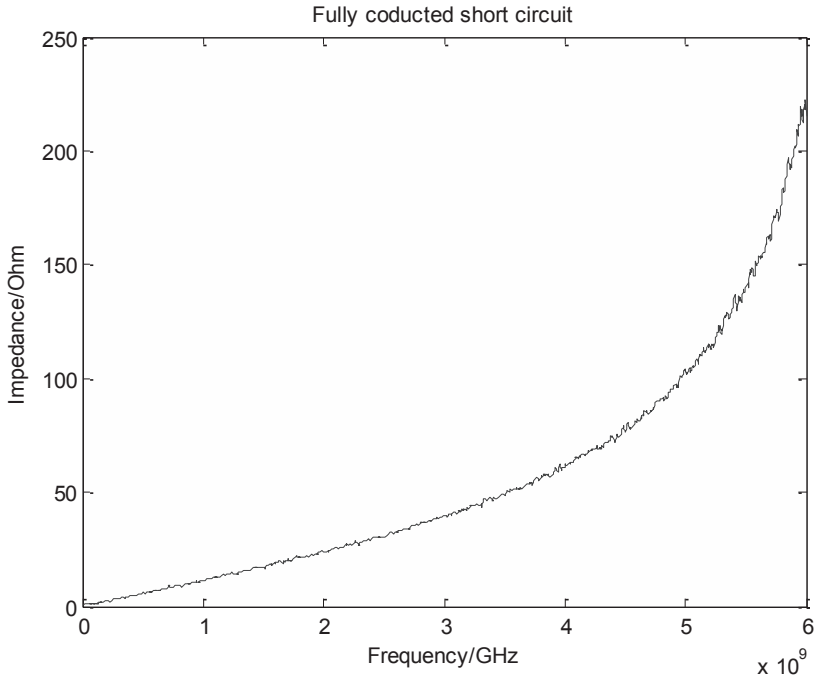


Fig.102. Impedanceof a short circuit with fully conductive pins

In conclusion, to create a very good short circuit SMA-connector, you have to shield the output of the SMA-connector by a conductive plane as shown in Fig.101.

O. Side effect of measuring reflected power, program 3

Implementing the DPI method this way did not really give good results. The main problem was very high peaks in the acoustical output behavior of the Hybrid test board. The high peaks are most probably caused by the measured reflected power. As we explained before, program 3 depends only on the difference between the incident and reflected power [7]. If the reflection value is very high (s11 close to 0 dB) at some frequency points the program tries to increase the incident power to overcome this problem. This can be the reason for these high peaks, but we cannot explain the large reflections, because we do not see them when we perform s11-parameter measurements with the network analyzer, see Fig.103.
The results of program 2 and 3 can be compared between Fig.104, Fig.105. The peaks can obviously be seen in Fig.104, which is the result of program 3, while there are no peaks in Fig.105, which is the result of program 2.

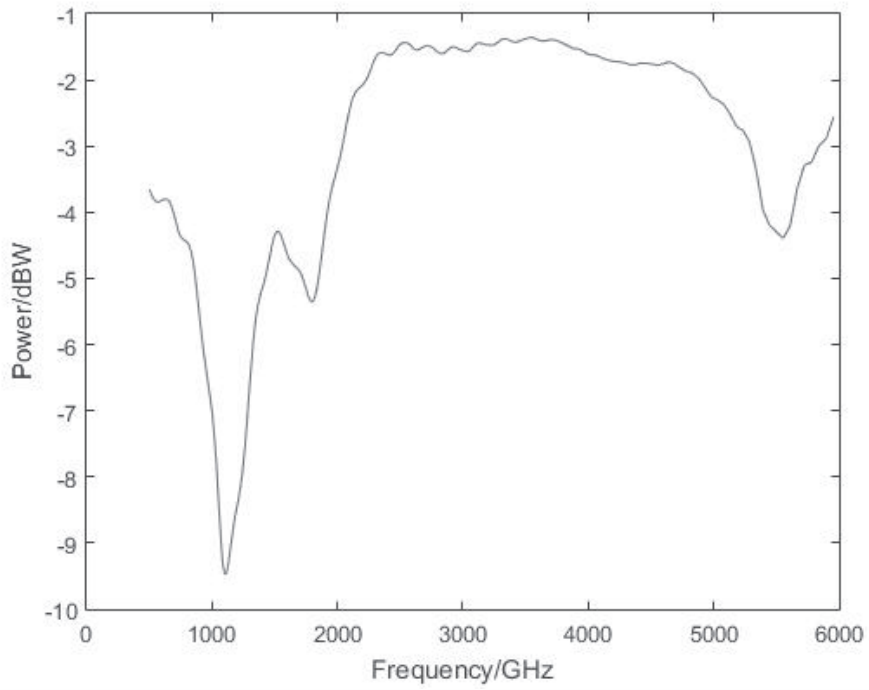


Fig.103. The s11-parameter measurement for Hybrid 2.

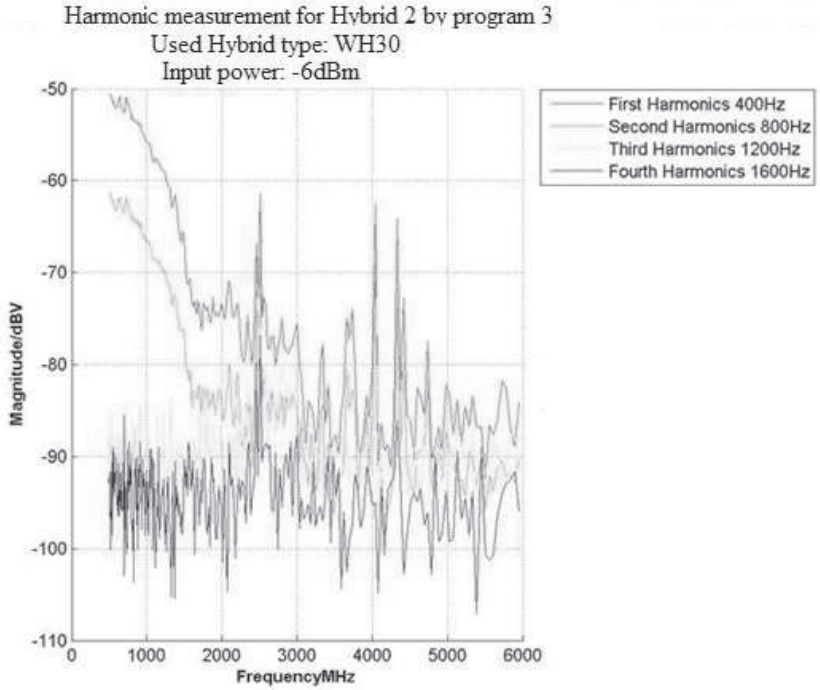


Fig.104. The result of using program 3

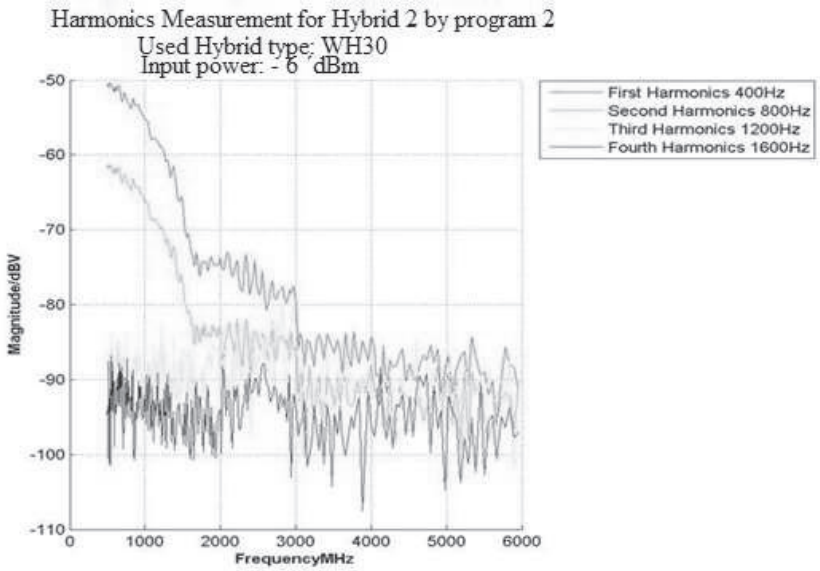


Fig.105. The results of program 2

P. Full frequency range

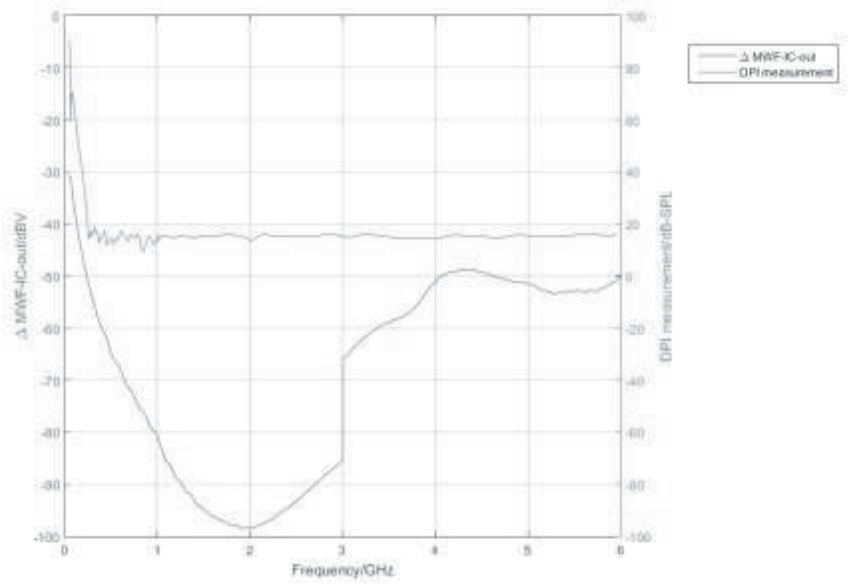


Fig.106. The full frequency range for Hybrid test board with TCOILN&P connection

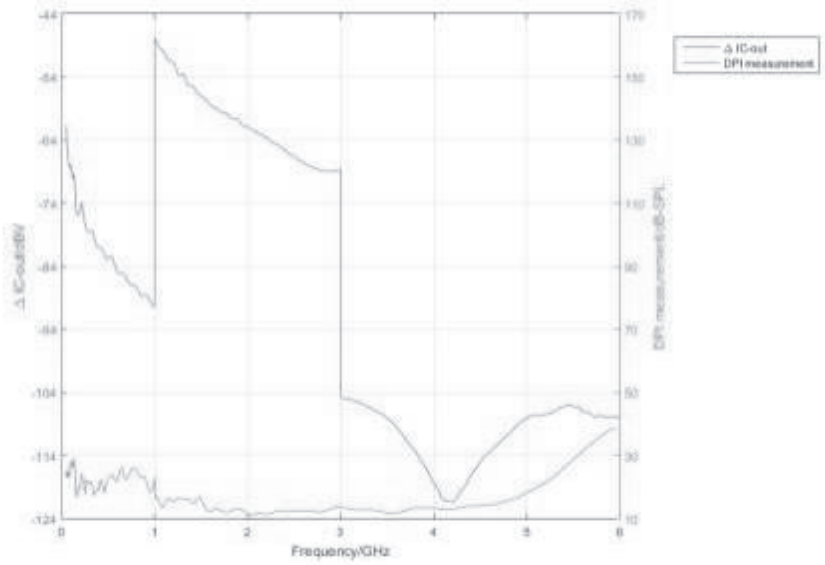


Fig.107. The full frequency range for microphone test board

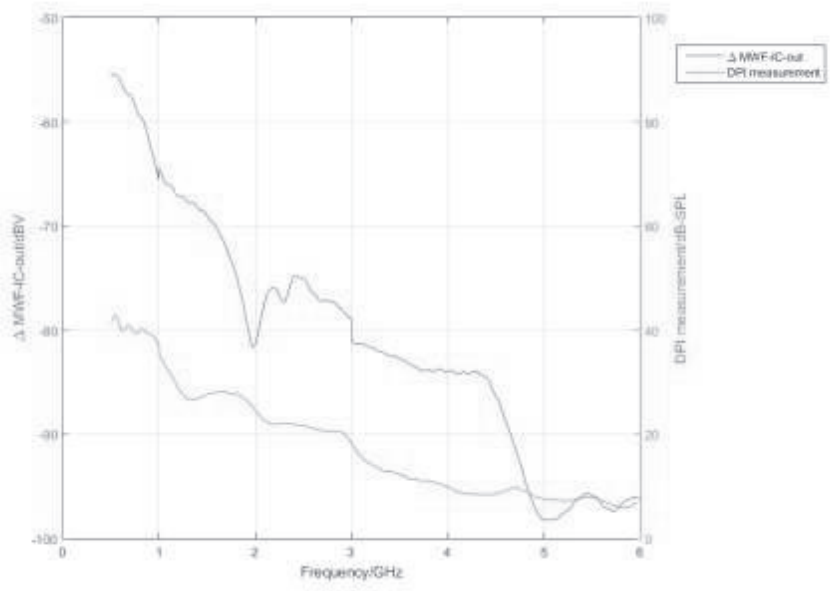


Fig.108. The full frequency range for Hybrid test board with MIC1 connection

We had to split the whole frequency range of 50 MHz – 6 GHz into 3 parts to get a reasonable complexity for the RLC circuit models and to perform an input impedance match between measurement and simulation. After combining the results of 3 frequency ranges we got large errors at the borders of adjacent frequency ranges as it is shown in Fig.106 and Fig.107**.** For a better impedance match adjacent frequency ranges should overlap.

Q. Julstrom correction

MIC1 and TCOILN/TCOILP:

After doing measurements for all the six orientations, the maximum between each orthogonal orientation and its opposing is taken. The maximum sum formula can be applied after that:

$$MAX_{odd} = MAX(+X1, -X1) + MAX(+Y1, -Y1) + MAX(+Z1, -Z1)$$

The output of the formula above represents the ORIL. This ORIL is converted to dB. The gain is subtracted from ORIL to calculate the IRIL.

IT'IS Foundation demodulator circuit calibration data and Julstrom method

After taking measurement for all the six orientations a correction for each measured frequency will be applied to these measurements using IT'IS foundation

calibration data. Each frequency in the calibration data has an input and output voltage. The output of each frequency that is measured by the GTEM is equivalent to the output voltage of the calibration data. The matlab program finds the equivalent RF input voltage for this (demodulated) output voltage and saves it in a new array, see the matlab code in section "Demodulator circuit code".

Afterwards the Julstrom approach is applied for the RF input voltage as follows

You can follow the same step as above, but now you must use the following maximum sum formula instead:

$$MAX_{even} = \sqrt{MAX(+X1, -X1)^2 + MAX(+Y1, -Y1)^2 + MAX(+Z1, -Z1)^2}$$

R. GTEM Cell Input Power Corrections:

Considered steps:

- Define the forwarded power from the network analyzer with -10dBm.
- Measure the transmission coefficient as S21 [dB].
- The output power is the sum between S21 [dB] and the forward power [dBm].
- Correct your forward power by using the calibration data of the GTEM cell.
- Convert the measured S22 parameter to impedance
- Calculate the corrected output power using the formula below:

Corrected_Output_Power= -10 dBm + (Corrected_Forward_Power - (-10dBm)) + S21

To calculate the input voltage (Vemf or open-circuit foot point voltage), we take the measured output power of the L-shaped antenna delivered into a 50-Ohm load. The L-shaped antenna is irradiated by an E-field of 50V/m and has a distinct orientation with respect to the H- and E-field vectors in the GTEM cell.
V_out / V_emf = 50 / (50 + Z_ant) =>V_emf = V_out * (50 + Z_ant) / 50

V_emf, Z_ant are complex values! Z_ant was derived from the S22-parameter.
V_out may be assumed as a real value (across the 50 Ohm resistor)!

V_out [V] = sqrt(50 * P[W]) = sqrt(50 * 1e-03 * 10^(P_out [dBm] / 10) ;
with 0 dBm = 1 mW

With P_out replaced by P_out_corr (from above) you get

V_emf [V] = (50 + Z_ant) / 50 * sqrt(50 * 1e-03 * 10^(P_out_corr [dBm] / 10)

S. Matlab code

Demodulator circuit code

```
% File name: JulStromCalculationForDemodulatorCircuitMIC1.m

%uploading the data to the defined variables below and
adding them to one martix
inputDataArray = [HIMIC1A0Data, HIMIC1A90Data,
HIMIC1A180Data,HIMIC1A270Data, HIMIC1B0Data, HIMIC1B180Data,
HIMIC1C0Data, HIMIC1C180Data];



% Defining a variable for the corrected data
outputCorrectData = [];
% Correcting by using sensor calibrating data will be
implemented here usingMr Kuehn measurements

for i = 1:8
% uploading sensor calibrating data:
Calibration =
dlmread('PhonakSensor01_CH2__20151003.txtPhonakSensor01_CH2_
_20151003.txt.calParam','', 5, 0)';

originFreq = Calibration(1,1:end)';
% Reading the measured data:
Maximal_sum_dB_ORIL = inputDataArray(:,i);
a = [];
b = [];
ResultBefore = [];
% Interpolating the calibrated data to match the samples
frequencies with the measured data
InterpolatedCalibratedData = [];
InterpolatedCalibratedData = [WantedFrequency(1:286)];
for i = 2:14
          F = griddedInterpolant(originFreq,
          Calibration(i,1:end)');
newCalibratedData = F(WantedFrequency(1:286));
InterpolatedCalibratedData =    [InterpolatedCalibratedData,
newCalibratedData];
end

dlmwrite('InterpolatedData.csv',
InterpolatedCalibratedData,';');
% Iterating through the whole frequency range
for i = 1:size(WantedFrequency(1:286),1)

        format long
```

```
% Reading the frequency, calibration error and minimum and
maximum voltage:
n=i; %n = 62, 2950MHz
    f=InterpolatedCalibratedData(n,1);
    errdB=InterpolatedCalibratedData(n,2);
    VfitRFinMin=InterpolatedCalibratedData(n,3);
    VfitRFinMax=InterpolatedCalibratedData(n,4);

    ci=[];
for ii=5:14
        ci=[ci, InterpolatedCalibratedData(n,ii)];
end

%Finding the correct input power
Vrfin = linspace(VfitRFinMin,VfitRFinMax,1000000);
%Reading the equivalent output voltage for the chosen input
voltage above.
Vrfout = polyval(ci,Vrfin);
%Converting
result = (Maximal_sum_dB_ORIL(n) - 131.4);
wantedFreq = WantedFrequency(n);
% d = find(Vrfout>-70.375, 1)
d = find(Vrfout> (Maximal_sum_dB_ORIL(n) - 131.4), 1);
%Using the position number to read out the output and input
voltage and save them in a separated array
a = [a; Vrfout(d)];
b = [b; Vrfin(d)];

end
outputCorrectData = [outputCorrectData, b];
end
%Declaring the corrected data.
Corr_HIMIC1A0Data = outputCorrectData(:,1);
Corr_HIMIC1A90Data = outputCorrectData(:,2);
Corr_HIMIC1A180Data = outputCorrectData(:,3);
Corr_HIMIC1A270Data = outputCorrectData(:,4);
Corr_HIMIC1B0Data =  outputCorrectData(:,5);
Corr_HIMIC1B180Data = outputCorrectData(:,6);
Corr_HIMIC1C0Data = outputCorrectData(:,7);
Corr_HIMIC1C180Data = outputCorrectData(:,8);

% Finding the maximum between the orientation measurements

% Maximum between A0 and A180
maxofA = [];
for i = 1:size(Corr_HIMIC1A0Data,1)
    t = [Corr_HIMIC1A0Data(i), Corr_HIMIC1A180Data(i)];
maxofA = [maxofA; max(t)];
```

```
end
% Maximum between B0 and B180
maxB0B180 = [];
for i = 1:size(Corr_HIMIC1B0Data,1)
    t = [Corr_HIMIC1B0Data(i), Corr_HIMIC1B180Data(i)];
    maxB0B180 = [maxB0B180; max(t)];
end
% Maximum between C0 and C180
maxC0C180 = [];
for i = 1:size(Corr_HIMIC1C0Data,1)
    t = [Corr_HIMIC1C0Data(i), Corr_HIMIC1C180Data(i)];
    maxC0C180 = [maxC0C180; max(t)];
end

% Converting to the linear scale
Out_linear_maxA = 10.^(maxofA/20);
Out_linear_maxB = 10.^(maxB0B180/20);
Out_linear_maxC = 10.^(maxC0C180/20);
%Applying the maximum sum of Julstrom method
Maximal_sum =  Out_linear_maxA + Out_linear_maxB +
Out_linear_maxC;
%Converting to dB scale
Maximal_sum_dB_IRIL = 20 .* log10(Maximal_sum);
%Plot whatever you want after that.
```

Julstrom calculation for Golden HI

```
% File name: JulStromCalculationForGolden_HI1_MIC1.m
% You should make sure that you do not go over 4 GHz because
the limit ofMr. Kuehn measurements

HIMIC1A0Data,HIMIC1A45Data
HIMIC1A90Data,HIMIC1A135Data, HIMIC1A180Data,
HIMIC1A225Data,HIMIC1A270Data, HIMIC1A315Data, HIMIC1B0Data,
HIMIC1B180Data, HIMIC1C0Data,HIMIC1C180Data
% Finding the maximum between the orientation measurements

% Maximum between A0 and A180
maxofA = [];
for i = 1:size(HIMIC1A0Data,1)
    t = [HIMIC1A0Data(i), HIMIC1A180Data(i)];
maxofA = [maxofA; max(t)];
end
% Maximum between B0 and B180
maxB0B180 = [];
for i = 1:size(HIMIC1B0Data,1)
    t = [HIMIC1B0Data(i), HIMIC1B180Data(i)];
    maxB0B180 = [maxB0B180; max(t)];
end
```

```
% Maximum between C0 and C180
maxC0C180 = [];
for i = 1:size(HIMIC1C0Data,1)
    t = [HIMIC1C0Data(i), HIMIC1C180Data(i)];
    maxC0C180 = [maxC0C180; max(t)];
end

Out_linear_maxA = 10.^(maxofA/20);
Out_linear_maxB = 10.^(maxB0B180/20);
Out_linear_maxC = 10.^(maxC0C180/20);

Maximal_sum = Out_linear_maxA + Out_linear_maxB +
Out_linear_maxC;
Maximal_sum_dB_ORIL = 20 .* log10(Maximal_sum);

Maximal_sum_dB_IRIL = Maximal_sum_dB_ORIL - 46.5;
Gain = 46.5;
HI1MICData = Maximal_sum_dB_IRIL;
```



LUND
UNIVERSITY

Series of Master's theses
Department of Electrical and Information Technology
LU/LTH-EIT 2016-490

http://www.eit.lth.se